Vertical-cavity surface-emitting lasers: Polarisation and external cavity effects

Badr, N. M.

Award date:
1995

Awarding institution:
University of Bath

VERTICAL-CAVITY SURFACE-EMITTING LASERS: POLARISATION AND EXTERNAL CAVITY EFFECTS

Submitted by N. M. Badr
for the degree of PhD
of the University of Bath
June 1995

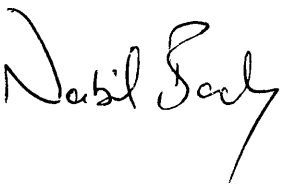

ProQuest LLC
789 East Eisenhower Parkway
P.O. Box 1346
Ann Arbor, MI 48106-1346

بِسْمِ الآبِ و الإبْنِ و الرُوحِ القُدْس

To my mum

Abstract

A theoretical two-mode rate equation model of a vertical-cavity surface-emitting laser is constructed incorporating thermal effects on wavelength, and two-mirror optical feedback. The experimental polarisation resolved light-current characteristics of the birefringent laser cavity are simulated. The model predicts static polarisation switching under stronger coupled cavity feedback, better spontaneous emission coupling, larger wavelength splitting or smaller optical loss anisotropy.

Static polarisation switching under polarised optical feedback is performed experimentally and is accompanied by a drop in the total power output. All-optical dynamic polarisation switching is attained at 1.5 GHz and is limited by the sensitivity of the detector. Theory reveals that switching is caused by large and mutual gain suppression supported by coupled cavity constructive interference.

The observed drop in total optical output power is associated with a rise in the carrier concentration of the laser. The subsequent modulation of the device bias voltage is measured for the first time in a semiconductor laser and is found to depend on the feedback power and the polarisation angle. This modulation reaches ~ 10mV both above and below threshold and is lowest for maximum cross-coupling between the polarised modes.

Exploiting this voltage modulation, the VCSEL is used as a source of polarised optical output and as a detector of polarisation rotation induced by the polar Kerr effect. The magnetic pattern of a magneto-optic material is successfully observed through the laser voltage. In such operation a VCSEL is envisaged as a compact alternative to the cumbersome optical head used in magneto-optic data storage applications.

Contents

Chapter 3: Coupled cavity VCSEL model

Chapter 4: Polarisation switching

Chapter 5: Magneto-optic data detection

Conclusion

Appendix

Preface

Semiconductor lasers are utilised not only in optical fibre communications but also in a variety of scientific, industrial and military equipment. Perhaps more significant though, is their recent utilisation in the personal and domestic environment, such as laser printing and optical data storage.

The introductory chapter describes traditional edge-emitting lasers and their characteristics, and highlights their limitations. A preview of the new class of vertical-cavity surface-emitting lasers (VCSELs) demonstrates their advantages and potentials especially in polarisation switching and optical processing. Also reviewed is optical data storage technology, in comparison with magnetic storage, to assess the possible improvements that VCSELs may offer by replacing edge-emitting lasers.

Chapter two is a general exposure to the present state of VCSEL technology. Commencing with the basic physical principles and processes of laser operation, it continues to establish the laser cavity design. The behavioural characteristics of VCSELs are also described with particular attention to their optical polarisation diversity. An account of recent developments in microcavities, two-dimensional arrays and integrated lenses demonstrates the current interest in fulfilling the potential of VCSELs.

Subsequently, chapter three examines the unusual characteristics of one device (VCSEL #1) in comparison with reported observations, and provides a theoretical account of its behaviour. This is formalised in a model that is solved numerically providing an understanding of the laser dynamics. Following its verification, the model is used to predict the polarisation behaviour under varied operation conditions.

The static and dynamic polarisation self-switching of VCSEL #1 under optical feedback is explored experimentally in chapter four. This all-optical behaviour is understood theoretically using the model previously developed. The chapter concludes with predictions regarding the bias voltage of the device under feedback.

The final chapter explores the response of the device bias voltage to polarised optical feedback, experimentally and theoretically. To our knowledge, this is the first such investigation of a semiconductor laser behaviour, and it leads to a novel application. The feasibility of this idea is investigated by utilising a VCSEL simultaneously as a laser source under feedback and as a detector of the magneto-optic polar Kerr effect.

In conclusion, all the chapters are summarised coherently outlining the work carried out and the results achieved. Finally, proposals for future work are recommended in the light of the understanding gained and the discoveries made.

Acknowledgements

I am deeply grateful to my family for supporting me throughout my research. I thank my supervisor Ian H. White for his encouragement and motivation. Special acknowledgement is due to Huw Summers for enlightening discussions and constructive criticism of this thesis, to Paul Snow for helpful explanations and to Frances Laughton for positive comments. Thanks are also deserved by members of the optoelectronics group for advice, cooperation and sense of humour.

I also acknowledge our industrial collaborators at Hewlett-Packard Laboratories: David Cunningham and Alistair Coles at Bristol, and Drs Tan, Houng and Wang at Palo Alto, California, for their support of the project.

Most of all I devote my warmest appreciation to my girlfriend Sandra for her sustained motivation and sacrifice, and for her scrutiny of this thesis.

CHAPTER

1

Introduction

This introductory chapter highlights the advantages of vertical-cavity surface-emitting lasers over their traditional edge-emitting relatives. Special attention is paid to the optical polarisation and its importance in various applications. Subsequently, a brief review of data storage technology and its limitations concludes with possible solutions offered by vertical-cavity lasers.

The first semiconductor lasers were fabricated in 1962 as simple p-n junctions with two cleaved facets. From those crude and inefficient lasers, the whole field of optoelectronics has developed. From a present perspective, traditional semiconductor lasers are limited by some of their characteristics because of their planar geometry and edge-emission. A recent arrival to the field, however, is the class of vertical-cavity surface-emitting lasers (VCSELs) which are on the verge of maturing in technology. Because of their unique surface geometry and their distinctive operation, they offer solutions to various problems.

The following is a brief review of the characteristics of edge-emitting lasers with an emphasis on their limitations that have fuelled the development of surface-emitters. A variety of technical aspects are covered concerning the use of lasers, and in particular applications requiring optical polarisation control. One specific application is that of optical data storage for which a review is provided in the latter part of this chapter.

1.1 Edge-emitting lasers

Originally, semiconductor lasers were fabricated as p-n junction diodes, and subsequent development has lead to a more sophisticated layer structure. When forward biased, the electron-hole recombination region forms the active gain volume of the laser, and two cleaved facets form the feedback mirrors. The operational wavelength range is determined by the gain spectrum of the active region material. Specific wavelength selection is achieved by interference between the mirrors within the optical cavity. One feature common to all edge-emitting lasers is that light propagation, amplification and emission are parallel to the plane of the junction, see figure 1.1. This essential architecture strongly influences their characteristics.

An edge-emitting laser emits light in a divergent elliptical beam that forms the far field pattern [1]. For a standard design most of the optical power of the approximately Gaussian profile beam is contained within a horizontal half-angle of ~ 15° and a vertical half-angle of ~ 30°. In order to capture most of the optical power emitted therefore, one requires a lens with a numerical aperture (NA) larger than 0.5. Moreover, when focussed the resulting elliptical focussed beam is unsuited for coupling to a standard circular profile optical fibre. This is evident in the low efficiency of power coupling from an

edge-emitting laser to a lensed fibre reported typically at 30% [2]. The need for a lens also complicates the optical alignment and its maintenance in a commercial system or even an experimental one.

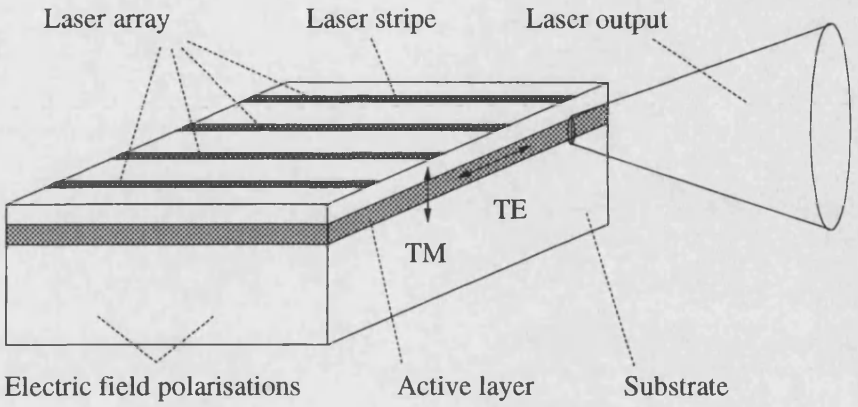

Figure 1.1: Illustration of an edge-emitting laser array: p-n junction, TE and TM electric field vectors and divergent elliptical output beam

One other problem is the difficulty of testing a laser before cleaving or etching the facets and observing the output. This inevitably reduces the yield, inhibits automated test and manufacture and maintains high costs, especially when monolithic arrays of lasers are required. Edge-emitting laser arrays are also clearly restricted to one dimension limiting the application of the technology in that respect.

Another difficulty common to the less sophisticated Fabry-Perot (FP) lasers is the inevitable hopping [1] between the densely packed longitudinal cavity modes that result from the long cavity length. This behaviour is highly detrimental to the error rate in long distance transmission systems and is overcome in the design of distributed feedback lasers (DFBs). Nonetheless, wavelength matching is a problem when coupling laser light into an FP optical amplifier. Other problems include large wavelength chirp [3] under pulsed operation, low modal confinement in the cavity cross-sectional plane and the ensuing unnecessary optical losses.

From a cavity cross-section perspective, an optical mode is given a transverse electromagnetic index (TEM_{pq}) [4] where p and q refer to the mode order along the

orthogonal cavity axes. It is common to apply TE_p and TM_q when referring to one dimension. The optical operation of an edge-emitting laser is usually dominated by a single fundamental transverse electric (TE ≡ TE_0) mode [4], i.e. electric field parallel to the junction plane. Second preference usually belongs to the fundamental transverse magnetic (TM ≡ TM_0) mode, i.e. magnetic field parallel to junction plane. Higher order modes are successfully eliminated by maintaining a thin and narrow active region that defines the viable mode. The distinction between TE and TM is caused by different effective facet reflectivities and different modal gains, each leading to unequal threshold currents.

In effect, an edge-emitting laser radiates a highly polarised optical output as required for many purposes. However, recently there has been interest in controlling the polarisation of a laser output for specific applications some of which are described below. Research has revealed that the intrinsic material gains of TE and TM modes may be altered by inducing strain in the active layer lattices. Consequently, edge-emitting lasers have been designed with pre-defined optical polarisation behaviour. Polarisation related issues will be detailed specifically in chapter two when describing the operation of a laser.

1.2 Surface-emitting lasers

Two categories of surface-emitting lasers (SELs) have been designed to alleviate the problems highlighted above and are illustrated in figure 1.2. Essentially, both designs redirect the output of edge-emitting lasers normally to the junction surface, effecting surface-emission. Output coupling components, such as etched mirrors [5] and distributed Bragg reflectors (DBRs) [6], are monolithically fabricated with the lasers. Although such SELs may be arranged in 2-D arrays that produce high optical power [1], they still exhibit other performance characteristics comparable to those of edge-emitting lasers.

The first accomplishment of a true surface-emitting laser with a vertical cavity (see figure 1.3) was reported in 1979 by Soda et.al. [7]. The high threshold current density of 11 kA/cm^2 together with the large diameter of 100μm necessitated cooling at the liquid nitrogen temperature of 77K and operation at a low duty cycle (<1%). The main problems

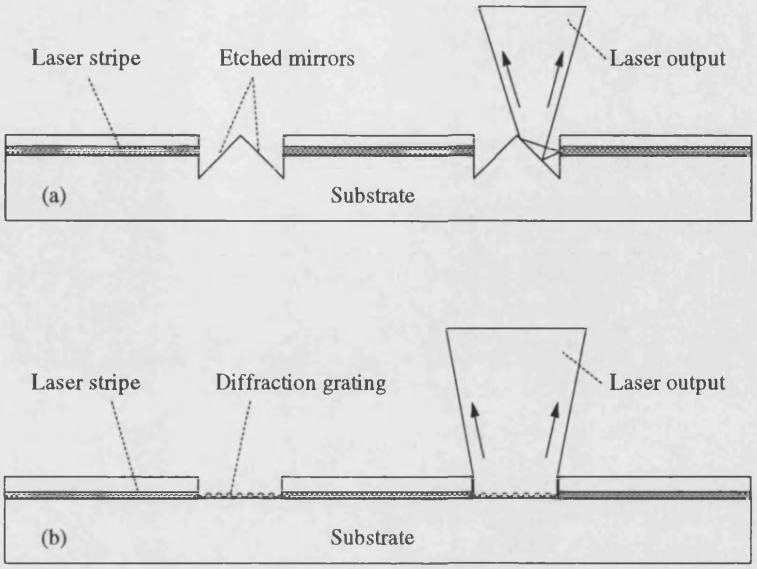

Figure 1.2: Two categories of surface-emitting lasers (SELs):
(a) etched-mirror SEL array and (b) grating-coupled SEL array

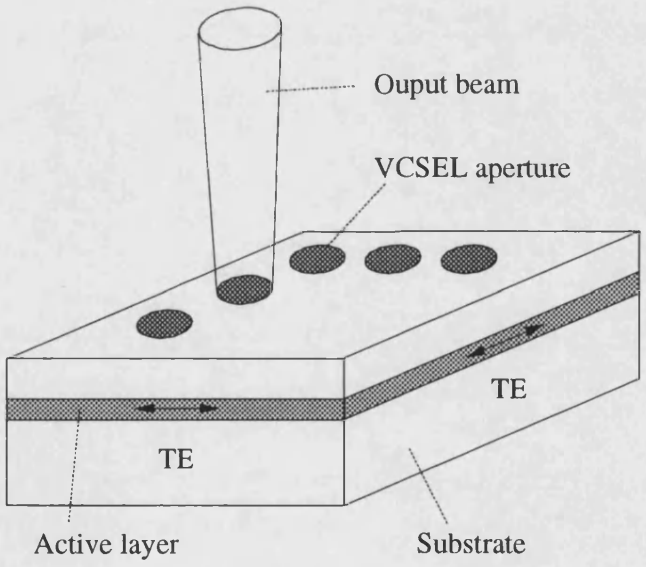

Figure 1.3: Illustration of a VCSEL array: p-n junction, TE electric field vectors and narrow circular output

were the low reflectivity of the multilayer dielectric mirrors, and the thin gain region. The high round-trip photon escape rate was balanced by the round-trip gain only at a very high injection current, and the heat generated would have been catastrophic without deep cooling. These problems have been overcome since then by phenomenal advances in high reflectivity mirror technology and by optimised cavity designs. Multilayer distributed Bragg reflectors (DBR) have been developed to reflect more than 99.5% of optical power. Vertical-cavity surface-emitting lasers (VCSELs) today operate without cooling at sub-milliamp threshold currents with up to 90% efficiency [8]. They vary in diameter from 100μm to only a few micrometers where the transition occurs to optically pumped microcavity devices.

The advantages of the VCSELs over their edge-emitting relatives are numerous. An immediate result of the surface emission is to remove the undesirable wide diffraction of the output beam. A typical far-field is circular in profile with a half-angle of approximately 4° (NA ≈ .07), dramatically improving coupling into optical fibre to ~ 90% [9]. This even allows the elimination of lenses altogether [10], promising easier and cheaper optical fibre interconnections. With this laser design, a short optical cavity is also possible and preferred to minimise the otherwise unnecessary losses of the passive layers adjacent to the active layer allowing the reduction of the cavity length to only a few micrometers. Hence, of all the possible longitudinal cavity modes, only one may fall within the gain spectrum and have maximum spatial overlap with the gain region, eliminating multi-longitudinal mode competition and the mode-hopping problem.

VCSELs may also be arranged in a two dimensional (2-D) array of almost any configuration. For example, a matrix of 27×27 VCSELs has been phase-locked [11] and other arrays of individually addressable VCSELs have been reported to successfully operate at room temperature. Such is the advantage of the surface architecture that each laser may be tested before cleaving the array from the wafer, perhaps allowing re-scheduling of the array and thereby improving the yield. VCSEL arrays may perform parallel optical communication between neighbouring electronic circuit boards or even multichip modules. The latter is approaching realisation as GaAs VCSEL substrates are integrated [12,13] on Si substrates bearing electronic circuits. Taken a step further, one may build other layers of optical devices on top of the VCSEL array to manipulate,

switch and process the lasers' outputs. This 3-D integration of optical devices and components is envisaged to be a possible route for optical processing and optical computing in the future. VCSELs have already been successfully integrated with optical modulators [14] and others have been converted to active AND logic gates [15] and logic inverters [16].

Considering that emission from a VCSEL is normal to the surface, the electric field of the output radiation is always parallel to the junction and is therefore TE polarised. Unlike edge-emitting lasers there is no intrinsic gain preference to a specific optical polarisation angle, but only a modal gain preference. Any deviation from circular symmetry of a VCSEL aperture leads to a transverse mode preference and thus to polarisation selection, much like in an optical fibre. Gain anisotropy may be induced, also, if a quantum well gain structure is fabricated with its layers tilted relative to the mirror structures, as explained in chapter two. Under suitable conditions of external injection though, a nearly symmetric circular VCSEL may be compelled to adopt a polarisation other than the naturally dominant one. Thus, VCSELs offer an underlying continuum of polarisation states of which to select the desired orientation with a minimum of effort and with good stability. This ability warrants investigations into the polarisation control of VCSELs and, in particular, under external feedback or injection.

1.3 Polarisation switching

There are several ways to modulate a laser beam with a signal such as amplitude, frequency and phase modulation. Alternatively, the polarisation direction may be modulated or switched to carry a signal, which offers a number of advantages. If the modulation is binary digital, then at any time the signal and its complement are present allowing easier logic manipulation. There is also an immediate improvement of 3dB in the signal to noise ratio compared with amplitude modulation for example. If amplifiers and waveguides are involved, then the constant optical power of a polarisation switched signal reduces multichannel cross-talk, further improving the system performance.

Considering the intrinsically isotropic gain of a VCSEL, it would seem possible to switch its polarisation under external injection or feedback. Such all-optical switching would not necessarily incorporate a change in the electrical state of the laser, i.e. the charge

carrier density, over short time scales (picoseconds). This operation therefore may reach ultra-high switching frequencies of the order of 100GHz [17]. Over longer time scales though (nanoseconds), polarisation switching may entail a change in the carrier concentration, particularly if the gain is highly anisotropic or bistable-type behaviour is exhibited.

The wavelength chirp that is characteristic of a modulated laser output would also be minimized dramatically, improving the signal quality and further reducing noise. Such signals would be square or rectangular in shape, and therefore would be suitable for digital subcarrier multiplexing (SCM) [18]. SCM may be applied to an optical carrier by modulating it at several microwave frequency channels, each of which further to carry a signal modulation [19]. Currently, there is great interest in employing SCM in optical fibre links for cellular communication networks [20,21] and for remote delivery of video services [22].

A more immediately tenable benefit of all-optical polarisation switching is pulse re-timing and re-shaping of injected optical signals [23]. If long distance transmission is required, a polarisation maintaining fibre is necessary to preserve a polarisation switched signal. Alternatively, filtering the signal with a polariser before transmission renders it suitable to a polarisation non-maintaining fibre. Subsequently, it may be re-converted to a polarisation switched signal by appropriate injection into a VCSEL.

When all-optical processing is possible in 3-D integrated optical circuits, the optical polarisation may be the preferred property to carry binary code. This would be aided by the availability of passive polarisation filters (polarisers), rotators (half-wave plates) and neutralisers (quarter-wave plates). The active elements, such as VCSELs and polarisation insensitive modulators [23], are capable of supporting, amplifying, selecting and modulating a continuum of polarisation orientations, and may also be designed to recognise two predetermined orthogonal axes. Meanwhile, and not so far from data processing, lasers have already entered the computer market in the form of the CD laser. VCSELs are expected to advance optical data storage technology even further.

1.4 Digital data storage

Data storage has been traditionally dominated by magnetic recording, from the early audio tape to the more recent video tape and magnetic disk media. Digital data storage is under continuous pressure to achieve larger data capacities and faster data transfer rates to fulfil the capabilities of modern computers. In the past two decades data storage has relied mainly on a combination of media for data retrieval. Fast data access (~ 70ns) has been provided by the temporary dynamic random access memory (DRAM) and permanent read-only memory (ROM). Although slower to access and usually physically non-portable, permanent and re-writable data is delivered by the magnetic hard disk drive (Winchester technology). Portable alternatives are available in the flexible disk, commonly known as the floppy disk (or diskette) and the much slower magnetic tape. Their unsatisfactory lower data density and slower access, however, are the forces behind the recent developments in the newer optical storage media. Although so far data processing is achieved electronically, its communication and storage are turning to optics.

There are presently three main methods of optical data storage: the compact disk read-only memory (CD-ROM), the write-once read many times memory (WORM or CD-R) and the magneto-optical disk (MO and MD). They all supply an unprecedented large volume of data in a compact, stable, and, invaluably, a portable medium. The following reviews are brief descriptions and comparisons of the commercially available media in terms of performance, potentials and limitations. Table 1.1 compares the best performance offered at reasonable cost by each storage medium at present.

1.4.1 Magnetic hard disks

Modern computers rely primarily on magnetic hard disks (Winchester technology) [24] for fast, random access to large volumes of re-writable data. A hard disk drive incorporates a stack of disks mounted on a common spindle driven by a motor that ensures a constant angular velocity (CAV) up to 7200 rpm. Read/write heads are mounted on swinging arms, each reaching between a pair of disks, and independently controlled by an electromagnetic actuator servo mechanism. The assembly, illustrated in figure 1.4, is encapsulated in an evacuated environment to minimise the drag force on the disks and their surface contamination by particles.

The actuators provide random access to any track on any surface of the disk. When the disk is formatted, special data sequences are stored on parts of the surface and used in signalling the head position to the servo control. Each arm carries two heads, one per surface, except the outermost arms which carry one head each. A hydrodynamic bearing is generated at a slider-disk interface, providing a small but stable spacing (~ 0.5 μm) between the heads and the disk.

The read/write functions are implemented by the magnetic head which stores data as a series of digital bits (figure 1.5) in a spiral track on the surface. The track spacing is determined by the head alignment tolerance and the tracking mechanism. The size of a bit depends on the head width and the magnetic material resolution which is improved by using thinner and higher quality substrates. With a track spacing as small as ~ 6μm, a bit density of ~ 20 kb/mm (kilobit/mm), the best total disk capacity currently stands at 11 GB (Gigabytes). Performance is also measured by the data flow rate which increases with bit density and with rotation rate, and is currently at 87 Mb/s (megabit/sec).

Another aspect of the disk drive performance is the average access time. This is the total of the average head seek time between two random tracks, and its settling time, in addition to the latency time. The latter is the time taken to reach the required sector on the track. Since, on average, the required sector is 180° away, i.e. on the other side of the disk relative to the head, the latency time is that taken for half a revolution. The access time depends on the heads and actuators used, while the latency time is shortened by faster rotation. However, it is common for 50% to 60% of all seeks to be of zero length because the data required often neighbours the data already read. Access time is short for program downloading but not necessarily for user data retrieval, and the statistics obviously depend on the nature of data mostly read or written. Presently, though, the best hard disks offer an average access time of ~ 9ms, most of which is latency time.

The head design, rotational velocity and tracking tolerances have improved at a rapid rate that still show no signs of levelling. The fundamental limits of the technology are estimated within an order of magnitude of the present performance [25]. However, the small gap between disk and head, the small magnetic head core and the narrow track leave little tolerance for misalignment and necessitate the permanent contact between

head and disk. The storage medium and drive unit are therefore combined in one assembly which is heavy (upwards of 0.5 kg) and essentially not portable. A notable exception is a detachable hard drive of 171 MB capacity used when high information security is paramount. The limitation of non-portability has been the main motivation for the development of the floppy disk to carry data on a light re-writable medium.

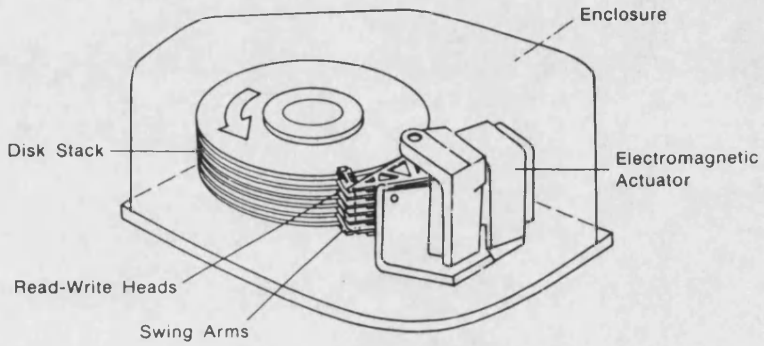

Figure 1.4: Hard disk drive contents, after [24]

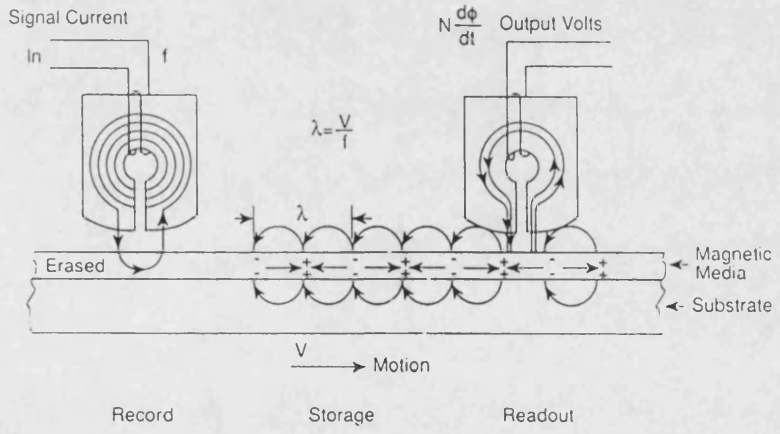

Figure 1.5: Magnetic head read/write functions in a hard disk drive, after [24]

1.4.2 Floppy disks

The floppy [24] is similar to the hard drive in principle but the gain in portability is lost in performance. The disk with its protective jacket is designed for easy insertion and removal from the disk drive. When mounted, the drive rotates the disk while the read/write heads access both disk surfaces through slots in the jacket. When functional,

the heads are in contact with the disk which is rotated at relatively low speed because of drag forces, reducing the data flow rate to ~ 200 kb/s. Unlike a hard disk, and to minimize wear, a floppy is not constantly rotating but spins up when access is required, further prolonging access time to more than a large fraction of a second.

The relatively low surface quality of the disk substrate and the inaccuracy of the disk clamp limit the track spacing to ~ 100μm. The most commonly used 3.5 inch floppy has a linear bit density of ~ 100 b/mm and a formatted capacity of 1.4 MB. Another major drawback of the floppy disk, however, is the susceptibility of the stored data to strong nearby magnetic fields commonly arising in everyday environment. The coercivity of a magnetic material is the minimum magnetic field necessary to change the magnetisation of the material, and it depends on its composition, structure and temperature. Optimally, the coercivity of the magnetic material would be high enough to secure the data stored from surrounding magnetic fields, and low enough to be adequately overcome by the field applied by the head when writing. While the floppy is suitable for transferring small quantities of data (~ 1MB), it is inadequate for the large data capacity and the high data security expected in many applications.

1.4.3 Magnetic tape cartridges

The oldest data storage medium took the form of magnetic tape [24] and provided serial access of analog and digital data. Despite the low data density of magnetic tape, it offers a high capacity (e.g. 80MB per cartridge) of multichannel re-writable data, fast data flow and portability in a variety of formats. Its very slow access times of seconds or minutes, however, limit its present and future utilisation to audio and video storage, and to archiving and backing up computer data.

1.4.4 Compact disk (CD-ROM)

Compact disk (CD) technology [26-28] was introduced commercially in 1982 as a read-only medium of digital audio albums. It had been preceded by the less successful LaserVision video storage medium first released in 1972. In 1986 the CD entered the computer digital storage market providing a large data capacity pre-recorded optically on a portable disk. The spiral data architecture is much the same as that of magnetic

disks but the physical phenomenon utilised is that of optical interference. Bits are impressed onto the transparent polycarbonate substrate to form depressed *pits* (or raised plateaux) surrounded by *land* area, see figure 1.6. An aluminium layer provides optical reflections and is protected by a third layer that shields the impression from direct external defacing.

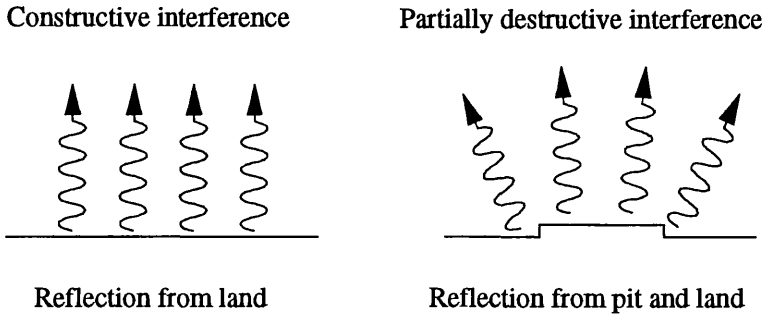

Figure 1.6: Detection of data pits on CD by destructive interference and scattering

Data detection takes place by focussing a laser beam through the substrate onto the track while spinning the disk. A CD laser is composed of AlGaAs/GaAs operating at 780nm and its beam is optically manipulated to form a circular spot ~ 1.2μm in diameter. The spot reflects coherently from land area but is reflected partly in antiphase by pits, interfering destructively and thereby modulating the optical beam. The small width of a pit is certain to scatter the reflected light also, further reducing the detected power. Each pit is a quarter of a wavelength deep (130nm, the refractive index of polycarbonate is 1.6), 0.5-0.6μm wide and at least 0.5μm long.

The track spacing and the bit spacing are limited not by the spot size but by its Airy rings formed due to diffraction from the focussing optical system, see figure 1.7. The nearest any bit can be to another is ~ 1.6μm, coinciding with the first Airy ring minimum (~ 2λ) and introducing least crosstalk, although recent designs set the track spacing at 1.3μm. The pit length indicates a sequence of identical binary digits corresponding to pulse code modulation (PCM). Therefore, the resulting linear bit density is somewhat variable and depends on the actual data and the coding, but the expected total capacity of a standard single-sided 5.25 inch disk is ~ 640MB.

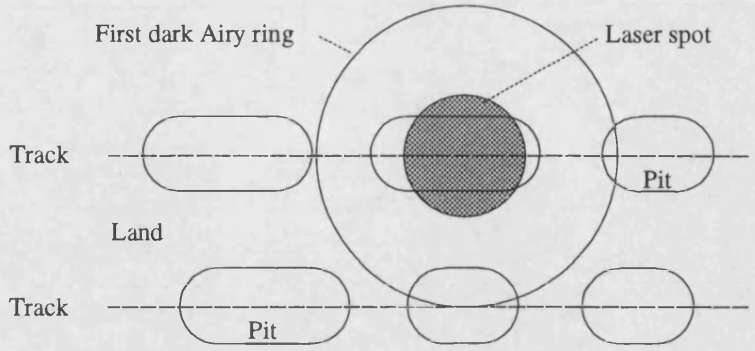

Figure 1.7: Placing neighbouring tracks at the first dark Airy ring

The compact disk is a constant linear velocity (CLV) medium which was originally set at 1.2m/s or 1.4m/s. Naturally, this requires a change of rotation rate when accessing different tracks, leading to a variable rotation rate of 200 rpm for the outside track and 500 rpm for the inside track. Because of the variable linear bit density, this is interactively adjusted to ensure a constant data flow rate of 150 kB/s (1.2 Mb/s) which is adequate for audio tracks. Because of the non-contact data readout, CD-ROM disks are currently driven at up to six times the original velocity, providing a data flow rate of 7.2 Mb/s. As for magnetic disks, track seeking is achieved by reading format information at designated periodic sectors on the disc. The total optical power required for this operation is ~ 2mW, easily within the capability of a semiconductor laser. A working optical system (figure 1.8) also includes more optical components arranged to perform focussing and tracking. Weighing between 18g and 60g, therefore, a CD is very light, allowing acceleration and deceleration as appropriate within an average access time of 130ms.

CD-ROM technology provides a massive data capacity in a permanent form. Although the substrate surface is ~ 1 mm from the lens focal plane, excessive defacing may introduce detection errors and degrade the system reliability. It is the non-contact optical detection however, that allows the inexpensive portability of the floppy while rivalling the high data capacity of the hard disk and adding inherent data security. Consequently, the remaining limitations are the lack of recordability and the long access time due to the change in angular velocity.

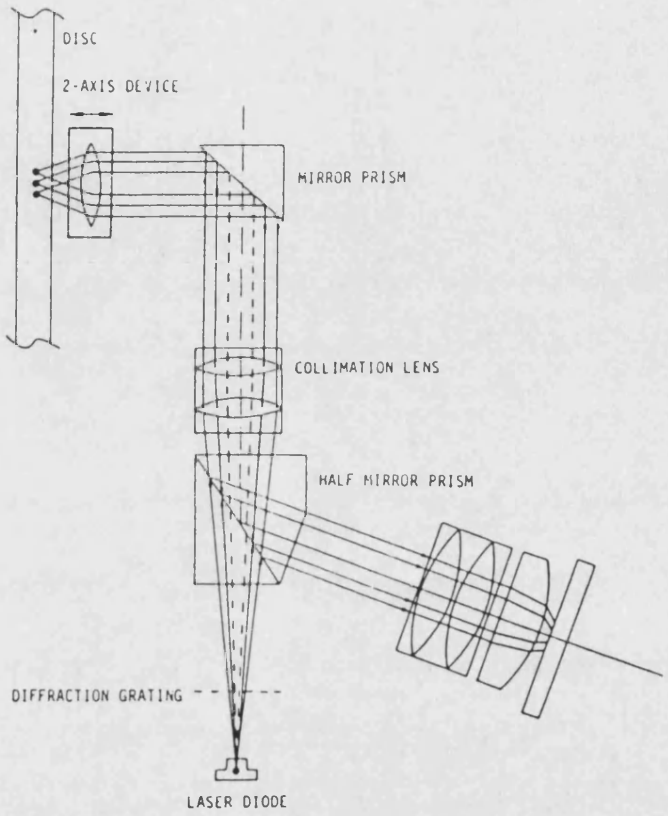

Figure 1.8: Optical arrangement of a CD-ROM optical pickup head, after [28]

The access time may be improved by adopting a CAV operation which shifts the limitation to the random seek time and the latency time. Mounting the laser, the detector and all the optical components on an optical head leaves it far too massive to move promptly. This problem is minimised by fixing all the optical components, except the essential beamsplitting mirror and lens, which constitute the optical pick-up that is moved radially by an actuator arm. With this split-head arrangement, average access times better than 50ms may be obtained. Because of industrial standardisation, CAV operation may not be applied to old standard designs but only new designs or to other optical storage media, as discussed below. Usually, a voice coil is employed in performing small adjustments within the optical pick-up to focus the beam on the track, permitting access to ~ 1 MB of neighbouring tracks within 1ms. Additionally, higher angular velocities are being achieved to reduce the latency time.

1.4.5 Recordable compact disks (CD-R)

The effort to develop a recordable optical storage medium with a high storage capacity is based on CD technology but uses a writable medium [26]. Similarly to a CD, a CD-R also begins with an optically flat polycarbonate substrate. A green dye film is topped with a thin reflective gold coating, together forming the recording layer which is covered by a protective film. The principle is to use the laser to create *pits* by thermally ablating the recording medium. The recording process involves focussing between 4mW and 8mW of infra-red (780nm) laser power onto the absorbing green dye heating it up. Local melting of the recording layer and the substrate are followed by cooling and contraction of the dye. The reflectivity of the recording layer is thus modulated by the dye thickness and may be detected by a CD-ROM optical head. When writing data, tracking is achieved by following the reflection from a pre-groove that contains a control signal used to maintain a constant linear velocity.

Data may be recorded only once using this process which offers a method of permanently storing information away from the factory making it suitable for archiving or for limited scale replication. A CD-R, also known as write once read many times (WORM) medium, is essentially limited in similar ways to a CD, but is one step closer to re-writable optical storage. The current capacity of a double-sided 5.25 inch diameter CD-R of 1.3 GB. Utilising a split optical head arrangement and a CAV of 3600rpm, the average access time is ~ 40 ms.

1.4.6 Phase change re-writable disks

A more expensive alternative to the CD-R described above relies on the change in reflectivity [29] that accompanies the change in the state of a material. If a short powerful laser pulse is focussed on a thin layer of a crystalline material (e.g. GaAs and Ge-Te-SB alloy), the exposed spot cools down as an amorphous *pit*. The amorphous spot is less reflective than the surrounding crystalline *land*, see figure 1.9, and overlapping a succession of these spots modulates the length of the pit.

Originally conceived for WORM technology, the process is discovered to be reversible. It has been reported [30] that subjecting the spot to a longer but less energetic laser pulse can revert the spot to the crystalline state. Although the material phase change is not

complete (see figure 1.9), the change in reflectivity is substantial and compatible with CD-ROM reflectivity modulation. A double-sided 5.25 inch re-writable disk [31] offers a capacity of 1.0 GB and the disk drive system provides an average data transfer rate of 7.9 Mb/s and an average access time of ~ 40ms. Current research efforts into optical re-writable CDs are concentrated on finding the optimum materials and structures for optically erasable phase change media. However, the problem of the massive optical head and the slow access time remains.

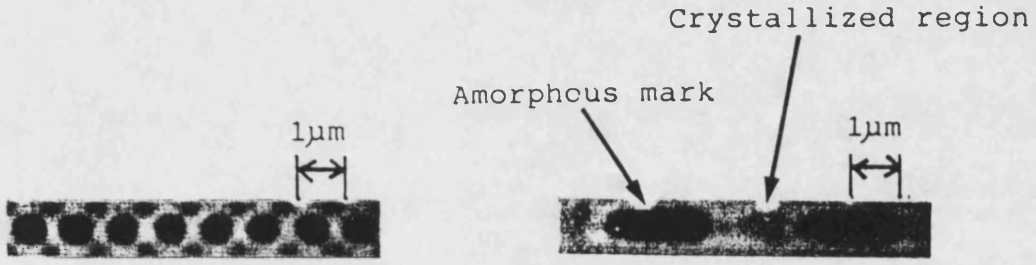

Figure 1.9: Phase change recording. Left: record marks at 1µm spacing. Right: record marks and erase-residues between them, after [29]

1.4.7 Magneto-optical data storage

Magneto-optic (MO) data storage [24,26,31,32] is based on the polar Kerr effect [33] which is also related to the Faraday effect. When plane polarised light is reflected from a magneto-optically active medium, its plane of polarisation is rotated by the Kerr angle θ_k. Hence as a focussed laser beam (~ 2mW) is reflected from the disk, its polarisation angle is modulated by data stored magnetically. Because of residual birefringence in the material, the polarisation rotation is usually accompanied by ellipticity.

The essential detection system [34], illustrated in figure 1.10, incorporates a polarising beamsplitter which directs the reflected beam to a quarter-wave plate to restore its linear polarisation state. A second polarising beam splitter is rotated at 45° about the optical axis and splits the beam into two similar fractions, which are detected by two photodiode assemblies. A rotation of the beam polarisation plane is translated to intensity modulation to both detectors, in complement. Recording is accomplished by focussing a powerful

laser pulse (5-10mW) on the medium, thereby heating it above its Curie point (or compensation temperature). An appropriate magnetic field applied by a coil on the other side of the disk magnetises the heated spot as it cools down, storing the data.

The first MO disk became available in 1988, and presently a 5.25 inch double-sided disk is capable of storing 1.7 GB while the smaller 3.5 inch double-sided MiniDisk (MD) alternative offers 230 MB. This technology adequately allows 10^9 erase/write cycles with a portable, secure and large data capacity. Current research into MO storage materials is exploring possible alloys (e.g. TbFe, Mn-Bi) and structures (e.g. PtCo multilayer) for optimum magnetic coercivity, optical reflectivity and Kerr angle. With an access time of 19ms (40ms for an MD), MO technology is very competitive when compared with CD-ROM and CD-R technologies. For obvious reasons though, see figure 1.11, the optical head is still too massive and sophisticated to approach the hard disk performance.

1.4.8 Future development

It is worth pointing out that data retrieved from any type of storage medium (except DRAM and ROM) is usually processed by error detection and correction algorithms to allow improvements in hardware that would otherwise produce unacceptable error rates.

In view of the brief descriptions of the various media, it is projected that using the shorter wavelength blue lasers (400nm) would allow a proportional improvement in the linear bit density and the track spacing. As a result, and while magnetic heads are near their size limitations, the optical storage capacity of a disk may be increased by a factor of ~ 4. Curiously, and as if a portable CD-ROM with a 640 MB capacity is not adequate, the development of the multi-level CD-ROM [36] is reported imminent. The proposed principle is to glue up to 10 CD-ROM disks in parallel and to focus the laser beam on the one disk of choice when reading. The disks have to be thinner, they can contain data on one side only, and they require a special driver which would be capable of reading normal CD-ROM. Using the new blue laser, a multi-level disk would have an unprecedented capacity of 15 GB in a portable form. This technique would not work in conjunction with MO storage because of the obvious degradation of signal.

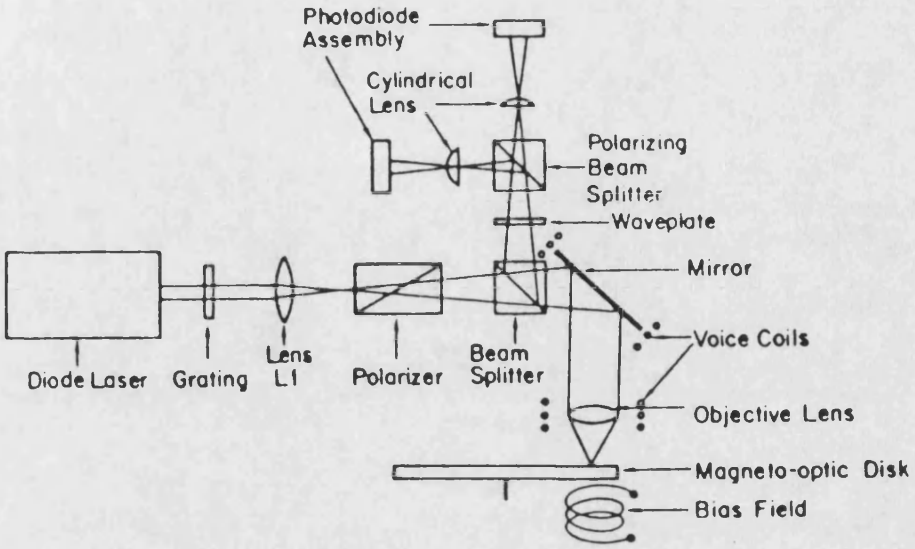

Figure 1.10: Optical pickup system for magneto-optic storage, after [34]

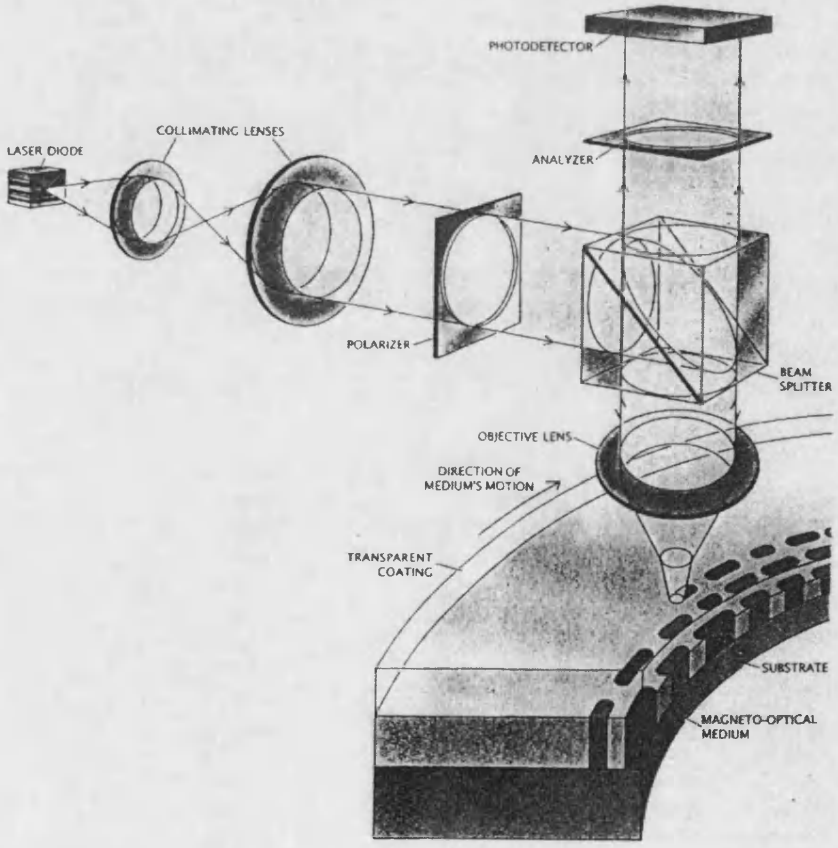

Figure 1.11: Illustration of optical pickup for MO storage, after [35]

Table 1.1: Present storage media system performance

Medium	Data stability	Read/write	Diameter (inch)	Usable surfaces	Storage capacity (MB)	Linear / angular velocity	Data rate (Mb/s)	Average access time (ms)	Linear bit density (kb/mm)	Track spacing (μm)
DRAM	Volatile	R/W	-	-	1	-		70ns	-	-
ROM	Permanent	R/pre-recorded	-	-	1	-		70ns	-	-
Hard drive	Unexposed	R/W	3.5	Up to 20	11 GB	7200 rpm	87	9	~ 20	~ 6
Mobile hard drive	Unexposed and lightweight (65g)	R/W	2	4	171 MB	4500 rpm	~ 20	16	~ 20	~ 7
Floppy	Magnetically susceptible	R/W	3.5	2	2.8	~ 300 rpm	200 k	> 0.5 s	~ 100 b/mm	~ 100
CD-ROM	Permanent	R/pre-recorded	5.25	1	640	(1 - 6) × 1.2 m/s	1.2 - 7.2	130	> 10	1.3
CD-R	Permanent	R/write-once	5.25	2	1.3 GB	3600 rpm	9	40	> 10	1.4
Phase change	Stable	R/W	5.25	2	1.3 GB	3600 rpm	9	40	> 10	1.4
MO	High coercivity	R/W	5.25	2	1.7 GB	3000 rpm	16	19	> 10	1.4
MD	High coercivity	R/W	3.5	2	230	3600 rpm	12	40	> 10	1.4

Despite optimism with respect to optical storage, digital data storage is unlikely to be monopolised by one storage medium in the near to intermediate term. It is likely that the present trend of using several media to store and retrieve information will continue. The preference obviously depends on the application, and while re-writable optical storage is available it is somewhat slower than the magnetic hard disk. If improvements in the lasers and optics of the read/write head reduce the access time significantly, optical storage may replace the hard disk altogether. In fact, optical data storage is progressing to replace conventional media of both still and motion photography.

Current efforts are directed at reducing the number of components of the head and reducing its mass. Apart from the present use of a split optical head where only the lens and a beamsplitter are moved, suggestions [25] include using fibre heads, holographic elements, non-mechanical scanners and integrated optics. An example of an integrated optical head [37,38] that includes a diffraction grating to couple laser light (surface emission) onto the disk and back to the laser for detection is reproduced in figure 1.12. It seems that VCSELs are well suited to enter optical storage technology, especially considering the possibility of integrated lenses.

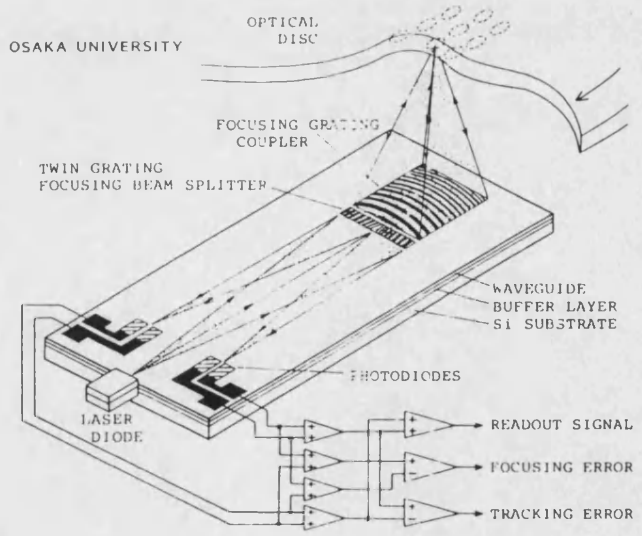

Figure 1.12: A suggested integrated-optical head for MO storage, after [37]

The drop in mass and complexity may plausibly afford the optical head a competitive access time and an interleaved architecture similar to the hard disk, further multiplying storage capacity. Moreover, although VCSELs are not available commercially as yet, it is likely that VCSEL arrays (with integrated lenses), will not be expensive. This may enable parallel multi-access to adjacent tracks, boosting the data transfer rate. Additionally, multiple independent and inexpensive optical heads may provide parallel access to remote tracks further improving the access time. Chapter five of this thesis will demonstrate an advantageous utilisation of a subtle VCSEL property in the detection of a pre-recorded magneto-optic pattern.

1.5 Conclusion

Semiconductor lasers are used in telecommunications and optical data storage amongst other applications. The edge-emitting architecture of traditional lasers is at present a barrier to their utilisation. Inefficient coupling to fibre, post-wafer level testing, demanding bulky lenses and one-dimensional limited arrays are all problems suffered by edge-emitters.

Vertical-cavity surface-emitting lasers are therefore designed to avoid such limitations providing, in addition, very short cavities, single longitudinal mode operation and potentially extremely low power consumption. Furthermore, their low polarisation selectivity may afford them a promising performance in polarisation logic and switching.

A brief review of magnetic and optical data storage technology is given, demonstrating that performance is undermined, to some extent, by the bulk and mobility of the optical read/write head. It is envisaged that VCSELs may alleviate this constraint especially with regards to magneto-optic storage.

1.6 References

[1] G.P.Agrawal, N.K.Dutta: *Semiconductor lasers* Van Nostrand Reinhold 1993

[2] M.C.Nowell, L.M.Zhang, J.E.Carroll, M.J.Fice: *Chirp reduction using push-pull modulation of three-contact lasers* Phot. Tech. Lett. **5** (12) 1993

[3] P.S.Griffin, I.H.White, J.E.A.Whiteaway: *Low linewidth enhancement factor for InGaAsP and InGaAlAs multiple quantum well lasers* Opt. and Quant. Elect. **23** 1991, pp.1031-1035

[4] H.C.Casey Jr., M.B.Panish: *Heterostructure lasers* Academic Press 1978

[5] Z.L.Liau, J.N.Walpole: *Surface emitting GaInAsP/InP laser with low threshold current and high efficiency* Appl. Phys. Lett. **46** (2) 1985

[6] N.W.Carlson, G.A.Evans, D.P.Bour, S.K.Liew: *Demonstration of a grating-surface-emitting diode laser with low threshold current density* Appl. Phys. Lett. **56** (1) 1990

[7] H.Soda, K.Iga, C.Kitahara, Y.Suematsu: *GaInAsP/InP surface emitting injection laser* Jap. J. Appl. Phys. **18** (12) 1979

[8] D.I.Babic, I.H.Tan, R.P.Mirin, J.E.Bowers, E.L.Hu: *Wafer fusion for optical communnication applications* CWB7 proccedings CLEO'95 Maryland, USA

[9] K.H.Hahn, M.R.Tan, S.Y.Wang: *Intensity noise of large area vertical cavity surface emitting lasers in multimode optical fibre links* Elect. Lett. **30** (2) 1994

[10] U.Fiedler, M.MIkulla, E.Zeeb, C.Jung, K.J.Ebling: *Hybrid integrated VCSEL-fibre module for efficient mode-locking* SL7.3 proceedings LEOS'94 Massachusetts, USA

[11] M.Orenstein, E.Kapon, J.P.Harbison, L.T.Florez, N.G.Stoffel: *Large two-dimensional arrays of phase-locked vertical cavity surface-emitting lasers* Appl. Phys. Lett. **60** (13) 1992

[12] D.L.Mathine, H.Fathollahnejad, R.Droopard, S.Daryanani, G.N.Maracas: *InGaAs quantum well vertical-cavity surface-emitting lasers integration onto silicon substrates* SL7.2 proceedings LEOS'94 Massachusetts, USA

[13] J.K.Tu, J.J.Talghader, M.A.Hadley, J.S.Smith: *Vertical-cavity surface-emitting lasers integrated onto Si by fluidic self-assembly* CPD1-1 proceedings CLEO'94 Maryland, USA

[14] A.Khan, K.Woodbridge, C.Roberts, G.Parry: *Modulation, chirp, and tunability properties of vertical cavity surface emitting lasers integrated with quantum-well modulators* CTuK18 proceedings CLEO/Europe'94 Amsterdam, The Netherlands

[15] W.K.Chan, J.P.Harbison, A.C.Von Lehmen, L.T.Florez, S.A.Schwarz: *Optically controlled surface-emitting lasers* Appl. Phys. Lett. **58** (21) 1991

[16] D.L.Huffaker, W.D.Lee, D.G.Deppe, C.Lei, T.L.Rogers, J.C.Campbell, B.G.Streetman: *Optical memory using a vertical-cavity surface-emitting laser* Phot. Tech. Lett. **3** (12) 1991

[17] W.H.Loh, C.L.Tang: *Numerical investigation of ultrahigh frequency polarization self-modulation in semiconductor lasers* J. Quant. Elect. **27** (3) 1991

[18] J.M.Senior: *Optical fibre communications, principles and practice* Prentice Hall international series in optoelectronics 1992 pp. 672-674

[19] J.B.Georges, D.M.Cutrer, M.H.Kiang, K.Y.Lau: *Multichannel millimeter wave subcarrier transmission by resonant modulation of monolithic semiconductor lasers* Phot. Tech. Lett. **7** (4) 1995

[20] H.Ogawa, D.Polifko: *Millimeter-wave fibre optics systems for personal radio communication* Trans. Micro. Theory Tech. **40** (12) 1992

[21] H.Jung, O.K.Tongus: *SCM optical fibre backbone network for microcellular communications: optimum network design considerations* ON4.3 proceedings LEOS'94 Massachusetts, USA

[22] J.O'Reilly, P.Lane: *Remote delivery of video services using mm waves and optics* J. Light. Tech. **12** (2) 1994

[23] F.Devaux, S.Chelles, A.Ougazzaden, A.Mircea, M.Carré, F.Huet, A.Carenco, Y.Sorel, J.F.Kerdiles, M.Henry: *Full polarisation insensitivity of a 20 Gb/s strained-MQW electroabsorption modulator* Phot. Tech. Lett. **6** (10) 1994

[24] C.D.Mee, E.D.Daniel: *Magnetic recording* Volume II: *Computer data storage* McGraw-Hill Book Company 1987

[25] R.Gerber, C.D.Wright, G.Asti: *Applied Magnetism* Kluwer Academic Publishers 1994

[26] Keith Howard: *Inside CD* Special issue with *What home entertainment* November 1994

[27] L.Purcell: *Super CD-ROM* Sams publications 1995

[28] Edited by L.Baert, L.Theunissen, G.Vergult, J.Arts: *Digital audio and compact disk technology* Sony service centre, Focal Press 1995

[29] Y.Miyauchi, M.Terao, K.Andoo, R.Tamura, N.Ohto: *Analysis of reproduced waveform in phase-change single-beam overwrite* 27B-4 proceedings ISOM Kobe, Japan 1979

[30] C.N.Afonso, J.Solois, M.C.Morilla, M.A.Ollacarizqueta: *Ultrafast erasable optical storage in Sb-rich GeSb films* CThI86 proceedings CLEO/Europe'94 Amsterdam, The Netherlands

[31] *Optical data storage* Technical specification published by Panasonic

[32] *Tosoh magneto optical disk cartridge* Technical report published by TOSOH

[33] E.Hecht: *Optics* Addison-Wesley publishing company 1987, pp.318-319

[34] M.H.Kryder: *Magneto-optic recording technology* J. Appl. Phys. **57** (1) 1985

[35] M.H.Kryder: *Operating pronciples of laser pickup for optical storage and retrieval* Scientific American 1987

[36] S.Baxter: *Real world, seeing is believing* Computer Shopper October 1994 page 417

[37] S.Ura, T.Suhara, H.Nishihara, J.Koyama: *An integrated-optic disk pickup device* J. Light. Tech. **4** (7) 1986

[38] S.Ura, H.Sunagawa, T.Suhara, H.Nishihara: *Focussing grating couplers for polarisation detection* J. Light. Tech. 6 (6) 1988

CHAPTER

2

The design and operation of a VCSEL

This chapter aims to give a general exposure to VCSELs and an understanding of their operation with particular attention to their optical polarisation behaviour. The chapter begins with an explanation of the heterostructure, the quantum well and carrier recombination mechanisms common to both edge-emitters and VCSELs. The design of a vertical cavity is introduced and the alternative transverse guiding structures are presented. Progress in achieving emission at different wavelengths by fabricating suitable material structures is also outlined. Subsequently, the operation of a typical VCSEL device is characterised and developments in 2-D arrays and microcavity devices are briefly reviewed. In conclusion, the prospects of the 3-D integration of VCSELs are considered.

A general introduction to both edge-emitting lasers and vertical-cavity surface-emitting lasers (VCSELs) has been given in the introduction chapter. Below is a description of the physical principles underlying the operation of a laser followed by a brief account of VCSEL technology.

2.1 The double-heterostructure and the quantum well

A modern semiconductor laser is based on the double-heterostructure [1] construction. An example of an undoped active layer double-heterostructure is illustrated in figure 2.1. It consists of a thin semiconductor layer sandwiched between two layers of wider band-gap materials. The n-type doped substrate is rich in electrons while the p-type doped grown layers are rich in holes. Under no applied field, carriers are diffused into the potential well and recombine in the active layer until their depletion induces an electric field that compensates for further diffusion and halts their spontaneous recombination. This field may be viewed as an equaliser of the otherwise different Fermi energy levels of the materials and as a barrier to carrier flow, as illustrated in figure 2.2a. Applying a forward voltage to the layered structure, however, displaces the Fermi levels correspondingly (figure 2.2b) and diminishes the carrier depletion region. When the applied voltage reaches the active layer band-gap voltage, the potential barrier is overcome, forward current begins to flow and the diode reaches threshold.

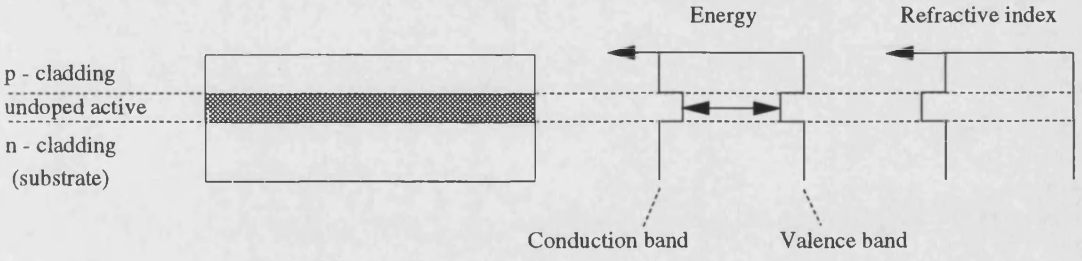

Figure 2.1: An example of the double-heterostructure, its band energy and index profile. The energy well confines charge carriers in the active layer and the index step confines a laterally propagating mode in an edge-emitting laser

This process of carrier recombination takes place in the active region and is partly optically radiative, therefore making stimulated emission feasible. The heterostructure layers are chosen so that the active layer acts as a potential well, i.e. a trap, for electrons

and holes alike. The active layer is selected with higher refractive index than the cladding layers, thereby providing optical guiding for a laser mode propagating along the layer and effecting an edge-emitting laser operation. This design is found to reduce recombination outside the active region in which the optical mode is confined. Thus the injection current required to achieve laser threshold is dramatically reduced.

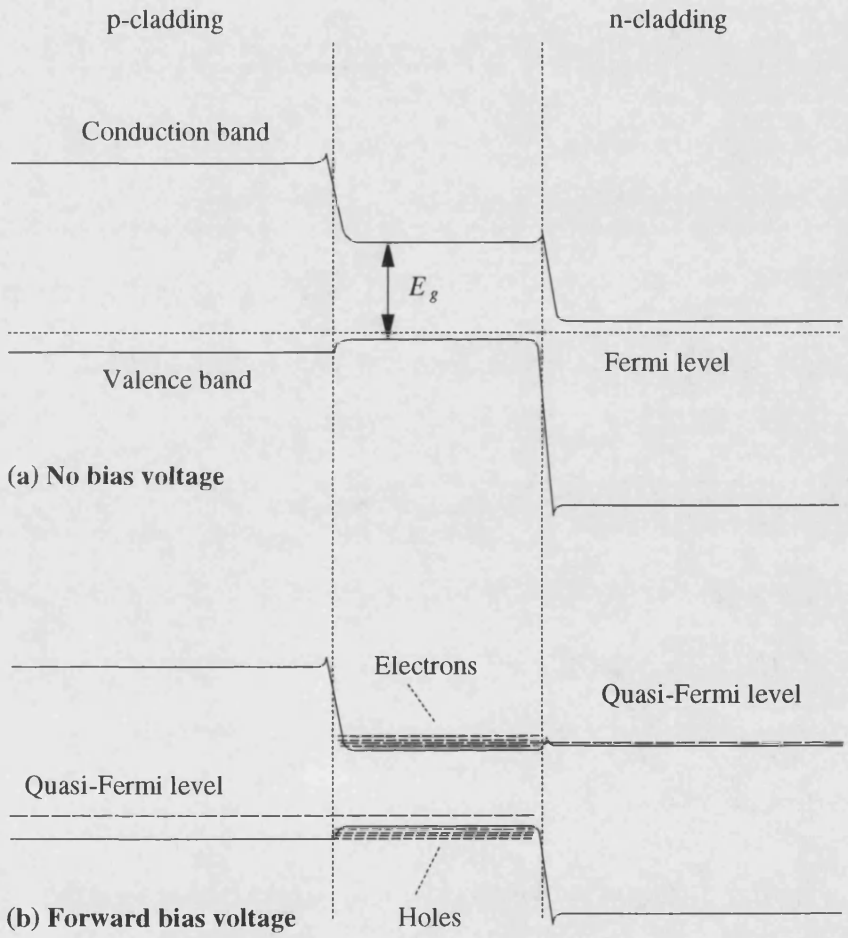

Figure 2.2: The Fermi level and energy-band across a double-heterostructure under (a) no external influence and (b) under forward voltage bias causing carrier recombination in the active layer

At this point it is useful to consider the carrier population statistics exemplified by the energy-wave vector diagram in figure 2.3 of a simplified band structure model. This is calculated from the quantum mechanical relation of a particle's energy to its momentum:

$$E = \frac{\hbar^2 k^2}{2m} \qquad \ldots\ldots \quad (2.1)$$

where the different effective masses of an electron, a heavy hole and a light hole, cause the difference in curvatures of the three parabolic bands. Since these particles are fermions, they are subject to the Fermi-Dirac statistics, generally expressed as:

$$f(E) = \frac{1}{1 + \exp[(E - E_f)/k_B T]} \qquad \ldots\ldots \quad (2.2)$$

where f is the occupation probability of a particle energy E in a band of a quasi-Fermi energy level E_f (E_{fc} for conduction electrons and E_{fv} for valence holes), while k_B is the Boltzmann constant and T the absolute temperature. The energy gap between the conduction band and the valence bands is E_g. Hence an electron-hole transition emits a photon of energy $E = h\nu$ roughly equal to $E_{fc} + E_{fv} + E_g$ carrying negligible momentum. As electrical pumping is increased, it leads to more band filling and the maximum emitted photon energy increases. This causes broadening of the gain spectrum and a shift of its peak towards shorter wavelength.

As the active layer is made thinner (~ 10nm), the potential well exhibits quantum effects, trapping the carriers and restricting their movements in the direction normal to the layers. This introduces a quantisation of the energy levels within the energy-bands perpendicular to the layers while preserving the general parabolic shape of the *bulk* (non-quantum) energy-bands parallel to the layers. Additionally, quantum effects on the carriers are observed in the absorption, emission and carrier transport characteristics of the quantum well (QW). It is also practical to grow several quantum wells one on top of another separated by barriers of a slightly wider band-gap material. This multi-quantum-well (MQW) structure accordingly enhances the average optical intensity in gain region of an edge-emitting laser.

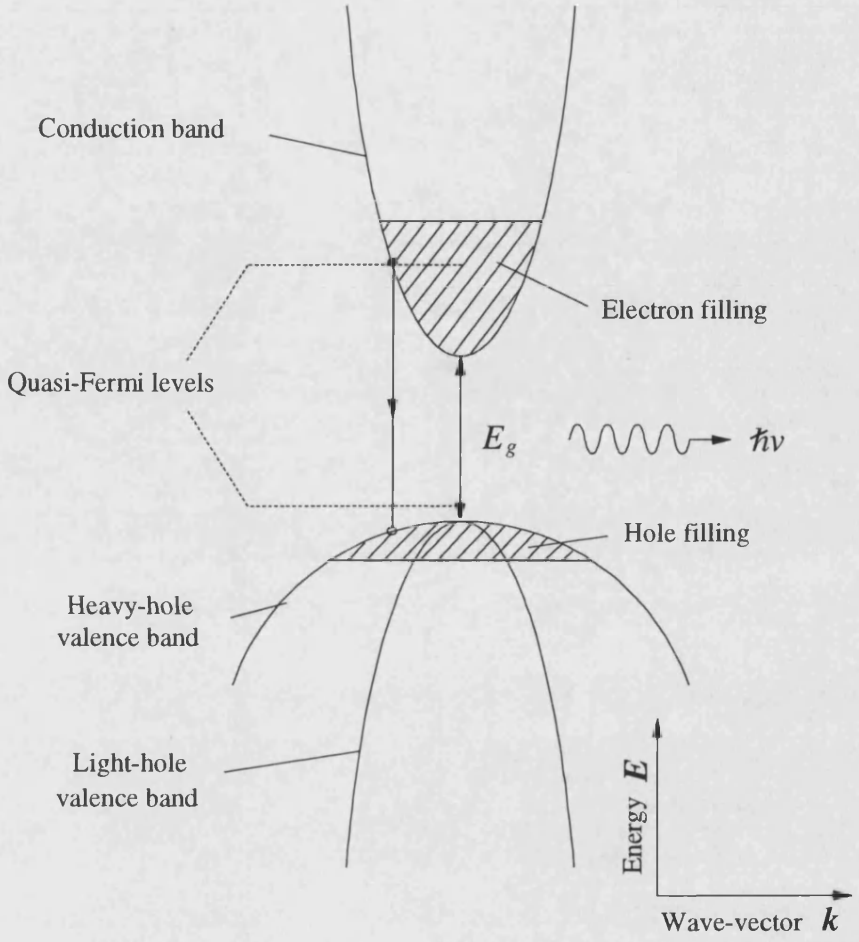

Figure 2.3: Diagram of energy versus wave-vector of the electrons, light and heavy holes, forming the conduction and valence bands, and illustrating a radiative transition

2.2 Carrier recombination and optical gain

As carriers are injected across the heterostructure, they accumulate in their respective energy bands awaiting spontaneous recombination. This occurs for many reasons [1] including recombination at defects, at surfaces and by the Auger process. Auger recombination involves at least three charge carriers and produces thermal or optical phonons and its rate is theoretically representable by $R_a = C N^3$. The Auger rate decreases rapidly at low temperatures and for wide band-gap materials because of the improbability of electron-hole pair interactions across the energy gap.

Lattice defects in the active layers produce a continuum of carrier states in a localised region where carriers may recombine non-radiatively within some diffusion length. A similar process occurs at the interfaces of the quantum well and barrier layers where lattice mismatch causes defects. Non-radiative defect and surface recombination occurs at a rate expressed as $R_d = A\,N$. The proportionality constant is dependent on the laser materials and structure and is expectedly significant for VCSELs with surfaces exposed to air.

Spontaneous recombination may also fruitfully radiate a photon which carries the energy lost by the electron-hole pair. This process is proportional to the densities of both types of carriers and hence is represented by $R_s = B\,N^2$ where B is the spontaneous emission constant. Conversely a photon of energy larger than that of the band-gap, passing through the active medium in thermal equilibrium, may be absorbed creating an electron-hole pair. This process appears as material absorption and is often used to excite the medium, i.e. to optically pump the carriers.

In principle, a photon may also stimulate the recombination of an electron-hole pair and the emission of an identical photon. This is the phenomenon of stimulated emission expressed by Einstein in 1917. The probability of stimulating such an emission grows in proportion to the populations of the conduction and valence bands (i.e. the density of excited carriers). The material absorption and stimulated emission are together representable as a gain per unit length $g = a\,(N - N_o)$, where a is the differential gain constant and N_o is the transparency carrier density. The latter is the carrier density at which the rate of photon absorption by the material is balanced by the rate of stimulated emission. The gain per unit time G is obtained by simply multiplying g by the optical group velocity.

In general, lasing action is seeded by spontaneous emission which radiates incoherent photons in random directions and within an optical spectrum determined by the energy bands and their filling. However, only a fraction of spontaneous photons are valid for stimulated self-sustaining emission. They must be emitted appropriately to resonate in the optical cavity, in terms of direction (solid angle accepted by the cavity) and

wavelength (cavity modes). This fraction is defined as the spontaneous coupling coefficient β, and its value depends on the laser structure but is typically between 10^{-5} and 10^{-3}.

2.3 Optical polarisation and transverse modes

The direction of the dipole moment of a radiative electron-hole recombination determines the polarisation of the radiation. If the wave-functions of a heavy-hole and a light-hole are resolved into axial components, then they are representable as [2]:

$$\Psi_{HH} = \frac{1}{\sqrt{2}}X + \frac{1}{\sqrt{2}}Y \quad \ldots\ldots \quad (2.3)$$

$$\Psi_{LH} = \frac{1}{\sqrt{6}}X + \frac{1}{\sqrt{6}}Y + \frac{2}{\sqrt{6}}Z \quad \ldots\ldots \quad (2.4)$$

where X and Y are wave-functions in the directions of orthogonal lattice axes in the (001) lattice plane, and Z is the <001> axis normal to that plane [3]. These equations demonstrate that TE polarisation is radiated by heavy-holes and light-holes while TM polarisation is radiated only by light-hole recombination with electrons. It is also noticeable that half of all light-hole radiation is TM polarised. In a bulk active layer the normalised sum yields equal emission probabilities into all three polarisation axes (X, Y and Z). Hence in a bulk edge-emitting laser TE and TM polarisations encounter identical gain coefficients. However, the active layer is vertically thin (~ 0.1 μm) and laterally comparatively wide (~ 3μm), forming a highly rectangular waveguide cross-section. This is designed to lead to a decidedly fundamental transverse mode operation in the vertical direction and to a strong preference to the fundamental transverse mode in the horizontal direction. It is also observed experimentally, and may be shown theoretically, that the preferred optical polarisation aligns the electric field parallel to the junction plan (TE). Some operating conditions though, may saturate the fundamental TE mode and encourage the fundamental TM mode or even the first order TE mode.

If the fundamental TE and TM modes coexist, then their lateral and vertical profiles are different. Therefore they are confined to different extents in the waveguide and experience different average (effective) refractive indices. As well as inducing wavelength splitting (birefringence), this waveguide (cavity) anisotropy results in

different refractive index discontinuities at the facets and thus leads to different reflectivities. Therefore TM polarised modes have higher thresholds than the equivalent TE polarised modes. All the while, the longitudinal mode order is determined by the effective optical length of the laser stripe that forms the Fabry-Perot cavity.

Replacing the bulk active layer with a quantum well construction serves only to reinforce the TE preference of the edge-emitting laser. Under no mechanical distortion, the gain material exhibits an electron to heavy-hole energy band-gap identical to the electron to light-hole band-gap. However, distorting the active layer lattice has dramatic consequences. The greater the dissimilarity between the lattice constants of two adjacent layers are (e.g. quantum wells and barriers), the greater is the lattice constant mismatch between them. The mechanical strain mutually exerted on both layers deforms their lattices. This distorts the band energies [2] of the heavy-hole and the light-hole in the quantum well differentially, see figure 2.4.

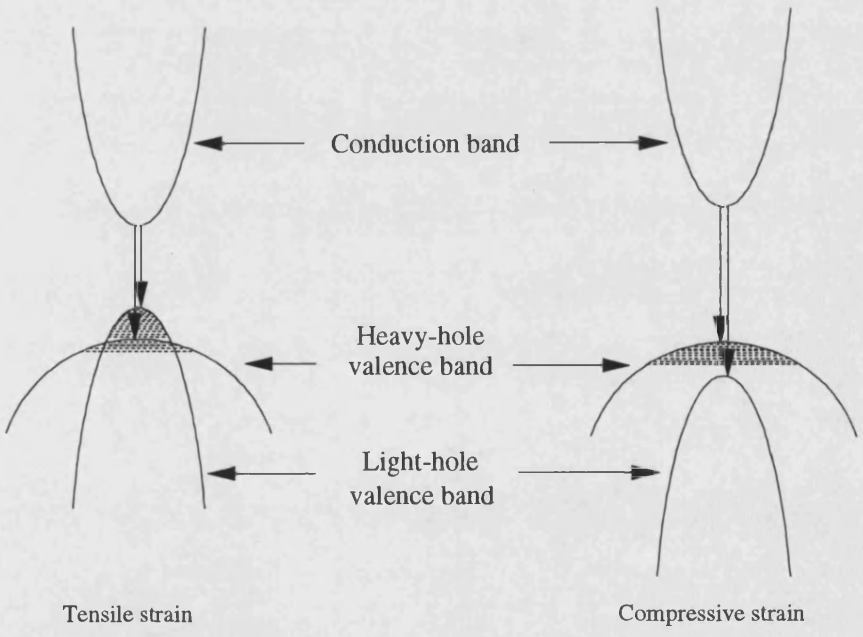

Figure 2.4: The effect of strain on the energy bands of the quantum well: (a) tension sustains light-holes and promotes TM emission while (b) compression favours heavy-holes which do not contribute to TM emission

It is found that tensile strain the junction plane reduces the mean band-gap, and more so the electron to light-hole band-gap. When carriers are injected therefore, they begin to fill the light-hole band first which provides better gain for TM than for TE modes thus counteracting the waveguide preference. Conversely, compressive strain in the junction plane increases the mean band-gap energy, and more so the electron to heavy-hole band-gap. This results in heavy-hole band filling first and almost eliminates TM gain altogether.

For a vertical cavity laser the optical mode polarisation aligns the electric field vector in any orientation in the junction plane, i.e. TE polarisation. Hence whether a bulk or a quantum well construction is utilised, there are no contributions to the lasing mode from TM polarised radiation. Ideally then, the gain is isotropic, and polarised transverse modes are selected by the cavity cross-section. In theory then, a circularly symmetric VCSEL should exhibit no polarisation selectivity. A slight departure from circular symmetry in the aperture, however, induces cavity anisotropy and birefringence.

2.4 The DBR stacks and the vertical cavity

The multilayer mirrors are grown of alternate layers of high and low refractive index each optically a quarter of a wave thick ($\lambda/4$). The index discontinuities at the interfaces cause backward reflections that interfere constructively. It can be shown from coupled-mode theory [4,5] that the maximum amplitude reflectivity of such a DBR mirror is:

$$|r_{DBR}|_{max} = \frac{(1-b)}{(1+b)} \qquad \ldots\ldots \quad (2.5)$$

where $b = (\mu_l / \mu_h)^{j+1}$ and j is the total number of layers. When $b \sim 0.1\%$, the intensity reflectivity approximates to $R_{DBR} \sim 1 - 4b$ and is limited ultimately by the optical scattering at the lattice interfaces. For a GaAs VCSEL operating around 980nm, the DBR stack is composed of AlAs/GaAs with a refractive index ratio [6] of ($\mu_l / \mu_h = 3.0 / 3.5$); 20 such layer pairs yield an intensity reflectivity of ~ 99.2%.

A bottom DBR stack of a bottom-emitting VCSEL often consists of 19.5 layer pairs while the top mirror often incorporates 24-30 layer pairs for a reflectivity near 99.8%.

The process of depositing these layers is laborious and complicates the fabrication, however, adding a metallic layer (silver or gold) to the top mirror inflates the reflectivity to 99.8% without further complications.

A typical DBR mirror reflectivity spectrum is illustrated in figure 2.5 revealing a broad and nearly square maximum. It is shown from coupled cavity theory [4,5] that the width of the reflection bandwidth is proportional to the index step of the alternate layers. The full-width half-maximum (FWHM) wavelength bandwidth of the amplitude reflectivity $\Delta\lambda$ is related not to the number of layers but to the refractive index step $\Delta\mu = \mu_h - \mu_l$ by:

$$\frac{\Delta\lambda}{\lambda} = \frac{2}{\pi}\frac{\Delta\mu}{\bar{\mu}} \qquad \ldots\ldots \quad (2.6)$$

This is of great importance when selecting the mirror materials as discussed in the following section. The square shape (sharpness of edges), on the other hand, is a function of the number of layer pairs.

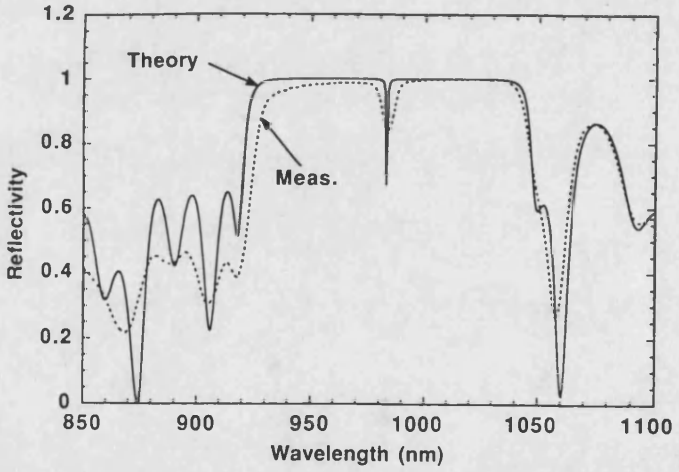

Figure 2.5: Experimental and theoretical intensity reflectivity spectrum of an unbiassed VCSEL. Note the dip at the cavity resonance wavelength, after [7]

The designed longitudinal cavity is often half a wavelength long with either a bulk active layer (figure 2.6a), a single quantum well (SQW) or multiple quantum wells (MQW) (figure 2.6b). Because of the higher average electric field for optimised SQW or MQW gain regions they are more efficient than a bulk gain region design. In a periodic gain

structure [8], the cavity is an integer number of half-wavelengths long (figure 2.6c). A quantum well is positioned at each peak of the standing wave maximizing the overlap of gain and optical field, and improving the conversion efficiency.

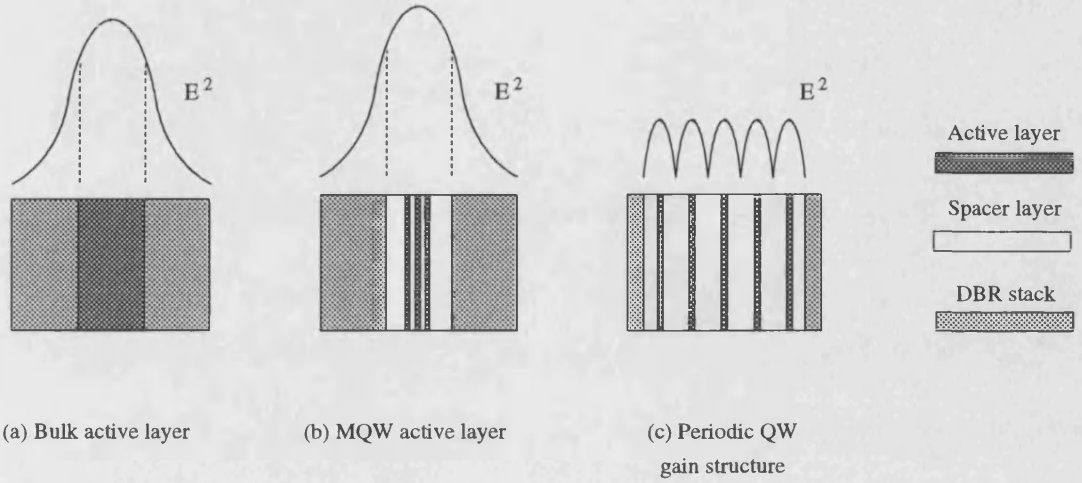

Figure 2.6: VCSEL longitudinal cavity design: (a) half-wavelength long with bulk active layer, (b) multi-quantum-well active layer, and (c) periodic gain structure

2.5 Semiconductor materials

The prime factor in chosing and developing semiconductor laser materials is the required wavelength of operation, which corresponds to the photon energy E_g. The first double-heterostructure edge-emitting lasers were based on AlGaAs/GaAs material systems [1], therefore providing gain in the wavelength range 0.7-0.9μm. Addressing optical fibre telecommunication requirements, however, new materials have been developed to exploit the low loss windows in the transmission spectrum of glass optical fibre at 1.3μm and 1.5μm [1]. By adjusting the mole fractions of $In_{1-x}Ga_xAs_yP_{1-y}$ layers on InP substrates, operation is achieved in the range 1.1-1.6μm.

The construction of a VCSEL is somewhat more intricate, though, necessitating DBR materials that match the lattice of the active medium and of low absorption at the operating wavelength. In addition, if the ohmic resistance of the DBR layer interfaces is high, the heat generated causes a shift in the operating wavelength, perhaps beyond the DBR reflectivity bandwidth. Operation around 980nm is obtained from InGaAs/GaAs active regions and AlAs/GaAs DBR stacks. VCSELs that operate around 850nm are fabricated

from GaAlAs/GaAs active regions and DBR stacks of similar materials but different aluminium mole fraction. Recently a 3-pair DBR stack with wide bandwidth (830-1370nm) was obtained using the high index step of GaAs and AlAs oxide ($\mu = 1.55$) allowing a threshold current of 0.33mA [9].

It has proven more difficult to fabricate VCSELs of InP based materials because of the resulting small index steps ($\Delta\mu \sim 0.3$) obtained from different InGaAsP compositions. This necessitates 40 layer pairs for a DBR to reach a suitable reflectivity, which has a small reflectivity bandwidth. This becomes a problem when the wavelength inevitably drifts due to Joule heating. Instead, DBR stacks are fabricated from high-low index dielectric materials [1] such as SiO_2-TiO_2 or Si-SiO_2. Alternatively the mirrors may be fabricated of AlAs/GaAs and fused to the InP active region [10]. Using such fabrication techniques, ~ 1.5μm wavelength VCSELs have recently been successfully operated at room temperature [11].

On the other hand, lasers operating in the visible spectrum (400-700nm) are of great interest for many applications including visible displays, molecular microscopy, laser printing and optical data storage. Visible edge-emitting lasers have utilised InGaAlP [1] for red emission (600-700nm) at room temperature and green (555nm) at low temperature. Currently, research is being carried out to develop other materials for blue-green emission. Operation at 496nm [12] and at 463nm [13] with CdZnSe/ZnSe at room temperature is obtained, even though with a short lifetime.

Similarly, red light VCSELs have also been realised [14] using AlGaInP gain materials and visible bandwidth DBR stacks, mostly consisting of 35-pairs of AlGaAs/AlAs ($\mu \sim 3.3/3.0$) and reflecting ~ 99% over the range of 625-675nm. Recently, though, it was uncovered [15] that a mere 4.5 pair DBR of thermally oxidised AlAs ($\mu \sim 1.55$) in conjunction with $Al_{.5}In_{.5}P$ yields a similar reflectivity over the much wider range of 635-967nm. Replacing the $Al_{.5}In_{.5}P$ with $Ga_{.5}In_{.5}P$, it is found that the reflection band shifts to 470-676nm.

2.6 Surface area and electrical injection

The area of a VCSEL is defined by one of two methods: index-guiding and gain-guiding, both illustrated in figure 2.7. Index-guiding is easily achieved by etching the grown layers down to the substrate or to the bottom mirror in an air-post structure [7]. This serves to confine the optical mode in the transverse dimension by the surrounding lower refractive index, much as in an optical fibre.

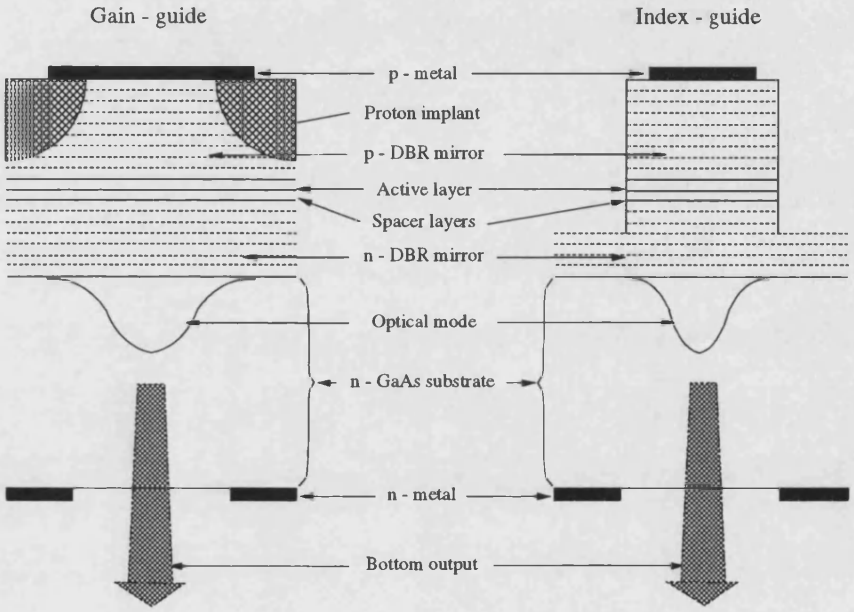

Figure 2.7: Guiding structures in VCSELs: (left) proton-implant leads to current funnelling and gain-guiding, (right) etched air-post provides index-guiding

Gain-guiding, on the other hand, is a process of guiding and funnelling the injected current so that the optical gain is localised laterally. This is accomplished by proton implantation [16] (high energy H^+ bombardment) into the DBR stack. Implanted protons immobilise the otherwise available carriers, creating a high resistivity boundary to the desired VCSEL surface. Unlike index-guided operation, gain-guiding does not define the gain area rigidly but is dependent on current spreading. The depth of the proton implant is also found to govern the leakage current and the average voltage across the p-n junction [17].

2.7 Optical losses and carrier effects

Photon interactions with the laser materials go beyond the absorption pointed out above. Photons are also absorbed by conduction band electrons that become free carriers, and photon scattering occurs at the interfaces of different material lattices. High current injection densities into VCSELs often lead to such high carrier density and thermal distribution profiles that the refractive index of the active medium is notably affected. It is the fundamental interactions of waves with matter that underlie these phenomena. The details of this interaction are beyond our scope, however, it is noted that an increase in the carrier density in the laser is accompanied by a fall in the refractive index [18] as well as a rise in gain. It is also noted from equation (2.2) that a higher junction temperature broadens the energy distribution of the carriers. Consequently, a rise in the junction temperature attenuates the gain and inflates the refractive index [18] while, conversely, an increase in the carrier density improves the gain and reduces the refractive index.

Because of the approximately parabolic carrier density profile [19,20] across a VCSEL, an index anti-guiding effect is experienced by an optical mode. In index-guided VCSELs, this is an effect that increases the threshold current. On the other hand, the heat generated in the DBR stacks usually results in a near-parabolic thermal profile [21]. The effect on the refractive index is that of guiding and is termed thermal lensing [22] which is conducive to lasing action near threshold. At higher injection currents though, thermal lensing restricts the mode laterally to the central gain region intensifying the stimulated emission there. Therefore, near the centre, carriers are depleted at a higher rate than near the perimeter causing the appearance of a *hole* in the spatial carrier profile [22], a process termed spatial hole-burning. The overall gain experienced by the mode is somewhat attenuated and the gain is compressed (self-saturated) [23] assisting the appearance of higher order modes. By the same token, when two or more modes overlap spatially, they attenuate each other's gain leading to gain suppression (cross-saturation) [23].

Another process that contributes to gain saturation is spectral hole-burning [1]. The shape of the gain spectrum is a reflection of the carrier recombination energy probabilities and is determined by the band-gap and the band filling. If carrier-pairs that contribute to emission at a particular wavelength are strongly stimulated to recombine, their supply

may not match their recombination and then leads to their depletion. This creates a *hole* in the gain spectrum [23] and saturates the gain only of that particular wavelength and a small bandwidth around it. The severity of this process depends material parameters, mainly the intra-band carrier relaxation time.

2.8 The output characteristics of VCSELs

The output power of an ideal laser below threshold is only the small sum of spontaneous emissions, but it is much larger and linear in relation to the injected current above threshold. The slope of this light-current (L-I) line is the external (differential) quantum efficiency η_e which naturally depends on the output mirror reflectivity. Therefore another parameter used to gauge the operation of a laser is the internal quantum efficiency η_i defined as the fraction of injected carriers converted to photons.

With the extraordinary reduction of VCSEL threshold currents [24], performance is often measured as the total power conversion efficiency, also termed wall-plug efficiency. This is defined as the ratio of optical output power to electrical input power. The best reported wall-plug efficiency for continuous-wave (cw) operation (dc drive) at room temperature is 50% [25] accompanied by a threshold of 9μA.

In practice, though, the efficiency of a VCSEL usually drops with increasing current. This is partly caused by gain saturation of the operating mode, and severe saturation may allow another longitudinal or transverse mode to dominate. Single-moded VCSELs often exhibit a roll-over in the L-I curve [26], see figure 2.8a, caused mainly by large changes in device temperature and hence in the longitudinal cavity optical length. This is followed by a shift in operating wavelength and a departure from optimum overlap between the optical mode and the gain region. This problem becomes less severe with increasing device diameter [27], see figure 2.8b, because of smaller current leakage, and better power dissipation via a wider single optical mode or multiple transverse modes.

The sensitivity of VCSELs to temperature changes may be used to tune the operation wavelength. Continuous tunability of 96nm has been achieved in a top-emitting device by controlling its temperature up to 200°C [28]. The device was operated cw and had a centre wavelength of 850nm.

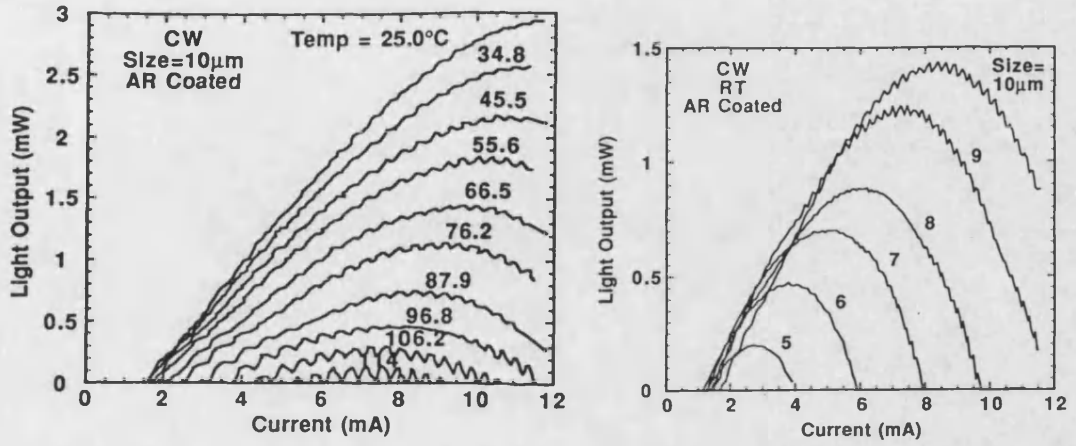

(a) (b)

Figure 2.8: Experimental VCSEL L-I curves: (a) of a 10μm device at a range of temperatures demonstrating the detrimental effect of heat on the device efficiency, and (b) of single-moded devices ranging in diameter from 5μm to 10μm, demonstrating an earlier roll-over for the smaller devices, after [7]

Except for periodic gain structured devices, a VCSEL operates in a single longitudinal mode owing to the short vertical cavity. However, similarly to an optical fibre, the transverse architecture of a VCSEL affords it a multi-transverse mode operation and unrestricted polarisation. Index-guided VCSELs have been defined with circular, elliptical, rhombus, dumb-bell and cross shaped apertures [29-31] for control of transverse modes and output polarisations. Circular air-post VCSELs have exhibited polarisation preference relative to a crystallographic axis. This is probably due to unintentional anisotropy introduced during the etching process [17].

Gain-guided VCSELs are usually defined with circular or square apertures, and sustain multi-moded operation more easily. This is because of their variable gain and refractive index profiles with injected current. If a VCSEL displays orthogonal polarisations simultaneously, in the presence of gain anisotropy or cavity anisotropy, the polarised modes experience a slightly different refractive index inducing spectral splitting [32].

The linewidth of a laser output is the spectral width of the lasing mode, and it may determine the laser's suitability for particular applications. Fundamentally, the linewidth is the inverse of the optical coherence time [33] of the laser emission. The latter may also be translated to the coherence length (quantum mechanically, the length of a photon packet) which is of great impact on interference effects.

In an experiment to measure coherence [34] under single-moded cw operation, a 15μm diameter VCSEL had a coherence time of 1.5ns (≡ 45cm) at best. An 8μm laser operating under similar conditions exhibited a maximum coherence time of 2.5ns (≡ 75cm). As each laser became multi-moded, the coherence collapsed to less than a millimetre because of mode-beating. Under single-mode pulsed operation, wavelength chirp due to thermal changes reduced the coherence time to a few centimetres normally, and to ~ 1mm at worst.

2.9 VCSEL arrays and microcavity devices

VCSELs arrays have been fabricated not only with identical devices but also with progressive wavelengths [35] such as the 7×20 VCSEL array with a wavelength separation of 3 Å. An 8×6 continuously tunable array of individually addressable devices has also been reported [36]. There are other examples of VCSEL arrays such as the matrix-addressed 10×10 pixel configuration [37] for optical displays. Another example is the 10×10 individually addressable array [38] capable of high speed (10GHz) signal modulation for optical interconnect applications. One of the main problems presented by closely packed 2-D VCSEL arrays is the thermal cross-talk [39] between adjacent devices. This is reported highly detrimental to the operation of phase-locked arrays and to the transverse mode and polarisation state of each laser. However, continuous reductions in threshold and improvement in conversion efficiency may eventually alleviate these thermal problems.

As half-wavelength cavity VCSELs are made with smaller diameters approaching a wavelength, a transition occurs to microcavity devices. They begin to show quantum effects that influence all aspects of their performance. In particular, a rise in the spontaneous emission coupling factor (β) has been measured experimentally [40] at ~ 0.1. The ultimate theoretically expected limit of this factor is unity [41] thereby

enhancing the internal quantum efficiency and approaching threshold-less operation. Despite the present technical problems with current injection, optically pumped microcavity laser arrays are considered potentially the ultimate laser light sources for photonics technology.

2.10 3-D integration

Because of their 2-D architecture, VCSELs are suitable for three-dimensional (3-D) stacking and integration whether achieved monolithically, or by fusing or bonding hybrid device layers. This applies to individual devices and to 2-D arrays of VCSELs and microcavities. New compatible devices and optical manipulation elements are constantly being developed for various purposes.

Parallel free-space optical interconnects as well as optical fibre links can be implemented with arrays of VCSEL but require optical elements for beam focussing and distribution. Therefore monolithic and hybrid arrays of microlenses have been engineered to complement the VCSELs. For example, a microlens array has been etched on the back of a bottom-emitting VCSEL array substrate [42] so that the output of each laser is focussed by a lens. The lenses ranged between 10μm and 200μm in diameter and were preset in focal length as required. A hybrid array of polyimide microlenses has similarly been integrated [43] with a VCSEL array and demonstrated suitable for multichip interconnection.

An alternative to refractive optics (utilising changes in refractive index) are diffractive optics (i.e. Fresnel elements). A Fresnel lens utilises diffraction from concentric circular apertures to cause constructive interference in a particular direction and thus to direct and focus a beam. An array of such lenses, also etched on the substrate, was fabricated [44] allowing on-axis focussing as well as 20° off-axis pre-determined beam control.

Top-emitting lasers have also had their share of lensed output design, most impressively the zone laser [45]. This includes a series of concentric zones etched on the topmost mirror layer. Each zone supports a lasing filament 180° out of phase with filaments the neighbouring zones. The overall effect is phase locking of the lasing supermode such

that the output interference is at a single point on the axis. This self-lensing was accurately designed to focus the supermode of the 120μm diameter VCSEL at an on-axis point 300μm above the surface achieving a diffraction limited beam waste of ~ 8μm. Further, it has been demonstrated that the focal length of a zone plate may be altered [46] by applying graduated voltages to successive contacts. The electric field is reported to change the refractive index between the contacts. Applying this idea to a VCSEL similar to the zone laser may be a way to realize variable focus VCSELs, advantageous for many applications.

Finally, and as an example of the versatility of the surface architecture, it is worth mentioning the vertical coupled-cavity micro-interferometer. This is a variable wavelength filter of ~ 2.5nm bandwidth centred on 920nm and tuneable over 32nm by the application of a voltage between 0V and 14V. It utilises an variable thickness air cavity between a GaAs gain region and a controllable suspended reflective membrane (Au/SiNH/GaAs) which replaces the output mirror [47].

2.11 Conclusion

An understanding of the physical principles that underlie the operation of a laser, and the processes that determine its behaviour, have been established in this chapter. Progress in many aspects of VCSEL technology is also outlined to convey the depth of interest in developing these devices. The main concern of this work subsequently will be the polarisation behaviour of VCSELs particularly under external feedback.

2.12 References

[1] G.P.Agrawal, N.K.Dutta: *Semiconductor lasers* Van Nostrad Reinhold 1993

[2] E.P.O'Reily: *Valence band engineering in strained-layer structures* Semicon. Sci. Tech. **4** 1989, pp. 121 - 137

[3] D.Vakhshoori: *Symmetry considerations in vertical-cavity surface-emitting lasers: Predictions of removal of polarisation isotropicity on (001) substrates* Appl. Phys. Lett. **65** (3) 1994

[4] A.Yariv: *Quantum electronics* John Wiley & Sons 1989

[5] L.A.Coldren, R.S.Geels, S.W.Corzine, J.W.Scott: *Efficient vertical-cavity lasers* Opt. Quant. Elect. special issue on microresonator devices **24** (2) 1992

[6] R.S.Geels, S.W.Corzine, L.A.Coldren: *InGaAs vertical-cavity surface-emitting lasers* J. Quant. Elect. **27** (6) 1991

[7] R.S.Geels, B.J.Thibeault, S.W.Corzine, J.W.Scott, L.A.Coldren: *Design and characterization of In_2Ga_8As MQW vertical-cavity surface-emitting lasers* J. Quant. Elect. **29** 12 1993

[8] S.W.Corzine, R.S.Geels, J.W.Scott, R.H.Yan, L.A.Coldren: *Design of Fabry-Perot surface-emitting lasers with a periodic gain structure* J. Quant. Elect. **25** (6) 1989

[9] M.H.MacDougal, P.D.Dupkus, V.Pudikov, H.Zhao, G.M.Yang: *Ultralow threshold current vertical-cavity surface-emitting lasers with AlAs oxide-GaAs distributed Bragg reflector* Phot. Lett. **7** (3) 1995

[10] D.I.Babic, I.H.Tan, R.P.Mirin, J.E.Bowers, E.L.Hu: *Wafer fusion for optical commumnication applications* CWB7 CLEO'95 Maryland, USA

[11] C.L.Chu, Z.H.Zhu, Y.H.Lo, R.Bhat, M.Hong: *Low-threshold 1.57μm VC-SEL's using strain-compensated quantum wells oxide/metal backmirror* Phot. Tech. Lett. **7** (5) 1995

[12] D.Herve, E.Molva, L.Vanzetti, L.Sorba, A.Franciosi: *Microgun-pumpued blue-green laser* CMH1 proceedings CLEO'95 Maryland, USA

[13] P.Kelkar, V.Kozlov, H.Jeon, A.V.Nurmikko, D.C.Grillo, J.Han, M.Ringle, R.L.Gunshor: *Blue ZnSe quantum well diode laser* CMH5 proceedings CLEO'95 Maryland, USA

[14] M.H.Crawford, R.P.Schneider Jr.: *Performance of high-efficiency AlGaInP-based red VCSELs* CWB1 CLEO'95 Maryland, USA

[15] M.H.MacDougal, S.G.Hummel, P.D.Dapkus, H.Zhao, Y.Cheng: *Epitaxial (Al,Ga)InP-oxide distributed Bragg reflectors for use in visible wavelength optical devices* IEEE Phot. Lett. **7** (4) 1995

[16] C.J.Chang-Hasnain, M.Orenstein, A.Von Lehmen, L.T.Florez, J.P.Harbison, N.G.Stofel: *Transverse mode characteristics of vertical cavity surface emitting laser* Appl. Phys. Lett. **57** (3) 1990

[17] C.J.Chang-Hasnain, J.P.Harbison, G.Hasnain, A.C.Von Lehmen: *Dynamic, polarization, and transverse mode characteristics of vertical cavity surface emitting lasers* J. Quant. Elect. **27** (6) 1991

[18] H.C.Casey Jr., M.B.Panish: *Heterostructure lasers* Academic Press 1978

[19] N.K.Dutta: *Analysis of current spreading, carrier diffusion, and transverse mode guiding in surface emitting lasers* J. Appl. Phys. **68** (5) 1990

[20] D.Vakhshoori, J.D.Wynn, G.J.Zydzik, R.E.Leibenguth, M.T.Asom, K.Kojima, R.A.Morgan: *Top surface emitting lasers with 1.9V threshold voltage and the effect of spatial hole burning on their transverse mode operation efficiency* Appl. Phys. Lett. **62** (13) 1993

[21] R.Michalzik, K.J.Ebeling: *Modelling and design of photon-implanted ultralow-threshold vertical-cavity laser devices* J. Quant. Elect. **29** (6) 1993

[22] G.C.Wilson, D.M.Kuchta, J.D.Walker, J.S.Smith: *Spatial hole-burning and self-focussing in vertical-cavity surface-emitting laser diodes* Appl. Phys. Lett. **64** (5) 1994

[23] G.P.Agrawal: *Gain nonlinearities in semiconductor lasers: Theory and application to distributed feedback lasers* J. Quant. Elect. **23** (6) 1987

[24] J.W.Scott, B.J.Thibeault, D.B.Young, L.A.Coldren, F.H.Peters: *High efficiency submilliamp vertical cavity lasers with intracavity contacts* Phot. Tech. Lett. **6** (6) 1994

[25] K.Lear, K.D.Choquette, R.P.Schneider Jr., S.P.Kilcoyne, K.M.Geib: *VCSELs with 50% power-conversion efficiency* CTuB2 CLEO'95 Mayland, USA

[26] J.W.Scott, R.S.Geels, S.W.Corzine, L.A.Coldren: *Modelling temperature effects and spatial hole burning to optimise vertical-cavity surface-emitting laser performance* J. Quant. Elect. **29** (5) 1993

[27] W.H.Loh, C.L.Tang: *Numerical investigation of ultrahigh frequency polarization self-modulation in semiconductor lasers* J. Quant. Elect. **27** (3) 1991

[28] R.A.Morgan, M.K.Hibbs-Brenner, T.M.Marta, R.A.Walterson, S.Bounnak, E.L.Kalweit, J.A.Lehman: *200°C, 96nm wavelength range, continuous-wave lasing from unbonded GaAs MOVPE-grown vertical cavity surface-emitting lasers* Phot. Tech. Lett. **7** (5) 1995

[29] K.D.Choquette, R.E.Leibenguth: *Control of vertical-cavity laser polarisation with anisotropic transverse cavity geometries* Phot. Tech. Lett **6** (1) 1994

[30] T.Mukaihara, F.Koyama, K.Iga: *Engineered polarisation control of GaAs/AlGaAs surface-emitting lasers by anisotropic stress from elliptical etched substrate hole* IEEE Phot. Tech. Lett. **5** (2) 1993

[31] Y.A.Wu, C.J.Chang-Hasnain, R.Nabiev: *Transverse mode selection with a passive antiguide region in vertical cavity surface emitting lasers* Phot. Tech. Lett. **6** (8) 1994

[32] A.K.Jansen van Doorn, M.P. van Exter, J.P.Woerdman: *Effects of transverse anisotropy on VCSEL spectra* Elec. Lett. **30** (23) 1994

[33] E.Hecht: *Optics* Addison-Wesley publishing company 1987, pp.318-319

[34] J.L.A.Chilla, B.Benware, M.E.Watson, P.Stanko, J.J.Rocca, C.Wilmsen, S.Feld, R.Leibenguth: *Coherence of VCSEL's for holographic interconnects* Phot. Tech. Lett. **7** (5) 1995

[35] C.J.Chang-Hasnain, J.P.Harbison, C.Zah, M.W.Maeda, L.T.Florez, N.G.Stoffel, T.Lee: *Multiple wavelength tunable surface emitting arrays* J. Quant. Elect. **27** (6) 1991

[36] L.Fan, M.C.Wu, H.C.Lee: *8 × 6 wavelngth-tunable vertical cavity surface-emitting arrays* SL5.3 LEOS'94 Massachusetts, USA

[37] R.A.Morgan, G.D.Guth, C.Zimmer, R.E.Leibenguth, M.W.Focht, J.M.Freund, K.G.Glogovsky, T.Mullally, F.F.Judd, M.T.Asom: *Two-dimensional matrix addressed vertical cavity top-surface emitting laser array display* Phot. Tech. Lett. **6** (8) 1994

[38] B.Möller, E.Zeeb, T.Hackbarth, K.J.Ebling: *High speed performance of 2-D vertical-cavity laser diode arrays* Phot. Tech. Lett. **6** (9) 1994

[39] W.Nakwaski, M.Osinski: *Thermal-cross-talk effects in closely packed two-dimensional arrays of vertical-cavity surface-emitting lasers* CWF1 CLEO'95 Maryland, USA

[40] I.Vurgaftman, J.Singh: *Static, dynamic and spectral characteristics of microcavity surface-emitting lasers* **SL6.4** LEOS'94 Massachusettes, USA

[41] G.Shtengel, H.Temkin, T.Uchida, M.Kim, P.Brusenbach, C.Parsons: *Spontaneous emission factor and its scaling in vertical cavity surface emitting lasers* Appl. Phys. Lett. **64** (9) 1994

[42] E.M.Strzelecka, G.D.Robinson, M.G.Peters, L.A.Coldren: *Integration of vertical-cavity laser diode with refractive microlenses* CWF14 CLEO'95 Maryland, USA

[43] O.Blum, S.P.Kilcoyne, M.E.Warren, T.C.Du, K.L.Lear, R.P.Schneider Jr., R.F.Carson, G.Robinson, F.H.Peters: *Vertical-cavity surface-emitting lasers with integrated refractive microlenses* Elect. Lett. **31** (1) 1995

[44] T.Du, M.E.Warren, J.R.Wendt, G.A.Vawter, S.P.Kilcoyne, K.L.Lear, R.P.Schneider, A.J.Howard, R.F.Carson, J.C.Zolper: *Directional beam control using on/off-axis high-efficiency diffractive optics integrated on substrate-emitting vertical-cavity lasers* CWF15 CLEO'95 Maryland, USA

[45] D.Vakhshoori, M.Hong, M.Asom, R.E.Leibenguth, J.P.Mannaerts, J.D.Wynn: *Zone lasers* Appl. Phys. Lett. **65** (2) 1994

[46] F.Castro, B.Nabet: *Continuous variation in Fresnel lens focal length* EO4.3 LEOS'94 Massachusetts, USA

[47] M.C.Larson, B.Pezeshki, J.S.Haris: *Vertical coupled-cavity micro-interferometer on GaAs with deformable-membrane top mirror* IEEE Phot. Lett. **7** (4) 1995

CHAPTER

3

Coupled cavity VCSEL model

This chapter describes a theoretical model of a VCSEL that explains the light-current measurements and far field observations of VCSEL #1. This device is also used in experiments described in chapter four to obtain cw and dynamic polarisation switching, and in chapter five to investigate the effects of polarised feedback on the bias voltage of the laser. The model will subsequently be used as a theoretical basis to account for polarisation switching and laser voltage dependence on polarised optical feedback.

This chapter begins with the device characteristics followed by explanations of events that occur in the laser in terms of phenomena like coupled cavity effects, thermal lensing, gain guiding and spatial hole burning. A theoretical rate equation model is formulated to include these effects and is solved numerically simulating the laser operation. Results from the model realistically predict and explain cw and dynamic polarisation switching experimentally achieved in later chapters. To our knowledge this is the first theoretical analysis of a VCSEL in a coupled cavity.

3.1 Device and characterisation

Although many details about this laser have not been made known to us on account of industrial confidentiality, deductions may be made from observing the behaviour of the laser and making specific measurements. VCSEL #1 is designed for emission through the bottom mirror and through the substrate which is antireflection (AR) coated. The active region is composed of three In_2Ga_8As/GaAs quantum wells 80 Å thick and the laser is designed for operation at the optical wavelength of 980nm. It has a 10μm diameter circular aperture defined by proton implantation.

The laser chip is mounted on an 10mm × 10mm brass submount with a compact SMA connector for passing electrical drive to the device. The DC electrical characteristics of this laser are represented by the V-I curve in figure 3.1 demonstrating a forward laser resistance of approximately 60 Ω at threshold. The light output is collected by a 6.5mm laser diode lens with a numerical aperture of 0.5 which is much larger than that of the laser (~ 0.07). The optical power is measured by an HP-81521B optical head attached to an HP-8153A optical power-meter which is calibrated for the operating wavelength.

The cw polarisation resolved light-current (L-I) characteristics are shown in figure 3.2 and the threshold current is determined at 15.7mA by direct measurement. The operation at 21mA is single-moded at a wavelength of ~ 956nm as illustrated by the output spectrum in figure 3.3. The laser is pulse driven at a duty cycle of 7% and the linewidth is limited by an experimental resolution of 0.5 Å. It can be seen from the L-I curve that the laser operation is highly optically polarised and that the polarisation axes are fixed in direction. Most of the optical power is observed almost consistently in the dominant polarisation, referred to hereafter as P_a, whilst the subdued polarisation is referred to as P_b and appears briefly near 28mA.

The physical processes responsible for the unusual features of the L-I will be explained during the course of this chapter. One distinctive feature of the L-I curve is the very sharp laser turn-on. At first this behaviour was presumed to signify optical bistability which would be marked by a hysteresis loop [1,2]. However, specific search for such a loop in the L-I curve under an expanded injection current scale revealed no hysteresis.

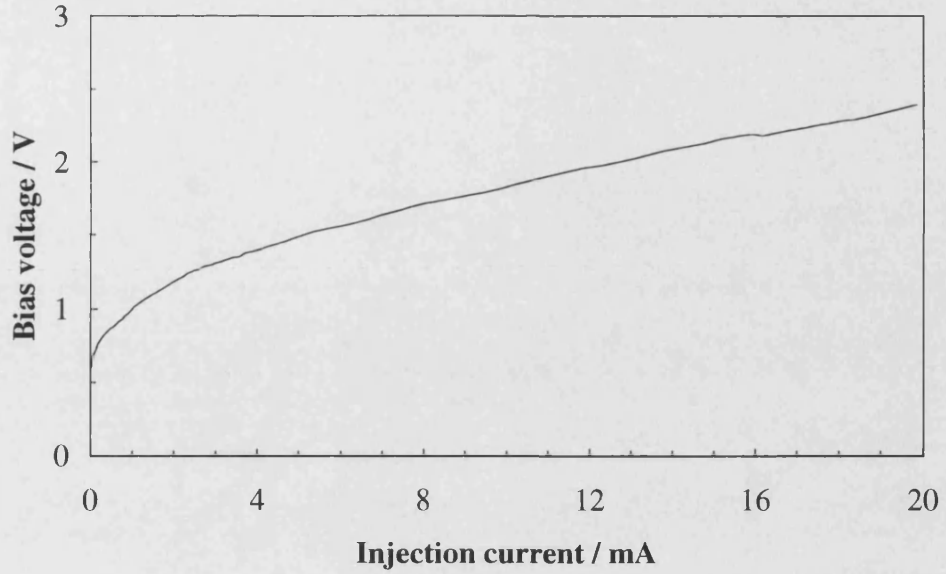

Figure 3.1: The voltage-current (V-I) characteristics of VCSEL #1

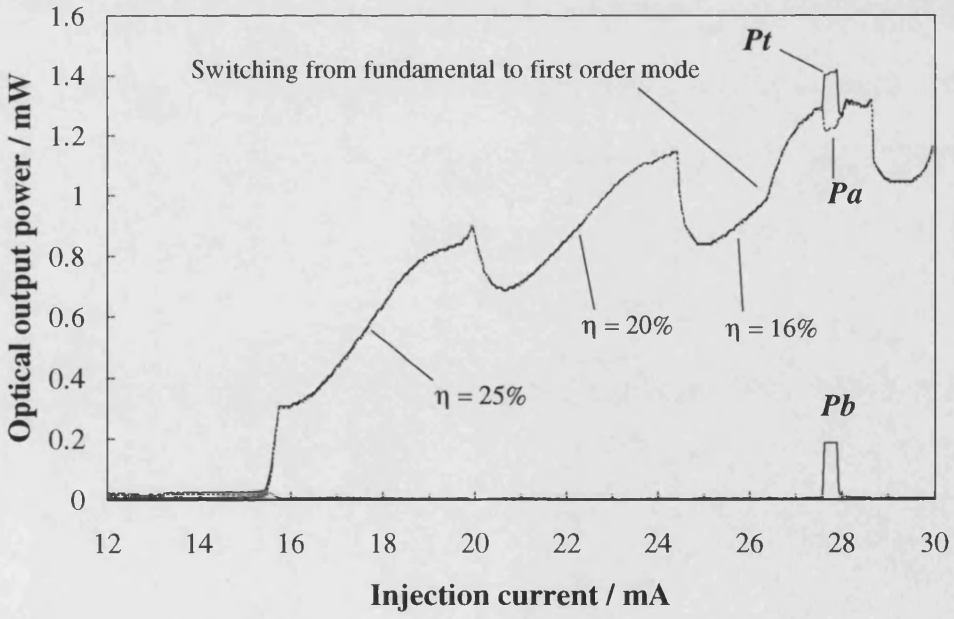

Figure 3.2: The light-current (L-I) characteristics of VCSEL #1

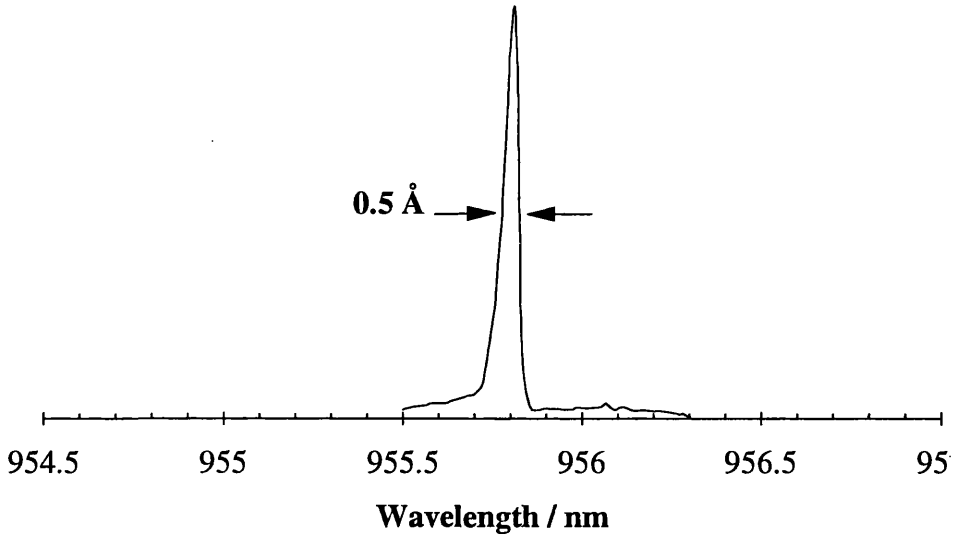

Figure 3.3: Laser output spectrum under 21mA current pulses and 7% duty cycle, illustrating FWHM of 0.5Å of spectral width as limited by equipment resolution

In addition, the laser may be operated so that the optical output power varies *continuously* along the steep curve and may be positioned anywhere on that part of the curve, unlike the sudden jump characteristic of bistability.

3.1.1 Coupled cavity effects

The deep kinks in the L-I curve illustrated in figure 3.2 result from residual reflections from the imperfect AR coating applied to the GaAs substrate as schematically illustrated in figure 3.4. The substrate interface forms a resonant cavity with the output DBR mirror of the laser which is then coupled to the laser cavity creating interference effects. The effective mirror reflectivity is therefore wavelength dependent and oscillates periodically as the laser output wavelength drifts causing a modulation of the L-I curve. As can be seen from the L-I curve, this modulation has a somewhat uniform period of ~ 4mA.

Another indication of the device behaviour is the far field distribution. This was observed as a focussed spot incident on an infra-red detector card. The laser produces concentric

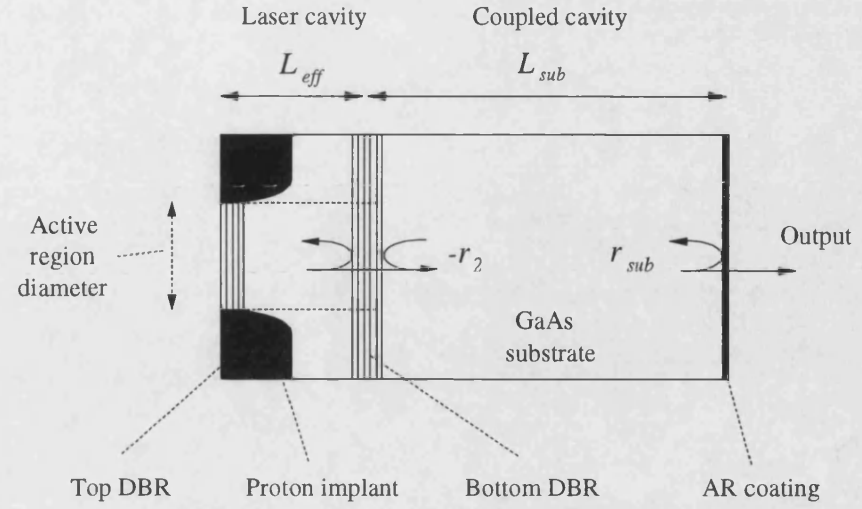

Figure 3.4: Schematic representation of the AR coating residual reflectivity forming a coupled cavity with VCSEL #1

rings of light, analogous to Newton's rings interference, that contract with increasing current injection. Laser emission perfectly normal to the substrate experiences an interference of some phase (either partly constructive or partly destructive) caused by the coupled cavity. Emission at some angle off the normal, however, experiences a different coupled cavity round-trip length, yielding interference of a different phase. Hence rings of alternate interference conditions are produced. At first an intense spot of light appears at the centre, but near 18mA it becomes dark until the surrounding ring contracts into a central spot at a still higher current. This process repeats at the succeeding peaks of the L-I curve. Similar behaviour has been observed and reported for other VCSEL devices [3-5] and is further evidence of the presence of a coupled cavity.

The first report of such effects in VCSELs was made by Geels *et. al.* [3], where a VCSEL with a non-AR coated substrate, reflecting ~ 30% of optical intensity, demonstrated a jagged but continuous L-I curve. They also examined the appearance of contracting circular rings in the far field pattern of a non-AR coated VCSEL [4]. This contrasted with the full disc far field pattern of an AR coated, but otherwise similar device, as illustrated in figure 3.5.

The work of Chang-Hasnain *et. al.* [6] in this respect is somewhat broader and addresses the enhancement and utilisation of coupled cavity effects in VCSELs. During their studies of the spectral evolution of a VCSEL output, they observe the inhibition of that laser from operating within wavelength windows 6 Å wide with a period of 19 Å. It is then demonstrated that the coupled cavity has the capacity to switch the laser on and off intermittently across its L-I curve [5] as represented in figure 3.6a. This is achieved by thinning the substrate to a 70μm thickness to reduce substrate absorption losses, and by specially polishing it to form a third mirror. For a 10μm gain-guided device with a threshold current of 15mA and a sharp turn-on similar to that of VCSEL #1, Chang-Hasnain also relates the individual peaks in L-I not to transverse modes of different orders, but to successive longitudinal external substrate cavity modes as demonstrated in figure 3.6b.

There is evidence that even VCSELs with AR coated substrates are prone to coupled cavity effects when the substrate refractive index changes with temperature [7]. This is confirmed by examining the evolution of a rather smooth L-I curve through a sequence of elevated operating temperatures, as illustrated in figure 3.7. As the substrate temperature approaches 114°C, ripples dominate the L-I of this 10μm diameter device. Such residual reflectivities are inevitable when operation deviates from the design conditions, for example as a result of high junction temperature. Others have reported "periodic ripples in the L-I curve" of an uncoated 8 × 8 VCSEL array [8] and "transverse mode switching" aided by "imperfect AR coating" in a 45μm diameter laser [9].

Our laser, however, suffers from kinks in its L-I curve deeper than those demonstrated in figure 3.7 (R ~ 1%) and not as profound as those in figure 3.6 (R ~ 30%). It is perceivable that the wavelength deviation (~ 960nm) from the design conditions (~ 980nm), coupled with an inaccuracy in the deposition of the AR coating, may effect a reflectivity of five percent (R ~ 5%). It is also possible that the refractive index of the AR coating material does not match the GaAs substrate interface with air. It is not known if the wavelength deviation is intentional, but it may easily be caused by a small inaccuracy in the thickness of the spacer layer between the DBR mirrors. This would yield a shorter laser cavity and hence a shorter fundamental longitudinal mode.

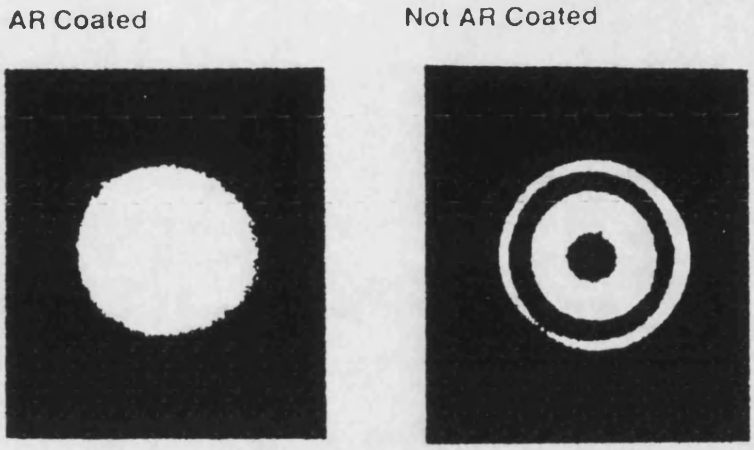

Figure 3.5: Far field pattern a of a 10μm bottom-emitting VCSEL with the substrate (a) AR coated and (b) not AR coated, after [4]

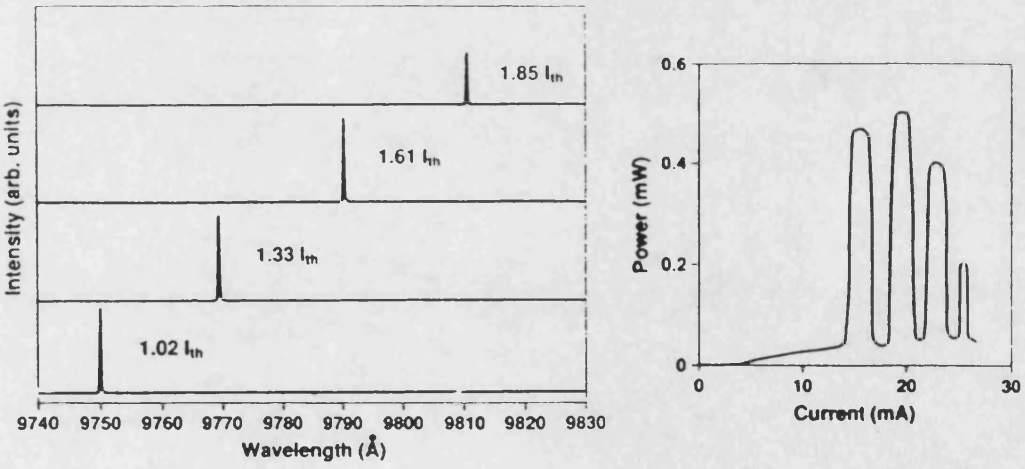

Figure 3.6: The coupled cavity effect on a 10μm bottom-emitting VCSEL with a polished substrate (R ~ 30%): (a) the L-I curve and (b) the wavelengths corresponding to the peaks of the L-I curve, after [5]

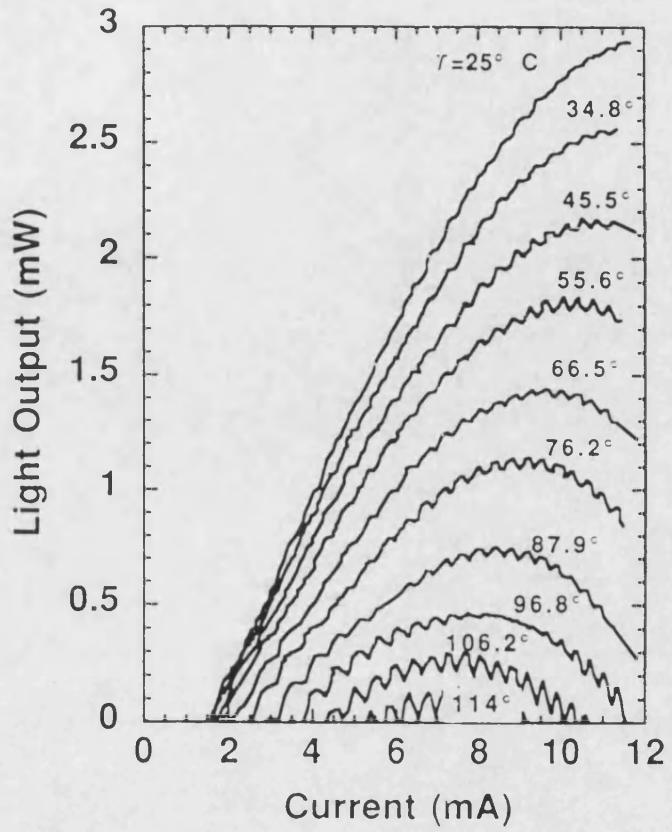

Figure 3.7: A bottom-emitting VCSEL L-I curve series demonstrating deeper L-I ripples with higher operating temperature which results from the deviation of the operation wavelength from the AR coating design wavelength (R < 1%), after [7]

It may be noticed that the kinks in the L-I are consistently sharper on the falling edge (high current side) than on the rising edge (low current side). This lop-sided appearance is consistent with other observations [3] and is probably caused by wavelength (frequency) pulling and pushing effects [10]. Lasers, like other physical systems, seek to operate in modes of lowest loss (the least action principle). Ideally, and in the absence of external feedback, the optical output power from a laser would increase steadily with current and the operation wavelength would change consistently. The coupled cavity, however, resists attempts by the laser to operate at wavelengths intermediate to its cavity modes, resulting in destructive feedback interference. The laser thus remains near the low loss wavelength until it can operate at the next external cavity mode window to where it rapidly scans its wavelength of operation. Such wavelength pulling has been demonstrated in injection locked lasers [11].

It is highly suspect that the sharp laser turn-on feature of VCSEL #1, illustrated in figure 3.2, is also related to the presence of the coupled cavity. The actual mechanism of switching is uncertain, but only in view of the many possibilities. It has been reported that a bistability hysteresis loop can be reduced in width by optical feedback [12] from a passive coupled cavity. This has been attributed to the phase detuning of the feedback or, equivalently, to the difference in the linewidth enhancement factors of the two sections. Presumably then for some configuration it is possible for the feedback to eliminate the hysteresis width altogether, with no serious attenuation of the sharpness. Without this coupled cavity VCSEL #1 may therefore show bistability resulting from one of many mechanisms [13-15] as other VCSELs have shown [1].

Alternatively theoretical and experimental studies demonstrate that external cavity laser systems with passive, active or saturable absorber slave cavities may exhibit bistability [2,16]. A passive slave cavity may similarly have the ability to induce near bistability, i.e. a sharp turn-on with a single L-I route and no hysteresis loop [17,18].

It is also a well documented fact that lasers demonstrate bistability within a temperature window outside which the bistability mechanism is ineffective [13,19]. Towards the edge of this temperature window the hysteresis loop narrows gradually until it vanishes leaving only a sharp switch-on. Yet another simple possibility for this sharpness is wavelength-pulling of the laser into operation due to the coupled cavity. For it is noted that the switch-on appears at only 4mA (one coupled cavity period) below the 20mA peak. At threshold therefore, the coupled cavity provides a positive feedback mechanism to the laser mode which is otherwise below its threshold current.

The model will be restricted to account for the coupled cavity but not the wavelength-pulling or any bistability. Despite its low reflectivity, it appears that the substrate facet has a deep effect on the laser operation. It is noted that both lasers [20,21] and VCSELs [22,23] have been reported to be highly sensitive to very small amounts of feedback. The depth of L-I modulation, the sharp switch-on and possible alteration of the laser bistability are stronger effects than expected from an external cavity. It is therefore worth pointing out that this coupled cavity has the following advantages which make it more effective than an external cavity: ***(i)*** one of its mirrors is the highly reflective VCSEL bottom DBR mirror; ***(ii)*** more importantly, the short length of the cavity (the

substrate thickness) renders multiple reflection well within the optical coherence length; *(iii)* the substrate material (GaAs) optical loss is smaller than normal (~30% per round trip) because of the thin substrate, resulting in a stronger interference effects.

3.1.2 Transverse modes and gain saturation

VCSEL #1 displays transverse mode switching at 26.5mA where the L-I curve slope increases abruptly. To understand this switching we will consider the evolution of the fundamental transverse mode. Although the carrier profile induces a de-focussing effect on the optical mode, this is overcome at threshold by gain-guiding and thermal lensing profile [4,6,24-26]. This results in the establishment of an approximately Gaussian fundamental transverse mode as illustrated in figure 3.8a. As this mode gathers power with increasing current, it depletes the local carrier concentration effecting spatial hole burning at the region corresponding to the mode peak. A flattening of the carrier profile is matched by a levelling of the carrier-induced refractive index, a reduction of the defocussing effect and of the modal gain. As the depletion continues, the carrier profile is depressed in the centre while it rises at the perimeter [4]. The gain is saturated by the presence of the mode and the carrier-induced refractive index profile acts as a lens focussing the mode, reducing its diameter [26] and producing a narrow and intense optical profile, see figure 3.8b.

Increasing the injection current further deepens the hole burning [27] and the self-saturation and reduces the gain of the fundamental mode. This causes the general decline in external differential efficiency η_e of the L-I curve and leads to the transverse mode switch near 26mA as illustrated in figure 3.8c. This switch is marked by a noticeable increase in the slope of the L-I curve as the laser efficiency is recovered.

3.1.3 Optical polarisation

A circularly symmetric fundamental mode is composed of two superpositioned degenerate linearly polarised (LP) components [28,29] as illustrated in figure 3.9. A circularly symmetric VCSEL would therefore exhibit an equal output power from both optical components. In practice, however, a slight misalignment in the fabrication, or

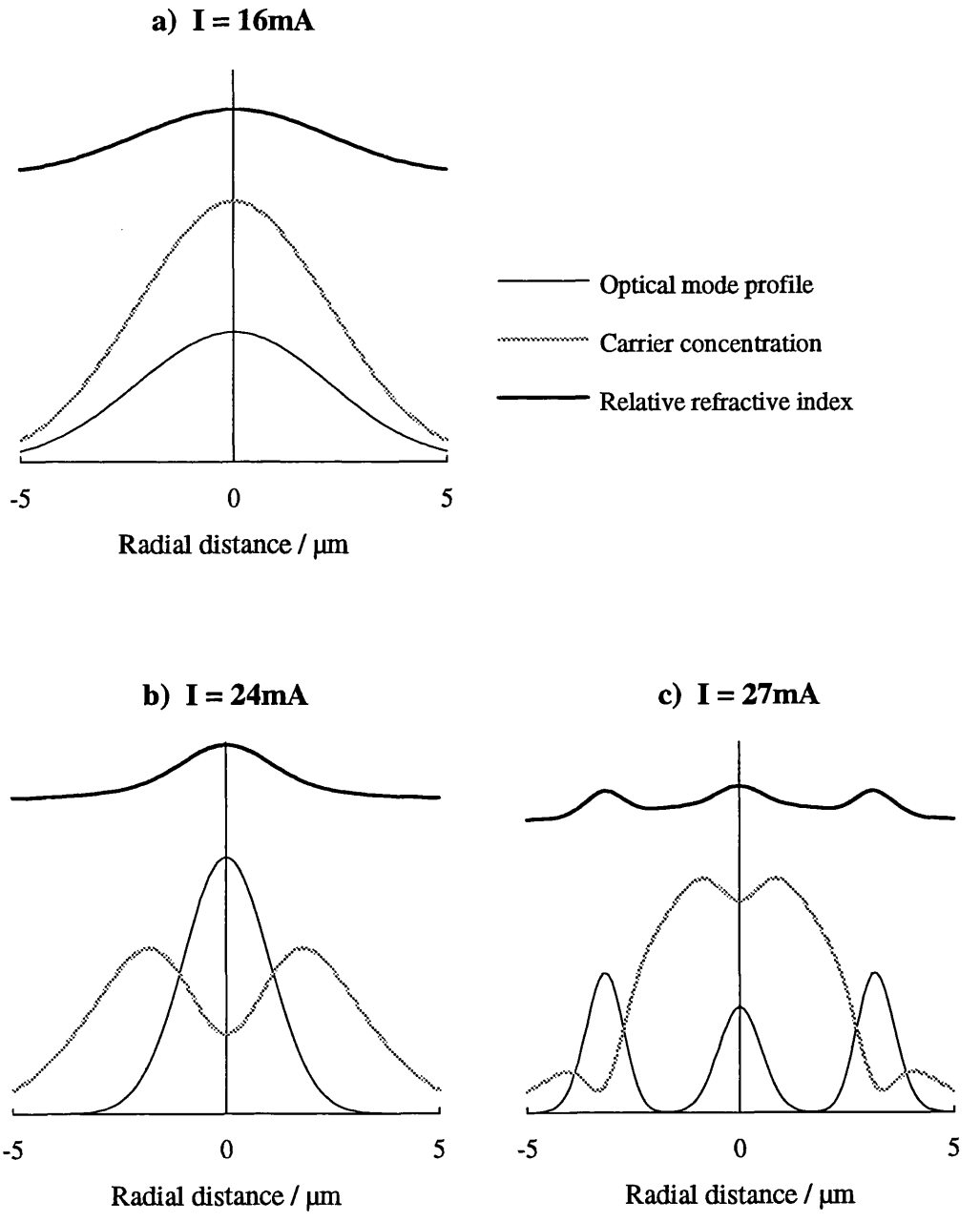

Figure 3.8: Schematic profiles across a 10μm diameter gain-guided VCSEL, of the carrier concentration, refractive index and optical mode, illustrating:
a) Gaussian mode above threshold,
b) gain saturation of fundamental transverse mode and
c) switching to first order transverse mode

an asymmetry in the proton implanted aperture could cause cavity anisotropy [6]. This will lift the degeneracy, and both modes may coexist, but will become spectrally distinct by a fraction of an angstrom [25].

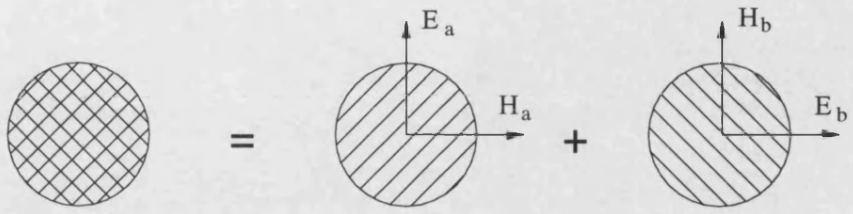

(a) Fundamental mode (b) Its modal components

Figure 3.9: Fundamental transverse mode and its polarised components

The non-symmetric carrier profile also leads to birefringence [30] and to the lifting of the polarisation degeneracy. An extreme example of this process is the generation of TE and TM modes in bulk edge emitting lasers. Such a phenomenon also takes place in optical fibres distorted by external mechanical pressure [31], and has been created in VCSELs by intentionally induced gain anisotropy [32] and cavity geometry anisotropy [33,34]. This leads to a lifting of the polarisation degeneracy and consequently to the spectral splitting of polarisations of each dumbbell-shaped mode by some fraction of an angstrom ($\delta\lambda_{ab}$ ~ .2 Å) [35,36]. The difference in modal width might lead to a higher threshold for one polarisation relative to the other and thus to a plane polarised operation until the laser cavity excitation energy is high enough to exceed the optical losses of the suppressed polarisation.

Despite the suppression of optical modes parallel to P_b in polarisation, the first order transverse mode of such a polarisation does make a sudden appearance as a flat peak near 28mA (figure 3.2). It disappears just as suddenly in a manner similar to the laser turn-on at threshold which may indicate a similar coupled cavity switch-on and switch-off effect. Recalling the wavelength dependence of the coupled cavity reflectivity and the spectral separation $\delta\lambda_{ab}$ of P_a and P_b, it is expected that the maximum reflectivity for each polarisation is reached at different laser drive currents. The appearance of P_b then

occurs when its reflectivity is strong enough to offset its losses, whilst the reflectivity of its opponent P_a is not yet at the peak. At that point conditions within the laser allow the presence of this polarised mode P_b and it effectively reaches its threshold. The height of the peak is consequently determined by the equilibrium obtained by the competing modes.

Another possible cause of polarisation anisotropy is polarisation hole burning. This has been observed in Erbium-doped optical fibres (EDFAs) [37,38] and Neodymium glass lasers (Nd:Glass) [39]. This anisotropy is more prominent at higher gain compression since it results from selective pump beam interaction with carriers and from polarisation-dependent gain, intrinsic to the amplifier medium. In essence, it is spectral hole burning of the carriers available to the dominant polarisation, leaving the other polarisation to experience a slightly different carrier concentration.

Evidently, conditions within the VCSEL #1 do not alleviate the suppression of the P_b polarisation at the first two peaks of the L-I curve at 18mA and 23mA, as they do at the third peak at 28mA. This will become more apparent in the discussion of the model results.

3.2 Model

In order to acquire a better understanding of the laser operation, a model is constructed that simulates the laser cw operation with a view to simulating and predicting the dynamic behaviour in the next chapter. First, it is useful to examine other models, their methodologies, assumptions and results.

Recently, theoretical studies of VCSELs have specifically targeted and modelled thermal effects, thereby accounting for the shape of the cw L-I curve which most VCSELs have in common. They typically demonstrate a declining external efficiency η_e, whereby the laser output reaches a maximum power followed by a rather more rapid fall. This display of negative external efficiency concludes in either laser shut-down or catastrophic termination. Considering also that pulsed L-I curves exhibit much less curvature than the cw L-I curves, it is not difficult to relate the roll-over to a rise in the device temperature. Several models have been formed by others to establish the details of this process [40-49].

One model of such behaviour formulated by Scott, Geels, Corzine and Coldren [40] accounts for Joule heating and the ensuing shift in operating wavelength. They also show from first-principle Fermi-level calculations that at sufficiently high temperatures the heterostructure becomes insufficient to confine the carriers. As a result carrier leakage becomes dominant and the threshold current increases dramatically. They also relate carrier leakage to the carrier concentration and temperature and include spatial hole burning. Thus, as the device temperature rises, the threshold current increases faster than the non-leaking portion of the injected current, resulting in an output power that actually decreases with current as observed.

This model, however, is formulated to describe a small single-moded index-guided bottom-emitting VCSEL with no possibility of mode competition. Furthermore, it does not account for the effect of heating on the reflectivities of the DBR mirrors. This is central to another model by Dudley *et. al.* [41] who considers the effect of heat generated within the top DBR mirror layers on their refractive indices, as well as the cumulative effect of increasing the mirror's reflectivity. This, it appears, simply confines more light inside the laser, reducing its external output efficiency at higher drive currents causing the roll-over in the L-I curve. This technique is proposed for modelling top-emitting

VCSELs, but not bottom emitters where the bottom mirror is thermally sheltered by the substrate and the device generally experiences better heat-sinking and a smaller temperature rise.

In another study the shift in operating wavelength is demonstrated to be five times slower than the shift in the spectral gain peak [42]. This causes lower differential gain and higher transparency carrier concentration leading to an increased threshold current and a negative external efficiency at higher injection [43].

There have been attempts at analytical solutions for VCSELs by Dutta [44], and numerical solutions of the inhomogeneous heat generation and dissipation within VCSELs [24,42,45-47] and their current spreading [48]. There are few, if any, self-consistent multimode models, as yet, that successfully calculate the spatial two-dimensional photon and carrier profiles with their mutual interactions. Not surprisingly so, for such models are computationally demanding and inherently difficult to stabilise.

Instead of replicating the models described above, however, it is prudent to perceive that they are aimed at understanding the general properties of VCSELs in order to acquire insight and achieve better designs. For our purposes though, and comparing the behaviour of VCSEL #1 with devices under modelling, it seems that a different perspective is needed.

Most VCSELs exhibit their maximum power before rolling over at drive currents exceeding four times their threshold ($4 \times I_{th}$). The relative roll-over current is even higher if they are small in diameter, e.g. typically 10μm [40]. Similarly, bottom emitting VCSEL, i.e. mounted p-side down [49], have better heat sinking and lower operating junction temperatures. If a VCSEL is fabricated especially with low top DBR mirror resistance [6], it rolls over at even higher currents. Comparing such performances with the multiple coupled cavity switching within twice the threshold current, it is apparent that thermal roll-over is slower in onset than the coupled cavity effect. In modelling VCSEL #1, one would then be justified in ignoring the roll-over effect with all its

temperature dependencies. Our model will be based on the coupled cavity effect and the only thermal effect necessary will be the wavelength shift with temperature to account for the kinks.

A suitable choice of model is a rate equation representation [50,51] of a lumped cavity, i.e. the material and mirror losses and the gain are assumed evenly distributed over the cavity. This contrasts with travelling-wave models [46] which account for standing wave interactions with the material and mirrors for which the calculation required is much more mathematically and computationally demanding. Due to the success of the standard rate equations in describing and predicting the behaviour of edge-emitting lasers, they are adopted and modified to model the performance of VCSEL #1. As a result of the lack of specific information about the material and structural details of this laser however, a standard structure is assumed as described below.

In order to obtain suitable elementary parameters for our model, we will seek to simulate a well behaved VCSEL first. If the effects of the coupled cavity were removed from the L-I of VCSEL #1, a threshold current between 16mA and 18mA would reasonably be expected. The external differential efficiency η_e can be safely assumed somewhat lower than the best slope of the L-I curve, where the external cavity allows the laser to rapidly catch up with its potential output. This occurs for each mode at the point of maximum slope, namely in the neighbourhoods of 16mA, 22mA and 26mA, where η_e is approximately 0.25, 0.20 and 0.16 mW/mA respectively, as obtainable from figure 3.2. The variation in slope is obviously an artifact of the changing effective mirror reflectivity, and in simulating the laser an external efficiency of ~ 0.18 mW/mA will be aimed for. Naturally, we will endeavour to find a set of laser parameters that yield a simulated performance matching the threshold current, external efficiency and output power level of the laser.

Since the laser operates in a single transverse mode below 26mA and its polarisation behaviour will be of interest in other chapters, it is reasonable to assume a single transverse mode operation and to design the model for a two-mode simulation, one mode per polarisation. What follows is a detailed and justified mathematical description which includes all the essential effects.

3.2.1 Rate equations

The model is based on a time-dependent representation which is foreseen as suitable for simulations and predictions of further dynamic behaviour as described in chapters four and five. All the symbols incorporated in the following equations are defined either in the text below or in table 3.1 where their values are also given. The rate of change of the photon density is expressed explicitly in the following relationship:

$$\frac{dP_i}{dt} = \Gamma_z \Gamma_{xy} G_i P_i + \beta B N^2 - \frac{P_i}{\tau_{P_i}} \quad \ldots\ldots \quad (3.1)$$

where P_i is the photon density of optical mode number i averaged over the laser cavity volume. The three factors contributing to this equation are defined below respectively:
i) The **stimulated emission rate** is identical to the rate of stimulated carrier recombination and proportional to the photon density and to the material gain.

The quantum wells are positioned at the peak of the standing-wave in the cavity. This positioning maximises the overlap of the gain region with the optical mode in the longitudinal direction. The longitudinal confinement factor Γ_z may be calculated [52] using:

$$\Gamma_z \equiv \frac{\int_{active} E^2(z)\, dz}{\int_{cavity} E^2(z)\, dz}$$

The laser operates in a single longitudinal mode which overlaps with the gain layers best. For a small total quantum well thickness, the above equation approximates to [52]:

$$\Gamma_z \sim 2\frac{\mu_{InGaAs} L_{QW}}{\mu L_{eff}} \quad \ldots\ldots \quad (3.2)$$

For our laser structure, Γ_z approximates to 3.6% [7] and is expectedly equal for all transverse modes.

Since the model combines spatial parameters, like gain and photon concentration and their spatial overlap is then accounted for by including lateral confinement factor Γ_{xy}. Nominally, for a particular mode this is a measure of the lateral overlap of the modal optical field with the gain profile in the lateral plane. Different transverse mode profiles

can therefore yield very different confinement factors. However, since our model is concerned with the fundamental transverse mode, which quickly reaches full lateral confinement as discussed in section 3.1.2 above, Γ_{xy} is assumed identically one.

ii) The **spontaneous emission rate** is a low level continuously occurring process of carrier recombination that generates incoherent photons. These photons range the whole gain spectrum seeding the growth of optical modes. The fraction of spontaneously emitted photons that contribute to the lasing mode is $\beta \sim (.1 - 2) \times 10^{-4}$. This magnitude is predicted by classical theory modified for VCSELs [53,54], and verified by experiments [55]. Above laser threshold this contribution remains unchanged and, compared to stimulated emission, pales into insignificance. CW power calculations are therefore insensitive to small inaccuracies in the spontaneous emission contribution. *iii)* The third term is the rate of photon loss which is accounted for by the **photon lifetime** discussed in section 3.2.2 next.

The rate of change of the average carrier concentration N is the sum of three terms:

$$\frac{dN}{dt} = \frac{\eta_{inj} I}{q\, Vol} - \Sigma G_i P_i - \frac{N}{\tau_N} \qquad \ldots\ldots \quad (3.3)$$

Firstly, there is the positive contribution of the **injection current density** per unit of active volume, that is the new carrier pairs available for recombination. The laser cavity volume for a circular VCSEL is estimated by assuming that current funnelling restricts the diameter to 10μm, and that the cavity length is the sum of the DBR mirror estimated penetration depths and the active region thickness. The current injection efficiency η_{inj} accounts for the current leakage past the active volume, and is determined by the quality of the proton implant. For simplicity this is taken as a constant fraction (65%) of the total injected current.

Secondly, the **stimulated carrier depletion** contributes negatively to equation (3.3) in a similar manner to that described for the photon rate equation (3.1). Finally, **spontaneous carrier recombination** introduces a loss process represented by the carrier lifetime τ_N such that:

$$\frac{1}{\tau_N} = A + B N + C N^2 \qquad \ldots\ldots \quad (3.4)$$

where A, B and C are the recombination constants, already discussed in section 2.2 (chapter two). The Auger recombination constant C is sometimes ignored in simulations of InGaAs stripe geometry lasers because of its small contribution at normal carrier concentration levels of say 3×10^{18} cm^{-3}. As it will turn out, however, VCSEL #1 reaches lasing at a carrier concentration of the order of 10×10^{18} cm^{-3}. Hence C makes a marked difference to the calculation and is retained in the carrier lifetime equation. More crucially, the process of carriers recombining not radiatively in the quantum wells but non-radiatively in the barriers is heightened. This is accounted for by increasing the value of the constant A from $\sim 3 \times 10^{8}$ s^{-1} to the more appropriate value of 10×10^{8} s^{-1} [56].

3.2.2 Mirror reflectivity and optical losses

Although the mirror details are uncertain, it is assumed that the top and bottom DBR mirrors are composed of alternating layers of AlAs and GaAs. Their respective intensity reflectivities will be given reasonable values as discussed in section 3.3 below.

The penetration depth into a multilayer mirror is calculated from coupled mode theory [51] using the relationship [49]:

$$L_{pen} = \frac{\tanh(\kappa_m L_m)}{2\kappa_m} \quad \ldots\ldots \quad (3.5)$$

where κ_m and L_m are the coupling constant and length of the mirror, respectively. For a mirror with defined interfaces between the layers, and therefore with sharp index steps, the coupling constant is calculated from $\kappa_m = 2\Delta n / \lambda$. The refractive index of AlAs is 2.95 and of GaAs is 3.52 effecting an index step of $\Delta n = 0.57$. Assuming the mirrors include 18.5 periods results in a penetration depth of 0.5μm, which is quite insensitive to the thickness of the mirror. This laser is most likely to have a 1 λ mirror spacing [45] which translates to λ/μ of real length. The effective optical cavity length is the sum of the penetration depths into both mirrors and the spacing thickness in between [7]:

$$L_{eff} = L_{top} + L_{bot} + L_c \sim 1.2\mu m \quad \ldots\ldots \quad (3.6)$$

A Fabry-Perot cavity of this length has a mode spacing of approximately 100nm as obtained from:

$$\Delta\lambda = \frac{\lambda^2}{2\mu L_{eff}} \quad \ldots\ldots \quad (3.7)$$

This free spectral range is much larger than the gain spectrum (up to 80nm at high carrier concentrations), hence allowing the existence of only one longitudinal mode in the cavity. This longitudinal confinement does not affect transverse mode profiles though.

The average lifetime of photons represents losses arising from interaction with the material and from the mirror transmission and absorption calculated from the both top and bottom mirror intensity reflectivities R_1 and R_2. Approximating the VCSEL cavity to a Fabry-Perot cavity with well defined reflectors, the following analytic representation of the photon lifetime is obtained:

$$\frac{1}{\tau_{P_i}} = \frac{c}{\mu}\left(\alpha - \frac{\ln(R_1 R_2)}{2L_{eff}}\right) \quad \ldots\ldots \quad (3.8)$$

The material losses are lumped into one constant α which is estimated to be between 30 cm^{-1} and 50 cm^{-1} [7,49,52,57]. This constant includes absorption by free-carrier interaction with photons in the active region, and absorption and scattering in the passive layers of the cavity.

When calculating the rate equations for two transverse modes, it is justifiable to assign a higher α value to the higher order transverse mode. Normally, the difference $\delta\alpha$ would be > 10 cm^{-1} [57]. Since the suppressed polarisation mode P_b suffers higher losses than its dominant counterpart P_a, it seems reasonable to associate a higher loss $\alpha_a + \delta\alpha$ with P_b compared with the loss α_a for P_a. This will be explored quantitatively when presenting the results of the model in section 3.3 below.

The output power from the bottom mirror is calculated by multiplying the energy per photon by their total number in all cavity modes and by their rate of escape, as follows:

$$P_{out} = Vol\,\Sigma_i P_i \cdot \frac{hc}{\lambda} \cdot \frac{c}{\mu}\frac{\ln(R_1 R_2)}{2L_{eff}} \cdot F \quad \ldots\ldots \quad (3.9)$$

The symbol h is plank's constant and F is the fraction of the total number of output photons that escape through the bottom mirror only:

$$F = 0.85 / \left(1 + \left(\frac{1-R_1}{1-R_2} \right) \sqrt{\frac{R_2}{R_1}} \right) \sim 0.8 \quad \ldots\ldots \quad (3.10)$$

The numerator accounts for the optical absorption (~ 0.1%) of the bottom mirror in relation to its transmittance (~ 0.6%).

3.2.3 Gain and saturation

The gain for each mode is given by the following linear dependence on carrier concentration:

$$G_i = \frac{c}{\mu} a_i (N - N_T)(1 - \varepsilon \Sigma_j P_j) \quad \ldots\ldots \quad (3.11)$$

where a_i is the differential gain and N_T is the carrier density within the quantum wells at transparency. The last factor in this equation, in this form, represents gain saturation [51,58] resulting mainly from spatial hole burning of the carrier density profile by the optical field in the cavity. The laser may also suffer from spectral hole-burning, but since the two-modes under consideration are very close in wavelength ($\delta\lambda_{ab} = \lambda_a - \lambda_b$), they would experience a similar gain saturation from this process.

While the value of a_i depends on the carrier concentration, the value of N_T relates more to the wavelength of operation. Since the laser operates at a wavelength largely displaced from the spectral gain peak, and to the short wavelength side, N_T is given the value of 1.5×10^{18} cm^{-3} as calculated by Summers *et. al.* [59]. As demonstrated below, the laser operates at very high carrier concentrations, e.g. 10×10^{18} cm^{-3}; where the appropriate value for a_i is very low at ~ 1.5×10^{16} cm^2 [59].

The gain spectrum varies with the carrier density but is potentially 60nm wide for this material composition at high carrier concentrations. The above representation though, assumes a flat spectrum and is justified by the small wavelength separation of the two polarised modes in question ($\delta\lambda_{ab} < 1$ Å). As explained above, the L-I region of interest to us is well below the thermal roll-over current for this device. The decline in η_e is

mainly a result of the spatial hole burning and gain saturation. The sudden reversion to high η_e by the first order mode, i.e. above 26.5mA, testifies to the minor role of thermal effects.

If the decline in η_e is to be portrayed by the model, gain saturation must be well represented in the equations. Unlike InGaAsP operating at 1.3μm and at 1.5μm wavelengths and AlGaAs operating at 870nm wavelength, InGaAs operating at 980nm is a comparatively new material in laser design. Previously, its use has been directed at semiconductor pump lasers rather than telecommunication lasers. Hence there is little published data regarding its saturation constants. However, the range of values for the gain saturation constant ε in InGaAs/GaAs edge-emitting lasers is reported between 2.5×10^{-17} cm^3 and 12×10^{-17} cm^3 [60] depending on the laser structure. It represents the average effect of hole burning at multiple standing wave mode peaks over the length of a stripe laser cavity. In contrast, VCSELs have mode profiles that are more localised within the cavity. Whereas equation (3.11) describes the average saturation for an average photon density over the cavity volume, we need the description of a more localised optical field.

Consider that, for a 10μm diameter VCSEL, the fundamental mode quickly shrinks to a diameter of 4μm at its narrowest, as measured experimentally [26] and calculated theoretically [24,26]. The optical intensity then, over the mode volume, is a factor of $(10 / 4)^2 \approx 6$ higher than the effect portrayed in edge-emitting lasers. The carrier profile at its centre however is depleted by the small but intense mode and their interaction is accentuated by this factor of 6. Therefore, it would be a more reasonable description of gain saturation to use a saturation constant ~ 6 times larger than a value obtained from edge-emitting laser measurements. A suitable average value for ε is then 30×10^{-17} cm^3.

It is worth pointing out that because of the high spatial overlap and spectral proximity (< 1 Å) of orthogonal polarisation modes of the same transverse order, they experience a similar gain saturation and gain suppression. Two transverse modes of different orders, however, have a poor spatial overlap, are spectrally more remote (~ 1nm) and thus do not suppress one another appreciably. Hence the first order mode above 26.5mA experiences little of the gain saturation that depreciates the

fundamental mode. Since our simulation extends only as far as orthogonal polarisations of the fundamental transverse mode though, the gain saturation in equation (3.11) is adequate.

3.2.4 Coupled cavity effects

So far the model is designed to simulate the operation of a well behaved VCSEL. In this section, we introduce the feedback from the coupled cavity formed with the AR coated GaAs substrate as illustrated in figure 3.4. Considering the short length of the substrate cavity (200μm) and in order to avoid the complications of time evolving feedback components, the effective reflectivity method is adopted. The laser is assumed to operate in a steady state relative to the coupled cavity round-trip time (~ 5ps).

It can be shown from standard coupled cavity theory [51] that the effective amplitude reflectivity of the bottom DBR mirror and the substrate/air interface together, in terms of their reflectivities is:

$$r_{eff} = r_2 - r_{sub}\frac{(1-R_2)\,t_{cc}}{1+r_2 r_{sub}\,t_{cc}} \quad , \quad t_{cc} = e^{2\pi i\, 2\mu_{sub}L_{sub}/\lambda} \qquad \ldots\ldots \quad (3.12)$$

where $r_2^2 = R_2$ and $r_{sub}^2 = R_{sub}$, t_{cc} is the interference term, L_{sub} and μ_{sub} are the thickness of the substrate and its refractive index. The substrate loss of ~ 30% per round-trip [7] is included in the substrate facet reflectivity R_{sub}. This equation includes the effects of multiple reflections within the substrate, i.e. the substrate Fabry-Perot cavity, and their contributions to the feedback into the laser. Obviously r_{eff} is a complex function and that must be considered when calculating R_{eff} which replaces R_2 in equations (3.8) and (3.9). The substrate cavity mode spacing is obtained from:

$$\Delta\lambda = \frac{\lambda^2}{2\mu_{sub}L_{sub}} \sim 8\text{Å} \qquad \ldots\ldots \quad (3.13)$$

It is also not difficult to perceive that the reflectivity is largely dependent on the wavelength of the lasing mode. In other words, the substrate cavity will promote an intermittent range of wavelengths by constructive interference feedback, while undermining its complement range by destructive interference feedback.

The overall effect caused by this external cavity depends on the laser wavelength, which is dominated largely by its drift rate with temperature $d\lambda/dT$. This has been measured by several researchers [7,33-35,43,45,53,61] and studied theoretically by others [41,42]. For a VCSEL this property is determined mainly by the rate of change of its temperature with drive current. A rise in the device temperature causes an expansion of the laser and mirror layers and more significantly an increase in their refractive indices [41]. The result is an optically longer cavity and hence a longer modal wavelength. It is perhaps interesting that the increase in the refractive indices of layers comprising the DBR mirrors leads also to a rise in the index step between the layers and hence to a reduction of the mirror penetration depths [41]. Yet, the overall effect is a longer VCSEL operating wavelength. Values quoted for small diameter gain guided VCSELs operating at a 980nm wavelength and mounted p-side down are approximately 0.8 Å/°C of shift towards longer wavelength [4,5].

In order to calculate the laser diode temperature rise above substrate temperature, which is cooled at a constant 16 ± 1 °C, it is related to the power injected into the diode by using the thermal impedance constant Z_s [40] and including an exponential correction factor for high temperatures:

$$\Delta T = Z_s (VI - P_{out}) e^{\frac{-\Delta T}{250°C}} \quad \ldots\ldots \quad (3.14)$$

where P_{out} is the total optical output power and I is the injected current at the bias voltage V. The exponential factor is introduced to account for the higher rate of heat radiation at higher temperatures and leads to a somewhat linear temperature curve with current. Using an approximation from the V-I curve of figure 3.1, which is valid above $0.5 \times I_{th}$, the voltage is represented analytically by:

$$V \approx 1.2\,Volt + .05\,Volt\,mA^{-1}\,I \quad \ldots\ldots \quad (3.15)$$

Z_s has been reported at a theoretical value of 1.1°C/mW and an experimental value of 1.0 °C/mW [4,40]. From these equations the wavelength drift with current injection and output power can be calculated and the coupled cavity effect can be included.

Table 3.1: Model parameters

Parameter description	Symbol	Value
Effective laser cavity length	L_{eff}	1.2μm
Average cavity refractive index	μ	3.4
Substrate thickness	L_{sub}	200μm
Refractive index of GaAs substrate	μ_{sub}	3.5
Laser cavity diameter	D	10μm
Wavelength of laser operation	λ	956nm
Transparency carrier density	N_T	1.5×10^{18} cm^{-3}
Linear gain coefficient	a	1.5×10^{-16} cm^2
Longitudinal optical confinement factor	Γ_z	3.6%
Lateral optical confinement factor	Γ_{xy}	1
Optical material loss for mode a	α_a	35 cm^{-1}
Optical material loss difference of modes a and b	$\delta\alpha$	~ 5 cm^{-1}
Spectral polarisation splitting of fundamental mode	$\delta\lambda_{ab}$	0.2 Å
Gain saturation	ε	30×10^{-17} cm^3
Non-radiative recombination constant	A	10×10^8 s^{-1}
Bimolecular recombination constant	B	1×10^{-10} cm^{3}s^{-1}
Auger recombination constant	C	3×10^{-30} cm^{6}s^{-1}
Spontaneous emission coupling factor	β	1×10^{-5}
Reflectivity of top mirror	R_1	99.8%
Reflectivity of bottom mirror	R_2	99.4%
Reflectivity of the substrate facet	R_{sub}	3.0%
Current injection efficiency	η_{inj}	0.65
Thermal impedance	Z_s	1.0 °C/mW
Drift rate of wavelength with temperature	$d\lambda/dT$	0.8 Å/°C

3.3 Simulation and results

In order to simulate the laser L-I output, the dynamic time-dependent rate equations are solved using a fourth order Runge-Kutta method for a small drive current, see flow chart in figure 3.10. When the solution stabilises, the current is incremented and thus a curve of output power versus injection current is built up. Solution stability is greatly simplified by limiting the number of simultaneous photon concentration variables (optical modes) to two.

The values found most appropriate for the DBR mirror reflectivities of the laser are $R_1 = 99.8\%$ for the top mirror and $R_2 = 99.4\%$ for the bottom mirror. These values yield a reasonable threshold current and differential efficiency as shown below. In the first instance, the residual substrate reflectivity R_{sub} is set to nil, $\delta\alpha$ to 3 cm^{-1} and $\delta\lambda_{ab}$ to 0.2 Å, the resulting L-I is illustrated in figure 3.11. It demonstrates a threshold current of ~18mA, an external differential efficiency η_e of ~ 18% mW/mA and a highly polarised optical output. The carrier concentration continues to rise above the threshold value of ~ 14×10^{18} cm^{-3} because of gain saturation. The output power reaches 1.5 mW at a drive current of 30mA and approaches 4mW at 50mA. The junction temperature rises monotonically to some 60°C above the substrate temperature. The effects of gain saturation appear above threshold in the declining external differential efficiency and the continually rising carrier concentration N. These features all seem reasonable and give confidence in the simulation.

The coupled cavity effect on the L-I is investigated by reinstating the substrate reflectivity R_{sub} with values ranging from 0.1% to 4.0%. Figure 3.12 illustrates P_a, P_b and the total output power P_t. A marked rise in P_b is caused by reflectivities above 2% and causes a reactive reduction in P_a in a manner very similar to the occurrence near 28mA of the experimental L-I. At such reflectivities the modulation in P_t deepens and the first kink begins to reach output powers of 0.5mW. It is also interesting to note the appearance of a little kink between 15mA and 16mA that resembles, at least in position, the turn-on of the laser.

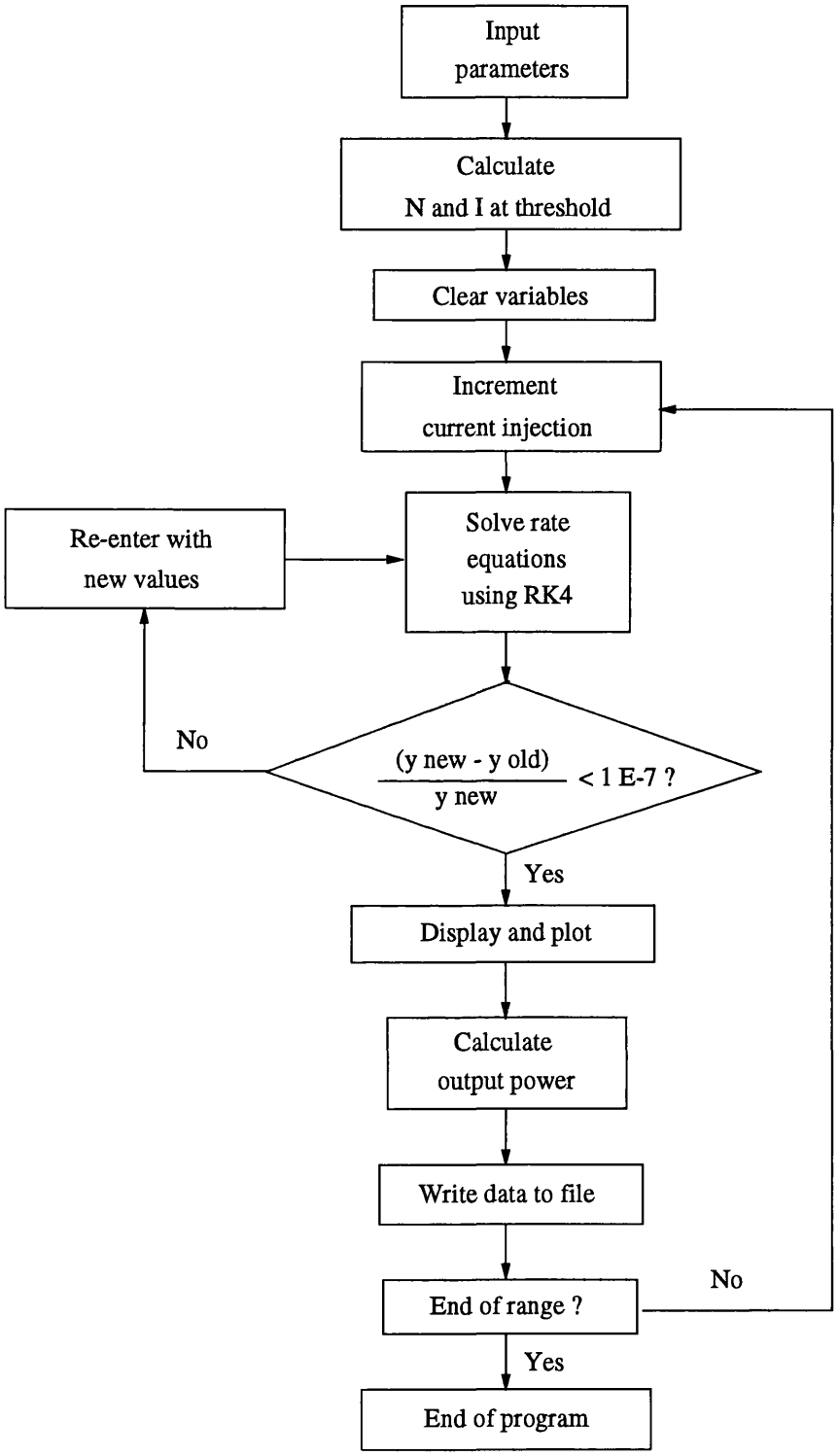

Figure 3.10: Program flow-chart illustrating the logic and sequence of model solution

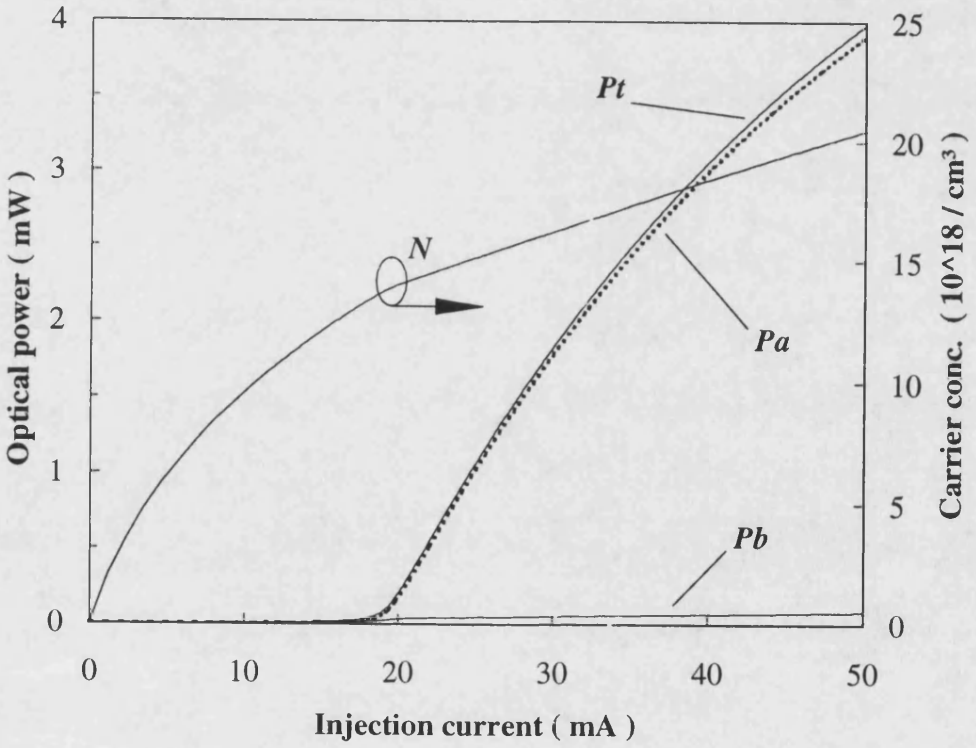

Figure 3.11: Numerical simulation of VCSEL #1 in cw operation vs. current I illustrating the carrier density N, the optical laser output total (P_t) and polarisation resolved (P_a and P_b))

Parameters: R_{sub} = 0.0% $\delta\alpha$ = 3.0 cm^{-1}
$\delta\lambda_{ab}$ = 0.2 Å β = 1 x 10^{-5}

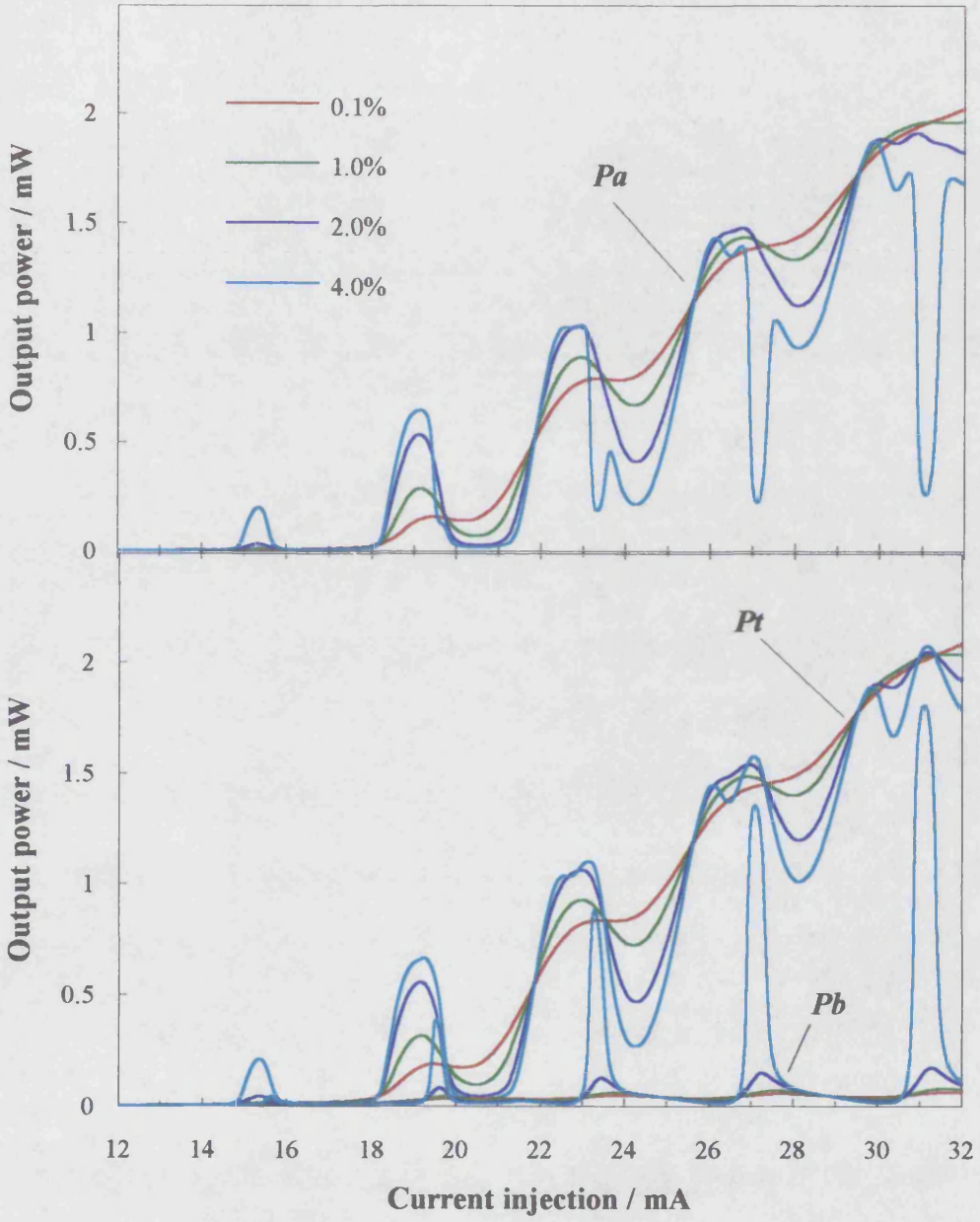

Figure 3.12: Numerical simulation of VCSEL #1 in cw operation vs. current I illustrating the carrier density N, the optical laser output total (P_t) and polarisation resolved (P_a and P_b))

Parameters: R_{sub} = 0.1% → 4.0% $\delta\alpha = 3.0\ cm^{-1}$
$\delta\lambda_{ab}$ = 0.2 Å $\beta = 1 \times 10^{-5}$

As discussed above, in practice the coupled cavity pulls the laser wavelength towards the peak reflectivity wavelengths of its reflectivity spectrum. Essentially, this allows the laser to optically dispense of more of the power injected electrically. Not including this wavelength pulling effect leads to the sinusoidal shape of the simulated output. If it is included, the rising side of each peak would start at a lower current and consequently be less steep. Each peak would persist for a slightly larger range of current because of the coupled cavity hindering the drift in laser wavelength. The falling side of each peak would be a sharper plunge because of the laser evading the low reflectivity wavelength band and passing through it swiftly.

In reality, the laser also exhibits transverse mode switching aided by transverse mode saturation of the fundamental mode. Although higher order modes are not included in the model, the simulation gives a reasonable and general model of the laser behaviour under varied parameters.

Setting R_{sub} to 3.0% and maintaining the wavelength splitting at $\delta\lambda_{ab} = 0.2$ Å and $\delta\alpha$ at 3 cm^{-1}, the L-I takes a shape that represents VCSEL #1 better, as illustrated in figure 3.13. Excluding the substrate loss of ~ 30% per round-trip, the substrate facet reflectivity would be in practice some 4.5%. Notice the modulation of the effective mirror reflectivity curves (R_{eff}) by ± ~ 0.25% resulting from the wavelength shift caused by thermal effects. This may seem like a trivial variation but the modulation in the effective intensity transmittance of the output mirror is then ± 0.25% ÷ 0.6% ~ 40%. The carrier density kinks are caused by carrier depletion by greater stimulated emission and lasing action at the peaks of the L-I.

Although a rise in effective reflectivity improves lasing conditions, an excessive rise reduces the output efficiency causing dips at the centres of the kinks. Similar behaviour is also observed in the device L-I characteristics at 28mA. The effective mirror reflectivity R_b displays a slight lag behind R_a, as expected from the wavelength splitting. On the falling side of the curves P_b therefore experiences a higher reflectivity than P_a which compensates for the larger optical loss. Hence, P_b appears at the corresponding current ranges and is very sensitive to the loss difference $\delta\alpha$ and the wavelength splitting $\delta\lambda_{ab}$.

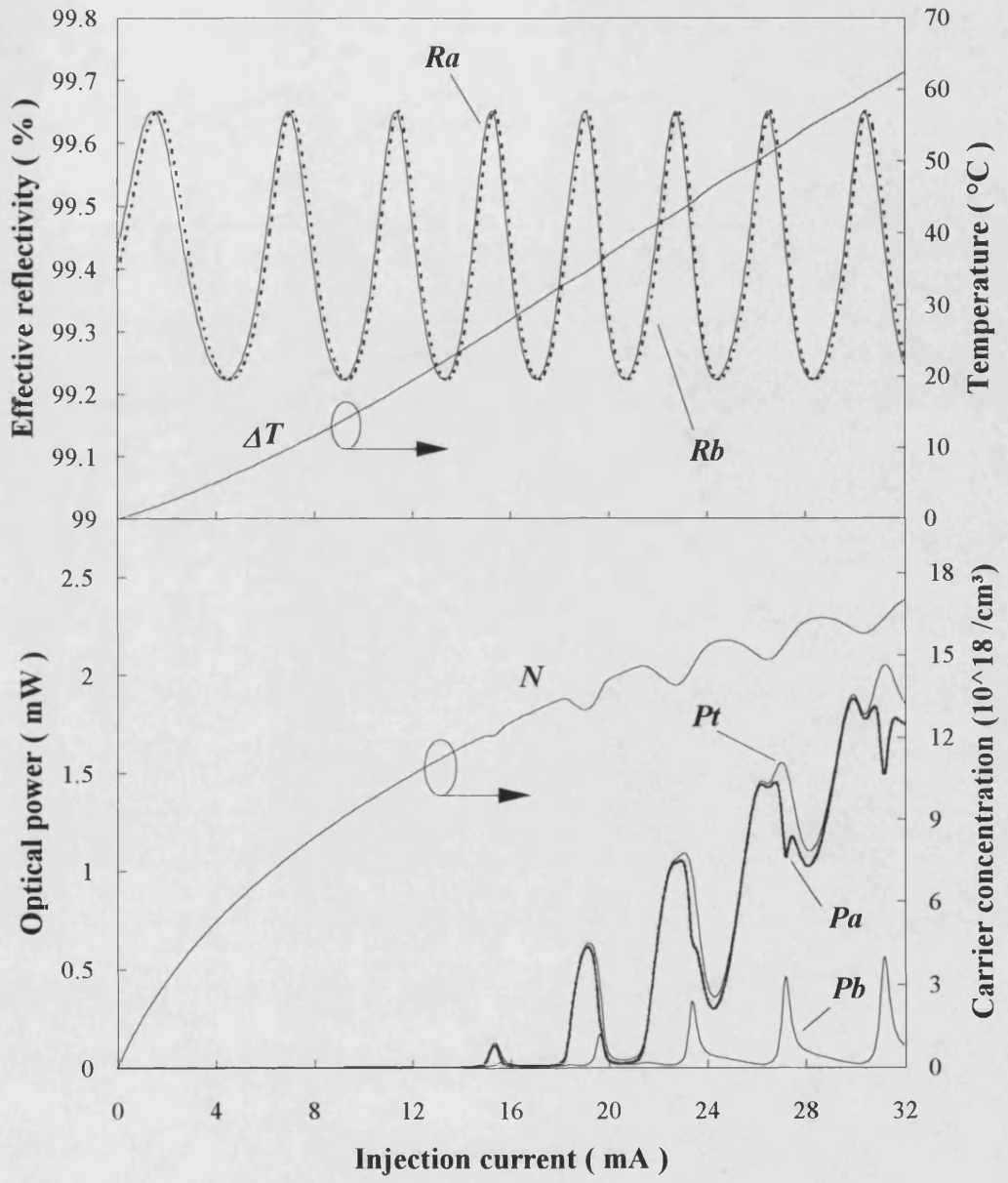

Figure 3.13: Simulation of VCSEL #1 in cw operation vs. current I illustrating:
- the effective output mirror reflectivity R_{eff},
- the junction temperature ΔT above the substrate temperature
- the optical output (total (P_t) and polarisation resolved (P_a and P_b)) and
- the carrier density N

Parameters: R_{sub} = 3.0% $\quad$ $\delta\alpha$ = 3.0 cm^{-1}
$\delta\lambda_{ab}$ = 0.2 Å $\quad$ β = 1 x 10^{-5}

It is also interesting to consider the effect of changing the spontaneous emission coupling factor (β) on the theoretical laser performance. Figure 3.14 illustrates the polarisation resolved L-I values of β from 1×10^{-5}, to 3×10^{-4} while $\delta\alpha$ is increased to 10 cm^{-1} in order to restrict mode *b* in power. The resulting P_a and P_t curves at high β are similar to those obtained experimentally, while the P_b curve better matches the experimental laser output below threshold, i.e. the sharp turn-on, at low β. However for the remainder of the modelling the spontaneous emission coupling is maintained at ~ 1×10^{-5} for both laser modes.

Investigating the polarisation response of the laser, we vary the wavelength splitting $\delta\lambda_{ab}$ from 0.1 Å to 0.4 Å while maintaining the modal loss difference at $\delta\alpha = 3$ cm^{-1} and β at 1×10^{-5}. The resulting L-I trend, as shown in figure 3.15, illustrates higher P_b peaks with increasing $\delta\lambda_{ab}$. This causes sharper reactive dips in P_a at the falling side of the kinks but does not affect the total output power P_t. This is explained by considering the competition between P_a and P_b. If their reflectivity curves are further out of phase, then the onset of P_b will be hindered by P_a only to a smaller extent and so it reaches higher maxima. It is obvious that above $\delta\lambda_{ab} = 0.3$ Å, the polarisations ratio of the output is very sensitive to the wavelength splitting. At the peaks of P_b, the optical loss difference is so small that it causes this sensitivity in output polarisation.

Alternatively, if the wavelength splitting is maintained at $\delta\lambda_{ab} = 0.2$ Å while the modal loss difference $\delta\alpha$ is varied between 1 cm^{-1} and 4 cm^{-1}, the effect is similar. Figure 3.16 illustrates that P_b remains weak at the peaks of P_a but rises rapidly at its expense just after these peaks only to subside again while P_a rises. Notice the resemblance this figure bears to the experimental L-I between 26mA and 28mA. It is possible then, that polarised modes of the first transverse order experience a smaller difference in modal losses or a larger spectral splitting, thus effecting the appearance of P_b at the third peak. Furthermore, using polarised optical feedback, the modal loss difference may be reduced, albeit artificially, to effect polarisation switching.

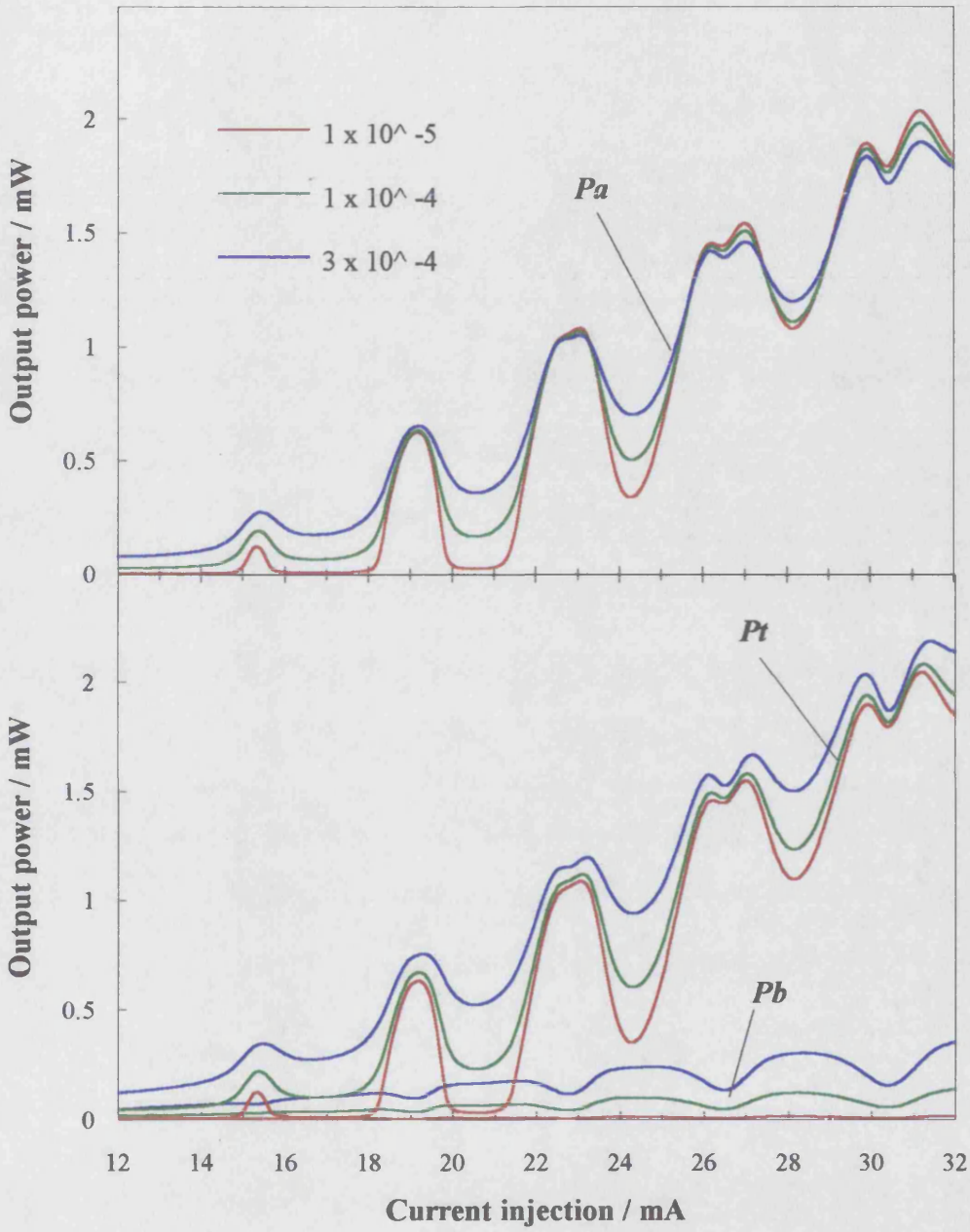

Figure 3.14: Numerical simulation of VCSEL #1 in cw operation vs. current I illustrating the carrier density N, the optical laser output total (P_t) and polarisation resolved (P_a and P_b))

Parameters: R_{sub} = 3.0% $\quad\quad$ $\delta\alpha$ = 10.0 cm^{-1}
$\delta\lambda_{ab}$ = 0.2 Å $\quad\quad$ β = 1 x $10^{-5} \rightarrow 3$ x 10^{-4}

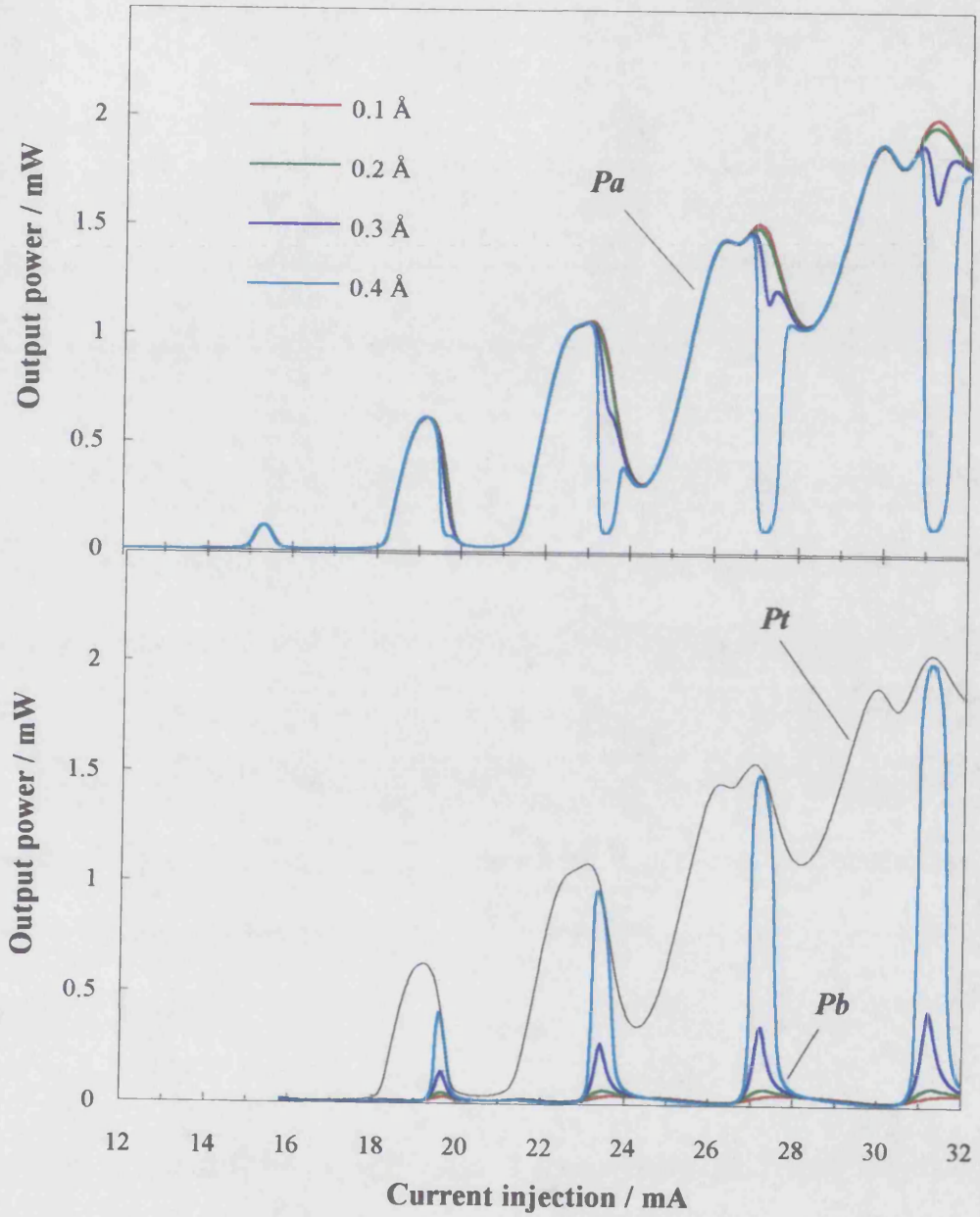

Figure 3.15: Numerical simulation of VCSEL #1 in cw operation vs. current I illustrating the carrier density N, the optical laser output total (P_t) and polarisation resolved (P_a and P_b))

Parameters: R_{sub} = 3.0% $\quad\quad$ $\delta\alpha$ = 3.0 cm^{-1}
$\delta\lambda_{ab}$ = 0.1 Å → 0.4 Å $\quad\quad$ β = 1 x 10^{-5}

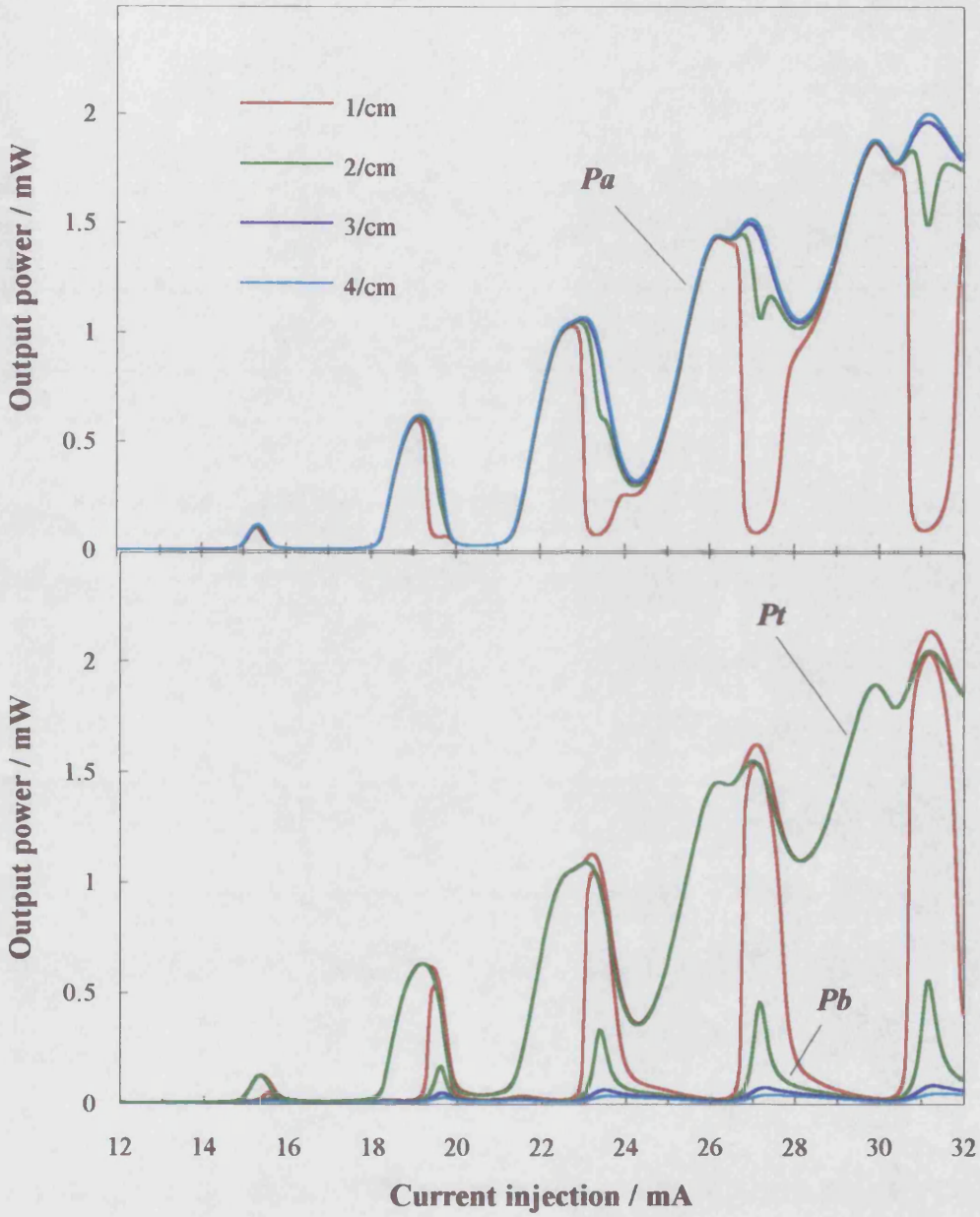

Figure 3.16: Numerical simulation of VCSEL #1 in cw operation vs. current I illustrating the carrier density N, the optical laser output total (P_t) and polarisation resolved (P_a and P_b))

Parameters: R_{sub} = 3.0% $\quad\quad$ $\delta\alpha$ = 1.0 cm^{-1} → 4.0 cm^{-1}
$\delta\lambda_{ab}$ = 0.2 Å $\quad\quad$ β = 1 x 10^{-5}

If we consider switching the polarisation of this VCSEL, or indeed a similar one, with optical feedback, then it is best to attempt that at the peaks of the suppressed mode P_b. It is the region near and just after the peaks of the dominant polarisation that would result in highest response to such feedback. This is the topic of the next chapter where experiments to induce cw and dynamic polarisation switching are carried out and the results are analysed theoretically.

3.4 Conclusion

The polarisation-resolved L-I behaviour of VCSEL #1 is attributed to residual gain anisotropy, cavity birefringence, a coupled cavity formed with the substrate and the inevitable device heating and wavelength drift. This coupled cavity VCSEL may be viewed as a simple, yet effective, 3-D integrated optical device consisting of an active laser and a passive element. A coupled cavity rate-equation model is constructed and used to estimate the internal laser parameters. It may also be used for designing VCSELs to display special coupled cavity effects. Because of interest in polarisation behaviour, the effects of several parameters on inducing cw switching are investigated. It is predicted that reinforcing the coupled cavity would deepen the L-I modulation and cause switching.

Similarly, it is anticipated that intensifying the cavity birefringence so as to widen the spectral splitting may be sufficient to cause polarisation switching. This may be achieved, alternatively, by reducing the loss of the suppressed polarisation, for example by applying suitable optical feedback to the laser. Such polarisation switching is anticipated to evolve near the peaks of the L-I curve and is pursued in the next chapter.

3.5 References

[1] D.G.Deppe, C.Lei, T.J.Rogers, B.G.Streetman: *Bistability in AlAs-GaAs-InGaAs vertical-cavity surface-emitting laser* Appl. Phys. Lett. **58** (23) 1991

[2] T.Fujita, A.Schremer, C.L.Tang: *Polarisation bistability in external cavity semiconductor lasers* Appl. Phys. Lett. **51** (6) 1987

[3] R.S.Geels, S.W.Corzine, J.W.Scott, D.B.Young, L.A.Coldren: *Low threshold planarised vertical-cavity surface-emitting lasers* Phot. Tech. Lett. **2** (4) 1990

[4] R.S.Geels, B.J.Thibeault, S.W.Corzine, J.W.Scott, L.A.Coldren: *Design and characterization of $In_{.2}Ga_{.8}As$ MQW vertical-cavity surface-emitting lasers* J. Quant. Elect. **29** 12 1993

[5] C.J.Chang-Hasnain, J.P.Harbison, C.Zah, M.W.Maeda, L.T.Florez, N.G.Stoffel, T.Lee: *Multiple wavelength tunable surface emitting arrays* J. Quant. Elect. **27** (6) 1991

[6] C.J.Chang-Hasnain, J.P.Harbison, G.Hasnain, A.C.Von Lehmen: *Dynamic, polarization, and transverse mode characteristics of vertical cavity surface emitting lasers* J. Quant. Elect. **27** (6) 1991

[7] L.A.Coldren, R.S.Geels, S.W.Corzine, J.W.Scott: *Efficient vertical-cavity lasers* Opt. Quant. Elect. special issue on microresonator devices **24** (2) 1992

[8] A.Von Lehmen, T.Banwell, L.Carrion, N.Stoffel, L.Florez, J.Harbison: *Pulsed and cw high temperature operation of $In_{.2}Ga_{.8}As$ strained layer vertical cavity surface emitting lasers* Elect. Lett. **28** (1) 1992

[9] J.D.Walker, D.M.Kuchta, J.S.Smith: *Vertical-cavity surface-emitting laser diodes fabricated by phase-locked epitaxy* Appl. Phys. Lett **59** 17 1991

[10] A.E.Siegman: *Lasers* Mill valley, Ca: Univ. Sci. Books 1986

[11] N.G.Basov: *The nonlinear optics of semiconductor lasers* proceedings of the Lebedev Physics Institute of the Academy of Sciences in the USSR, Nova, New York 1987, page 48

[12] A.Tomita, A.Suzuki: *Optical feedback effects on bistable laser diodes* Opt. and Quant. Elect. **19** Special issue on bistability in semiconductor lasers 1987

[13] H.Kawaguchi: *Absorptive and dispersive bistability in semiconductor injection lasers* Opt. and Quant. Elect. 19 Special issue on bistability in semiconductor lasers, 1987

[14] G.Roupars, A.Le Floch, G.Jezequel, R.Le Naour, Y.C.Chen: *The inhibition mechanism in Polarisation bistable semiconductor lasers* J. Quant. Elect. **23** (6) 1987

[15] Y.C.Chen, J.M.Liu: *Switching mechanism in polarisation-bistable semiconductor laser* Opt. and Quant. Elect. **19**, Special issue on bistability in semiconductor lasers, 1987

[16] T.Ogawa, Y.Ida, K.Hayashi: *Analysis of polarisation bistability of phase-shifted DFB laser due to TM light injection* J. Light. Tech. **10** (7) 1992

[17] G.P.Agrawal, N.K.Dutta: *Optical bistability in coupled-cavity semiconductor lasers* J. Appl. Phys. **56** (3) 1984

[18] Y.Mori, J.Shibata, T.Kajiwara: *Analysis of optical bistability in transverse-magnetic-wave-injected semiconductor lasers* J. Appl. Phys. **67** (5) 1990

[19] Y.C.Chen, J.M.Liu: *Polarisation bistability in semiconductor lasers* Appl. Phys. Lett. **46** (1) 1995

[20] D.S.Seo, J.D.Park, J.G.McInerney, M.Osinski: *Effects of feedback asymmetry in external-cavity semiconductor laser systems* Elect. Lett. **24** (12) 1988

[21] J.D.Park, D.S.Seo, J.G.McInerney, G.C.Dente, M.Osinski: *Low -frequency self-pulsations in asymmetric external-cavity semiconductor laser due to multiple feedback effects* Optics Letters **14** (19) 1989

[22] S.Jiang, Z.Pan, M.Dagenais, A.Morgan, K.Kojima: *Influence of external optical feedback on threshold and spectral charachteristics of vertical-cavity surface-emitting lasers* Phot. Tech. Lett. **6** (1) 1994

[23] T.Wipiejewski, K.Panzlaff, E.Zeeb, K.J.Ebling: *Characterisation of two-sided output vertical-cavity laser diodes by external optical feedback modulation* **SCL4.3** proceedings LEOS'93, California, USA

[24] D.Vakhshoori, J.D.Wynn, G.J.Zydzik, R.E.Leibenguth, M.T.Asom, K.Kojima, R.A.Morgan: *Top surface emitting lasers with 1.9V threshold voltage and the effect of spatial hole burning on their transverse mode operation efficiency* Appl. Phys. Lett. **62** (13) 1993

[25] C.J.Chang-Hasnain, M.Orenstein, A.Von Lehmen, L.T.Florez, J.P.Harbison, N.G.Stofel: *Transverse mode characteristics of vertical cavity surface emitting laser* Appl. Phys. Lett. **57** (3) 1990

[26] G.C.Wilson, D.M.Kuchta, J.D.Walker, J.S.Smith: *Spatial hole-burning and self-focussing in vertical-cavity surface-emitting laser diodes* Appl. Phys. Lett. **64** (5) 1994

[27] R.Michalzik, K.J.Ebeling: *Spatial hole burning in gain-guided vertical cavity laser diodes* **SCL3.1** proceedings LEOS'93, California, USA

[28] A.W.Snyder, J.D.Love: *Optical waveguide theory* Chapman and Hall, London, 1983

[29] A.H.Chern: *An introduction to optical fibers* McGraw-Hill, Japan, 1983

[30] A.K.Jansen van Doorn, M.P. van Exter, J.P.Woerdman: *Effects of transverse anisotropy on VCSEL spectra* Elec. Lett. **30** (23) 1994

[31] S.C.Rashleigh: *Origins and control of polarisation effects in single mode fibers* J. Light. Tech. **1** 1983

[32] T.Mukaihara, F.Koyama, K.Iga: *Engineered polarisation control of GaAs/AlGaAs surface-emitting lasers by anisotropic stress from elliptical etched substrate hole* IEEE Phot. Tech. Lett. **5** (2) 1993

[33] K.D.Choquette, R.E.Leibenguth: *Control of vertical-cavity laser polarisation with anisotropic transverse cavity geometries* Phot. Tech. Lett **6** (1) 1994

[34] K.D.Choquette, K.L.Lear, R.E.Leibenguth, M.T.Asom: *Polarisation modulation of cruciform vertical-cavity laser diodes* Appl. Phys. Lett. **64** (21) 1994

[35] K.D.Choquette, D.A.Richie, R.E.Leibenguth: *Temperature dependence of gain-guided vertical-cavity surface emitting laser polarisation* Appl. Phys. Lett. **64** (16) 1994

[36] S.Jiang, Z.Pan, M.Dagenais, R.A.Morgan, K.Kojima: *High-frequency polarization self-modulation in vertical-cavity surface-emitting lasers* Appl. Phys. Lett. **63** (26) 1993

[37] V.J.Mazurczyk, J.L.Zyskind: *Polarisation dependent gain in erbium doped fiber amplifiers* Phot. Tech. Lett. **6** (5) 1994

[38] C.R.Giles: *Suppression of polarisation hole burning-induced gain anisotropy in reflective EDFAs* Elect. Lett. **30** (12) 1991

[39] D.W.Hall: *Spectral and polarization hole burning in neodymium glass lasers* J. Quant. Elec. **19** 1983

[40] J.W.Scott, R.S.Geels, S.W.Corzine, L.A.Coldren: *Modelling temperature effects and spatial hole burning to optimise vertical-cavity surface-emitting laser performance* J. Quant. Elect. **29** (5) 1993

[41] J.J.Dudley, D.L.Crawford, J.E.Bowers: *Temperature dependence of the properties of DBR mirrors used in surface normal optoelectronic dvices* Phot. Tech. Lett. **4** (4) 1992

[42] J.Piprek, H.Wenzel, G.Sztefka: *Modelling thermal effects on the light vs. current characteristics of gain-guided vertical-cavity surface-emitting lasers* Phot. Tech. Lett. **6** (2) 1994

[43] B.Tell, K.F.Brown-Goebeler, R.E.Leibenguth, F.M.Baez, Y.H.Lee: *Temperature dependence of GaAs-AlGaAs vertical cavity surface emitting lasers* Appl. Phys. Lett. **60** (10) 1992

[44] N.K.Dutta: *Analysis of current spreading, carrier diffusion, and transverse mode guiding in surface emitting lasers* J. Appl. Phys. **68** (5) 1990

[45] R.Michalzik, K.J.Ebeling: *Modelling and design of photon-implanted ultralow-threshold vertical-cavity laser devices* J. Quant. Elect. **29** (6) 1993

[46] W.Jiang, J.Derickson, J.E.Bowers: *Analysis of laser pulse chirping in mode-locked vertical-cavity surface-emitting lasers* J. Quant. Elect. **29** (5) 1993

[47] W.Nakwaski, M.Osinski: *Thermal resistance of top-surface-emitting vertical-cavity semiconductor lasers and monolithic two-dimensional arrays* Elect. Lett. **28** (6) 1992

[48] W.Nakwaski, M.Osinski: *Current spreading and series resistance in photon-implanted top-surface-emitting lasers* **SCL4.5**, proceedings LEOS'93, California, USA

[49] R.S.Geels, S.W.Corzine, L.A.Coldren: *InGaAs vertical-cavity surface-emitting lasers* J. Quant. Elect. **27** (6) 1991

[50] J.E.Carroll: *Rate equations in semiconductor electronics* Cambridge University Press, 1985

[51] G.P.Agrawal, N.K.Dutta: *Semiconductor lasers* Van Nostrad Reinhold, 1993

[52] S.W.Corzine, R.S.Geels, J.W.Scott, R.H.Yan, L.A.Coldren: *Design of Fabry-Perot surface-emitting lasers with a periodic gain structure* J. Quant. Elect. **25** (6) 1989

[53] G.Shtengel, H.Temkin, T.Uchida, M.Kim, P.Brusenbach, C.Parsons: *Spontaneous emission factor and its scaling in vertical cavity surface emitting lasers* Appl. Phys. Lett. **64** (9) 1994

[54] Y.Suematsu, K.Furuya: *Theoretical spontaneous emission factor of injection lasers* Trans. IECE Japan **60** 1977

[55] F.Koyama, K.Morito, K.Iga: *Intensity noise and polarisation stability of GaAlAs-GaAs surface emitting lasers* J. Quant. Elect. **27** (6) 1991

[56] A.A.Bernussi, H.Temkin, D.L.Coblentz, R.A.Logan: *Effect of barrier recombination on the high temperature performance of quaternary multiquantum well lasers* Appl. Phys. Lett. **66** (1) 1995

[57] Y.A.Wu, C.J.Chang-Hasnain, R.Nabiev: *Transverse mode selection with a passive antiguide region in vertical cavity surface emitting lasers* Phot. Tech. Lett. **6** (8) 1994

[58] W.W.Chow, G.C.Dente, D.Depatie: *Saturation effects in semiconductor lasers* J. Quant. Elect. **23** (8) 1987

[59] H.D.Summers, P.Dowd, I.H.White, M.R.T.Tan: *Calculation of differential gain and linewidth enhancement factor in 980nm, InGaAs vertical cavity surface emitting lasers* Accepted for publication in Phot. Tech. Lett.

[60] J.Huang, L.W.Casperson: *Gain and saturation in semiconductor lasers* Opt. and Quant. Elect. **25** pp. 369-390 1993

[61] B.Lu, P.Zhou, J.Cheng, K.J.Malloy, J.C.Zolper: *High temperature pulsed and continuous-wave operation and thermally stable threshold characteristics of vertical-cavity surface-emitting lasers grown by metalorganic chemical vapor deposition* Appl. Phys. Lett. **65** (11) 1994

CHAPTER

4

All-optical Polarisation Switching

This chapter describes experimental and theoretical studies of the optical polarisation output of VCSEL #1. To begin with, the effect of a polarised optical feedback on the states of operation and polarisation of the laser is explored experimentally and analysed theoretically. Subsequently, a dynamic optical trigger is introduced to invoke continuous alternate switching in the output polarisation. The trigger frequency, determined by the external cavity optical length, is varied and polarisation switching is successfully achieved at frequencies exceeding 1GHz.

For a long time, semiconductor lasers have been observed to switch their polarisation states. Edge-emitting lasers may exhibit TE/TM switching under the influence TM optical injection [1] or feedback [2], injection current [3], temperature changes [4], and quantum well stress or strain [3]. By virtue of its cylindrical symmetry, an ideal VCSEL possesses a random polarisation state in the junction plane. A deviation from such symmetry induces a preferred polarisation axis [5-7], yet a high sensitivity of the polarisation state to variable influences is retained. VCSELs on the one hand exhibit polarisation axis rotation caused by thermal and carrier density changes [8], and on the other hand demonstrate axially fixed states of variable intensities. Power distribution may be modulated between the orthogonal axes of polarisation under the effects of temperature [9] and injection [10,11].

The process of dynamic polarisation switching is induced in semiconductor lasers in different ways. A laser may be modulated about the injection current where it switches polarisation [3]. This, however, is limited by the carrier response time and probably yields poorer results compared with intensity modulation techniques. Another method involves modulating an external cavity length [12,13] that forms a coupled cavity with the laser, where phase changes are sufficient to switch the polarisation. The well established method of using optical feedback (self-injection), commonly via a quarter wave plate, has yielded much faster operations. Such process was first reported by Davies, White and Carroll [14] and was accomplished in a twin-stripe edge-emitting laser obtaining a switching frequency of some 400MHz. A succeeding account by Loh *et. al.* [15] demonstrated a Fabry-Perot laser switched by a similar linear external cavity at 620MHz. Another endeavour by the same authors resulted in polarisation switching at 5GHz by resourcefully using a multisection ring external cavity [16].

VCSELs have also been subject to such attempts, such as reported by Pan *et. al.* who switched a polarisation bistable VCSEL at 6GHz [17,18]. Their result was achieved by merely contracting a linear external cavity to some 2.5 cm. In all the examples pointed out above, polarisation switching is induced at a point on the L-I curve where the two polarisations cross and switch over. A theoretical study of polarisation switching in semiconductor lasers using a travelling wave model has been carried out by Loh *et. al.* [19]. It indicates a risetime shorter than 10ps for the polarisation switching effect

which predicts the process to a reach ultra-high frequencies at hundreds of gigahertz. Experimentally, of course, this requires an optical cavity length of 3mm including all the optical components. The present limitation is then not fundamentally physical but solely technological. Edge-emitting lasers are not optically too long for ultra-high frequency switching, but require lenses and accurate external cavity alignment. VCSELs on the other hand, are designed for good coupling to external optical components even removing the need for lenses, e.g. substrate mirror coupled-cavity of VCSEL #1. They are also of a planar architecture and thus allow vertical integration of optical materials and devices. It is therefore envisaged that external cavities in the millimetre and submillimetre range are possible with VCSELs and will be realised in the near future.

The work below is motivated by two objectives. It aims at exploring the opportunity offered by the unique characteristics of VCSEL #1. At the kinks in the L-I, the suppressed polarisation is supported by the coupled cavity. The internal parameters of the laser, however, do not allow that polarisation to exist until the third kink. Hence, the effect of polarised optical feedback (POF) on the laser polarisation is investigated with particular interest in the kinks.

The second objective is to achieve dynamic polarisation switching. Externally triggered polarisation switching in edge-emitting lasers is facilitated by the low reflectivity of an uncoated or an antireflection (AR) coated facet. Such facets transmit a large proportion of the optical injection into the laser. VCSELs, however, may be limited by the low transmittance of the very high reflectivity distributed Bragg mirrors they incorporate, and therefore may be unsuited for such operation. Hence prior to attempting dynamic polarisation switching, it is necessary to assess the effect of POF on the laser state of polarisation.

4.1 Polarised optical feedback

VCSEL #1 is used for all experiments in this chapter and its L-I curve is presented in figure 4.1, for ease of reference. The following is a description of the experiments carried out to investigate the extent to which the polarisation behaviour of the laser may be influenced by self-injection.

4.1.1 Experimental arrangement

The following experiments with VCSELs are all conducted with thermal cooling of the laser at a stable temperature between 15°C and 17°C. As shown in figure 4.2, the laser is aligned in an external cavity using a horizontal HeNe beam such that the VCSEL output mirror is in the vertical plane. A 6.5 mm focal length laser diode lens collimates the laser beam for reflection by a high reflectivity (98%) external dielectric mirror. The mirror's glass substrate is wedge shaped to eliminate multiple external cavity formation. The polarisation state of feedback to the laser may then be controlled by rotating a polariser in the external cavity. A microscope slide functions as a low ratio beamsplitter allowing observations of the laser output with little disruption to the external cavity. Reflections from the latter are polarisation resolved by a second polariser (referred to as the analyser). The output is then focussed onto a detector and the electrical signal observed on an oscilloscope.

4.1.2 Electrical system

In order to prolong the laser life, the following measurements are obtained under pulsed operation. It is ensured, however, that the pulses are longer than a few microseconds to allow the settling of thermal transients. The differential electrical resistance of the laser above threshold is approximately 60 Ω, as can be derived from the V-I curve of figure 3.1. Matching the laser to standard 50 Ω transmission cables requires a resistance of an appropriate value in parallel with and in proximity to the laser as shown in figure 4.3. Therefore to measure the fraction of current injected into the laser only, a small probe resistance of 1.0 Ω is connected in series with the laser leaving the latter electrically slightly above ground. It is the probe resistor that is earthed rather than the laser in order to allow measurement of the voltage across it, and hence the current through it, using an oscilloscope. The circuit also includes three 0.28 V Ge diodes for protecting the laser from reverse pulses and a 4.7 V Zener diode as a barrier to high voltage drive. The laser submount is slotted on an electrically insulating perspex mount allowing the VCSEL to be driven with short square electrical pulses without the build-up of destructive electrical feedback.

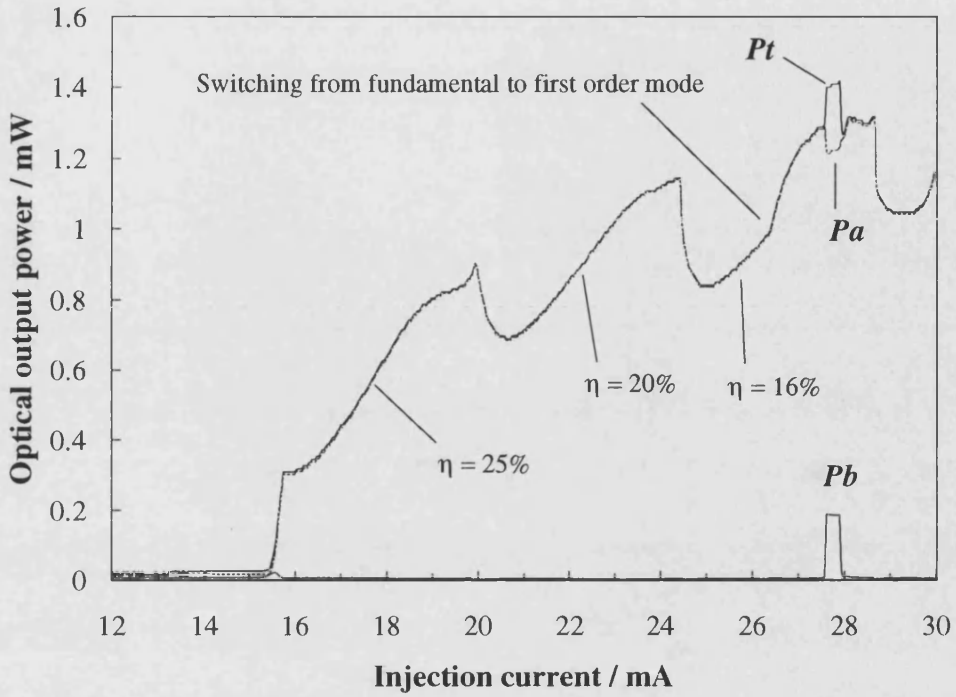

Figure 4.1: The light-current (L-I) characteristics of VCSEL #1

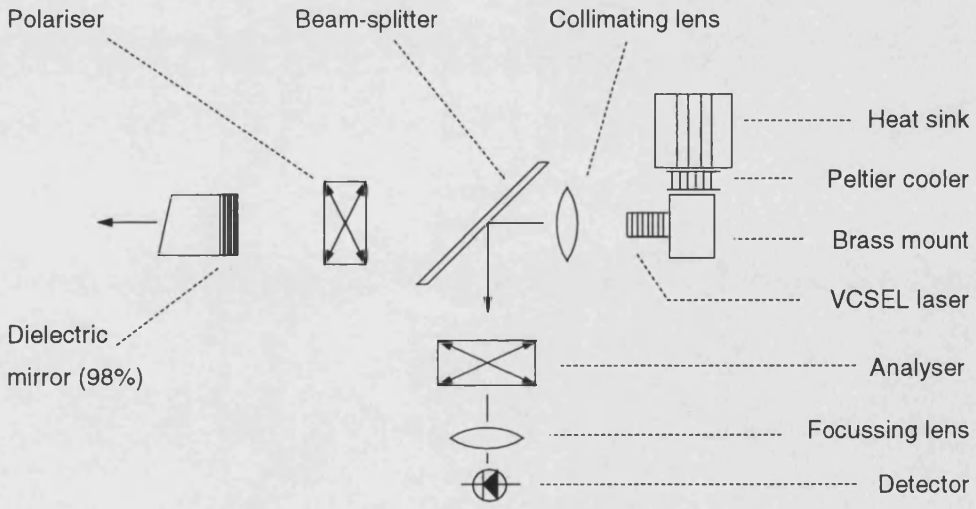

Figure 4.2: Experimental set-up for polarised optical feedback

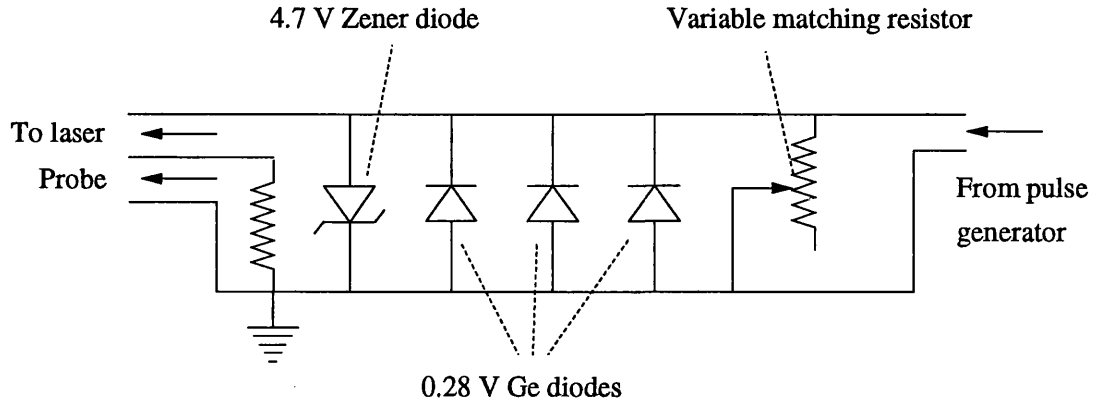

Figure 4.3: Matching circuit diagram for VCSEL #1

4.1.3 Laser output

Since the solitary laser output is predominantly P_a polarised, setting the polariser axis parallel to P_a only sustains the dominant polarisation causing no perceptible difference. Setting it parallel to P_b, however, reinforces the subdued polarisation causing a new equilibrium between the two polarisation states. Hence observing the laser output via the beamsplitter and the analyser provides an insight into the laser response. Oscilloscope trace plots of the P_a and P_b laser outputs under pulsed operation with and without external cavity P_b polarised feedback are obtained. They are plotted in figures 4.4 - 4.7 after adjustment for the beam splitter polarisation ratio and the analyser extinction ratio (polarisation crosstalk). The external cavity is 52.5 cm long and the plots are averages of 50 scans. The electrical pulses are around 45 μs long repeating at a period of 1 ms and reaching peak currents indicated approximately in the caption of each plot. The rising edge of each trace is therefore a rapid scan of the L-I curve up to the peak pulse current.

Figure 4.4 illustrates the laser switch-on at a slightly lower threshold current with the external cavity (14.8mA) than without (15.7mA). Whilst P_b is mostly minute, the power levels of P_a are not appreciably affected by the external feedback at that drive current. Figure 4.5, however, demonstrates the potential of external feedback to promote P_b within the laser at great expense to P_a and to the total output power, despite the high facet reflectivity characteristic of VCSELs. Figure 4.6 displays an insignificant P_b at 20mA, while figure 4.7 illustrates again the effect of polarisation redistribution at 23mA

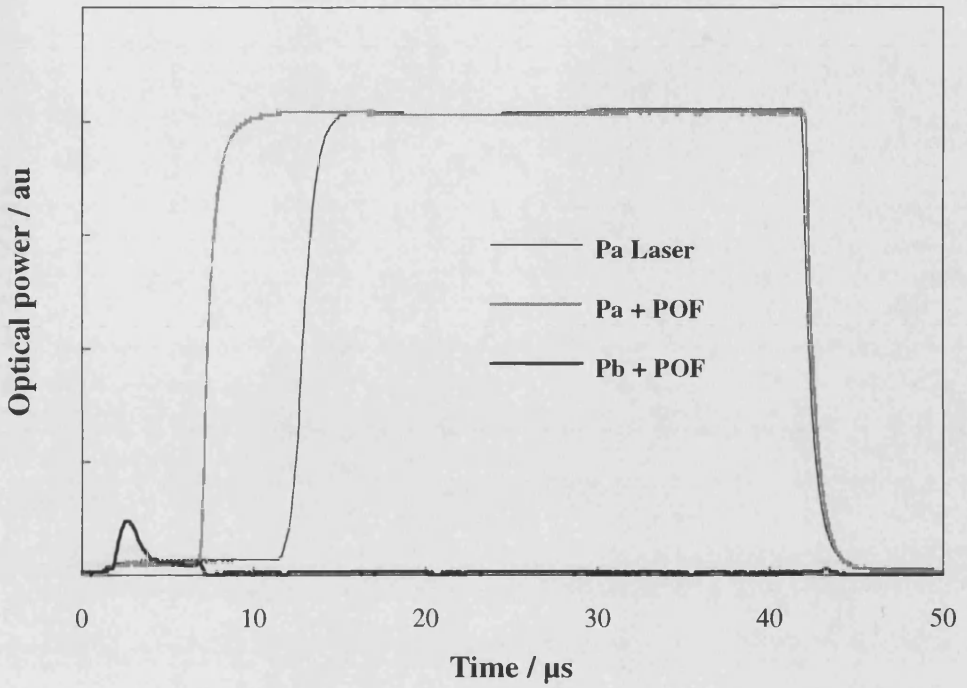

Figure 4.4: Laser response with and without POF (I ~ 16 mA)

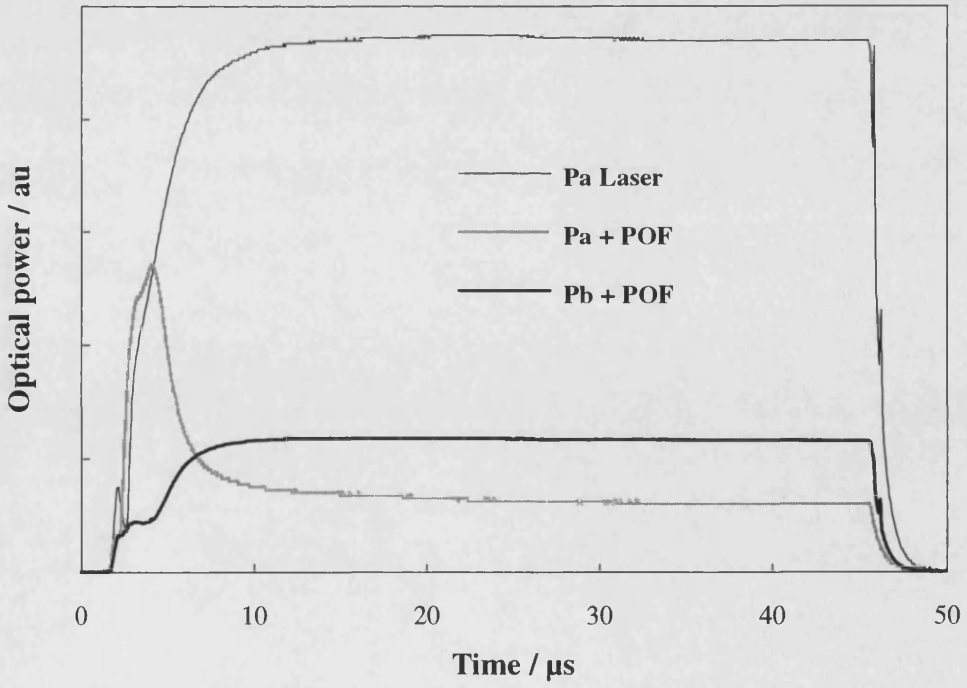

Figure 4.5: Laser response with and without POF (I ~ 18 mA)

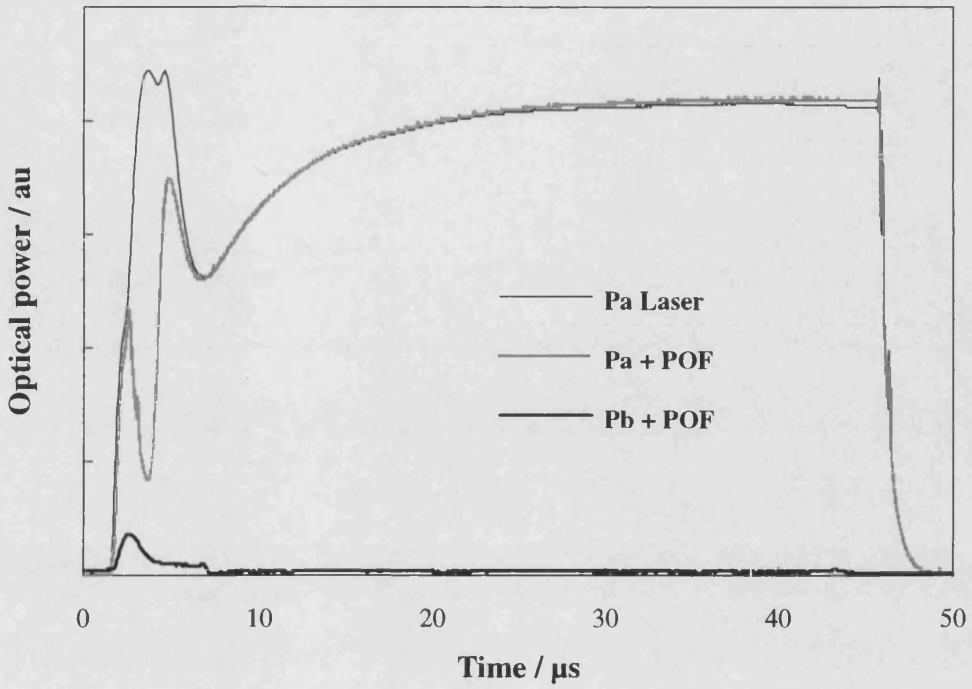

Figure 4.6: Laser response with and without POF (I ~ 20 mA)

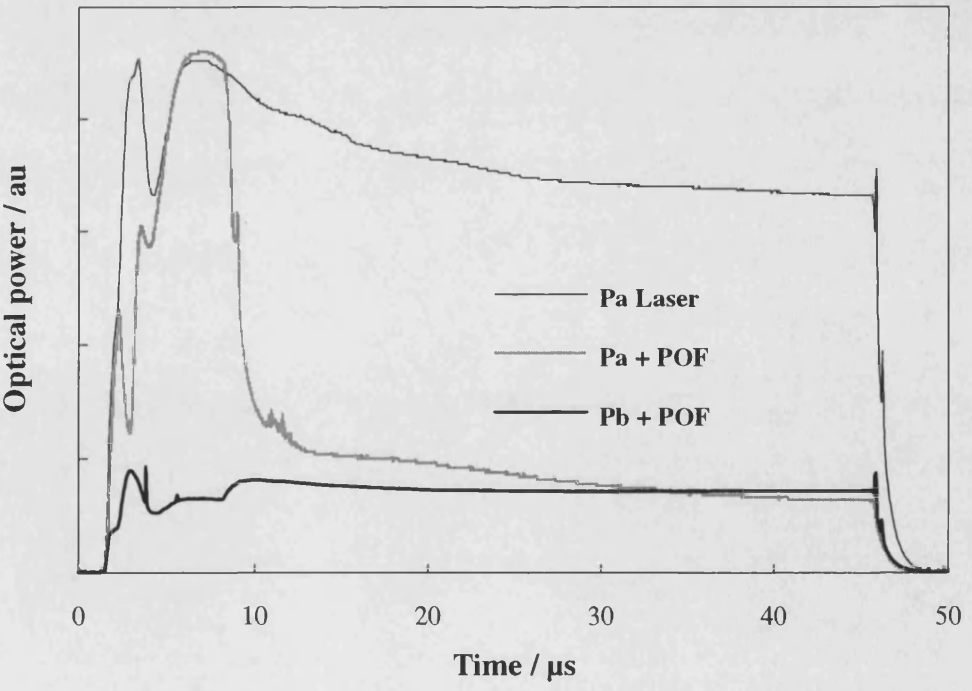

Figure 4.7: Laser response with and without POF (I ~ 23 mA)

and the total power reduction. The peak current corresponding to each figure was estimated from the probe pulse observed on the oscilloscope display. In both cases of figures 4.5 and 4.7 the optical output power was at its local maximum and was observed to decline at higher currents. The discrepancy between these peak currents and those of the cw L-I curve may be attributed to the pulsed injection and the ensuing dynamic thermal and wavelength chirp effects. Note that the polarisation switching effect is slightly greater in figure 4.5 than in figure 4.7. The plots illustrated are obtained at each particular current under the mechanical tuning (alignment) that maximises the switching effect. Furthermore, the best alignment differs slightly for different injection currents. This difficulty prevented the production of an L-I curve with POF.

The essential and noteworthy features of this behaviour are: *(i)* a large effect near the L-I kinks and a minute effect elsewhere; *(ii)* an incomplete but profound polarisation switching effect; *(iii)* a sharp reduction in total output power that correlates with polarisation switching; *(v)* repeatable and stable behaviour independent of the external cavity length; *(vi)* switching is restricted to a small current range of ~ 1mA near the peaks of the L-I curve. Such laser behaviour is unusual if not altogether novel [20]; modelling this operation therefore offers an insight into its origin.

4.2 CW polarisation switching model

The following theoretical consideration is an extension of the theory already developed in the previous chapter. It aims at understanding the effect of polarised optical feedback on the L-I output of the VCSEL in the continuous wave (cw) state. The problem of feedback from the substrate has been analysed and successfully applied as a coupled cavity which preserves coherence. However, semiconductor lasers including VCSELs are known for their sensitivity to small amounts of feedback [21]. There have been reports of extensive linewidth broadening under small amounts of feedback, hence causing coherence collapse. Miles *et. al.* [22] have found a reduction in the coherence length from 60 m to 30 cm at the meagre level of 0.2% feedback. Lenstra *et. al.* [23] reported that interferometer measurements of linewidth show a reduction in the coherence length by a factor of 1000 down to ~ 10 mm at the high power feedback levels

of 5% to 10%. Considering the high DBR mirror reflectivity of VCSELs, one expects small feedback levels (< 1%) and a coherence length comparable to 30 cm. An external cavity longer than ~ 15 cm then would qualify as a compound cavity [24,25].

Experimental evidence for the compound cavity feedback includes the following observations: ***(i)*** Once the external cavity is aligned, it is quite stable to angular tilt of the mirror and to general movement and oscillation of its position. If the mirror forms a coupled cavity with the laser, the operation state certainly would be very sensitive to such activity. ***(ii)*** The period of modulation of the L-I is around 4mA as caused by the very short substrate cavity (< 1mm). A coupled cavity some 50 cm long would undoubtedly modulate the L-I curve at a much higher rate. ***(iii)*** The positions of polarisation switching on the L-I curve are independent of the external cavity length, which proves the irrelevance of optical feedback phase. Hence in assessing the optical feedback effect on the laser operation, a compound cavity is assumed and all variables and functions will be in terms of optical intensity instead of amplitude. The polarisation switching cavity is illustrated in figure 4.8.

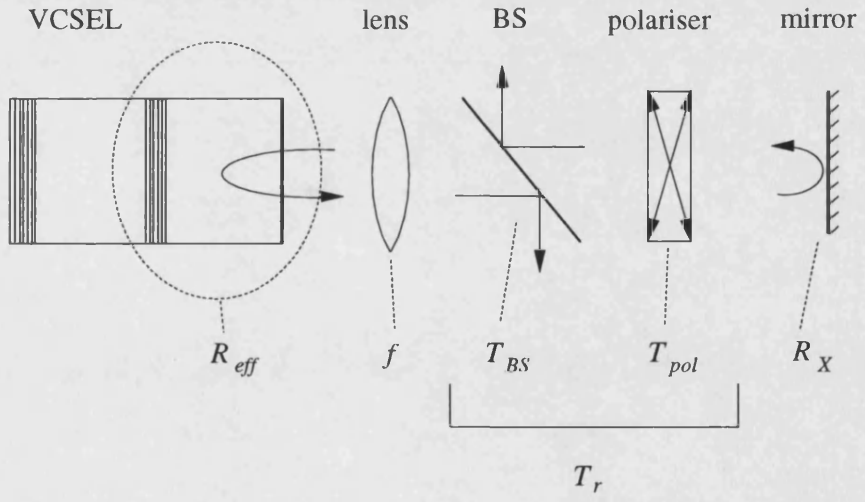

Figure 4.8: Compound cavity configuration for cw polarisation switching

The compound cavity is formed between the laser coupled cavity and the external mirror, both of which are highly reflective. For the purpose of numerical cw simulations, the compound cavity is condensed and represented by an effective reflectivity variable R_{FB}, as described below.

It can be shown that the laser experiences an effective compound cavity reflectivity of:

$$R_{FB} = R_{eff} + \frac{f(1-R_{eff})^2 T_r^2 R_X}{1-R_{eff} T_r^2 R_X} \quad \ldots\ldots \quad (4.1)$$

where $T_r = T_{BS}\, T_{pol}$ is the total optical loss within the cavity, f is the optical power coupling ratio from the lens to the laser cavity, T_{BS} is the transmittance of the beam splitter, T_{pol} is the transmittance of the polariser, and R_X is the external mirror intensity reflectivity. All these coefficients are in terms of the optical intensity rather than the optical field amplitude.

The polariser is aligned such that its polarisation axis is parallel to P_b and allows a large fraction T of that polarisation intensity through. It also allows a fraction X of the orthogonal polarisation intensity P_a through the extinction axis. For a good polariser, the extinction ratio X is very small, less than 10^{-3}. This ratio, however, is wavelength dependent and, while $T = 80\%$ for our polariser at 960nm, $X \sim 6\%$. Both beam splitter reflectivity T_{BS} and coupling factor f, are very high (> 95%) and contribute little to the external cavity losses.

During an external cavity round-trip therefore, P_b encounters a reflectivity of some 60% while P_a is subjected to a heavy loss returning a negligible 0.5%. Needless to say, most of the returned light is again reflected into the external cavity by the laser output mirror and the effect is that of multiple external cavity resonance.

If we were to take the effective transmission of our compound cavity as (1 - R_{FB}), we would be calculating the output through the external cavity mirror. Instead, we calculate the output from the beam splitter (*BS*) and in the process include the multiple reflections within the compound cavity. Thus the optical power incident on the detector from the beam splitter is :

$$P_{det} = \frac{P_{out}\, f R_{BS}}{1-R_{eff} T_r^2 R_X} \quad \ldots\ldots \quad (4.2)$$

where P_{out} is the laser output power calculated using equation (3.9) but replacing R_2 with R_{eff}, i.e. with no change from the model in chapter three. The main parameters in the equations are presented in table 4.1. Since figures 4.4 - 4.7 have been corrected for the reflectivity of the beam splitter R_{BS}, it is suitable to discard that factor from equation (4.2). However, whilst approaching unity for P_a on account of the high losses, the denominator is around 0.5 for P_b. In other words, extracting the output from the multiple resonance cavity artificially inflates the apparent P_b output by a factor of two.

Table 4.1: Compound cavity parameters

Parameter description	Symbol	Value
Reflectivity of external mirror	R_X	98%
Polariser transmissivity	T	80%
Polariser extinction ratio	X	6%
Coupling factor between lens and laser	f	95%
Beam splitter transmissivity	T_{BS}	96%

4.2.1 Simulation and results

When the output of the laser with POF as described above is compared with laser output without POF, it is found that the feedback makes no essential difference to the L-I. Merely adding the equations above to the model does not change its output markedly. Calculating the relative effect of the external cavity on the effective reflectivity, it is found that:

$$\frac{\delta R_{eff.b}}{R_{eff.b}} \approx 5x10^{-5} \approx -43\,dB \qquad \ldots\ldots \quad (4.3)$$

The actual power feedback is less significant still because the suppressed mode b does not reach its threshold in the simulation. It is not surprising then that this effect alone is not sufficient to model the laser behaviour. This conclusion is supported by the experimental observation that POF oriented along P_a has only a minute effect. Obviously, other processes need to be considered to account for the laser behaviour.

Highly nonlinear interactions caused by optical feedback and injection such as polarisation bistability [2,26] and wavelength bistability [27] were considered and their presence was investigated. This included increasing and reducing the injection current respectively to test for normal (S-shaped) bistability. Blocking the POF would also reveal the memory action of bifurcation bistability [28,29,30]. However, no such properties were found, thereby narrowing the options and leaving the possibility of high gain saturation, effecting high cross-coupling between modes [31].

The effect of feedback on semiconductor lasers has been studied experimentally [32] and theoretically [33] in several edge-emitting structures. It has been found that feedback effects on such lasers may be categorised into five regimes [34]: *(i)* At the weakest level of feedback of up to -80dB intensity ratio, the laser cavity is dominant. Depending on its phase, the feedback narrows or broadens the laser linewidth. *(ii)* A stronger feedback of up to -45dB, if in antiphase to the dominant laser mode, causes its apparent line splitting arising from rapid mode hopping. *(iii)* The third regime extends over a small range of feedback up to -40dB, when mode hopping is suppressed. This range appears as a transition between the surrounding regimes. *(iv)* Above -40dB feedback level, the effects displayed are independent of the feedback phase. Satellite modes appear around the main mode with a frequency separation similar to the laser relaxation oscillation [22]. Also the linewidth of the main mode broadens to tens of GHz because of coherence collapse induced by the feedback. *(v)* The final regime starts at a substantial feedback level of -20dB (1%), and typically requires an AR coated laser. There the external cavity dominates the laser operation often resulting in multimoded operation. At high feedback levels (~ 10%), each mode is highly coherent as observed form the linewidth narrowing.

The feedback level of our experimental configuration assigns the feedback to regime (ii), (iii), or (iv). However, as discussed above, since the laser output power and general behaviour is independent of the external cavity length, it is probable that the activity belongs to regime (iv) where coherence collapse occurs. The concept of coherence collapse induced by optical feedback offers a possible explanation to our observed laser behaviour. Theoretical accounts of such a phenomenon rely on the argument that the quantum fluctuations responsible for spontaneous emission are dominated as a noise source by fluctuations from the optical feedback [35,36]. Theory predicts that as

feedback from the external cavity does not correlate with the laser emission, it induces an effective rise in the spontaneous emission [23]. It is also reasonable to expect that the feedback is highly coupled to the laser mode in wavelength and even more so in angular distribution.

Let us assume that the feedback, imitating spontaneous emission, couples into and seeds a new mode of P_b polarisation. This mode may have unusual gain saturation characteristics effecting the observed behaviour. Investigating this possibility, the gain of equation (3.12) is replaced by:

$$G_i = \frac{c}{\mu} a_i (N - N_T)(1 - \varepsilon_{ii} P_i - \varepsilon_{ij} P_j) \quad \ldots\ldots \quad (4.4)$$

where ε_{ii} is the gain saturation factor of mode i and ε_{ij} is the gain suppression factor representing the effect of mode j on mode i. The previous model may be retrieved by setting all the gain saturation factors to 30×10^{-17} cm^3. A realistic L-I without feedback is modelled by maintaining a wavelength splitting ($\delta\lambda$) of 0.2 Å, a modal loss difference ($\delta\alpha$) of 10 cm^{-1} and a spontaneous emission coupling factor (β) of 5×10^{-5}. When the set of parameters in Table 4.2 is used, however, a marked reduction in the P_a optical power results, as illustrated in figure 4.9. At the delayed peaks of P_b and under constant current injection, the feedback effectively causes a polarisation switch. It is worth pointing out that a reported numerical simulation of first order mode polarisation switching in a bistable VCSEL under external injection indicates the possibility of optical logic gate operation [37]. Of interest also is a theoretical study by Buus [38] of possible unstable waveguiding in gain-guided VCSELs, particularly under small feedback.

The gain saturation values used in Table 4.2 to simulate polarisation switching may be justified by considering the lateral architecture of the gain region. It is conceivable that the focussed feedback light may deplete the thin gain region of carriers in a very localised manner. This could easily affect the saturation properties of the optical modes differently. Evidence for this behaviour may be observable in the real-time changes of the near field image of a VCSEL under varying injection current or optical feedback. The transverse mode distribution is readily influenced by small amounts of optical feedback, which is

not surprising considering the lack of a strong mode guiding mechanism in VCSELs. It should also be pointed out that using nonsymmetric gain saturation factors is a well established method for theoretically accounting for bistability in edge-emitting lasers.

As suggested in section 3.3 (chapter three), the spontaneous emission coupling (β_i) into a mode (i) seems to depend on the modal power P_i. The POF is possibly capable of redistributing the spontaneous emission coupling into each mode. It may also seed a new P_b such that it causes an extraneous gain saturation interaction between the two modes. Such gain interactions are well known to exist in various edge-emitting laser structures [28,39] and have been subject to many studies.

It is recognized that by involving gain saturation, the switching process demonstrated above also necessitates a change in the carrier concentration. Although this poses a limitation on the speed of response to the external trigger, such a process may be useful in low speed polarisation sensing applications. This possibility is considered in the next chapter, meanwhile the process of dynamic polarisation switching is further investigated below by introducing a trigger in the external cavity.

Table 4.2: Polarisation switching parameters

Parameter description	Symbol	Value without feedback	Value with feedback
Gain self-saturation of P_a	ε_{aa}	30×10^{-17} cm^3	50×10^{-17} cm^3
Gain self-saturation of P_b	ε_{bb}	30×10^{-17} cm^3	150×10^{-17} cm^3
Gain suppression of P_a by P_b	ε_{ab}	30×10^{-17} cm^3	150×10^{-17} cm^3
Gain suppression of P_b by P_a	ε_{ba}	30×10^{-17} cm^3	50×10^{-17} cm^3
Modal loss difference	$\delta\alpha$	10.0 cm^{-1}	4.0 cm^{-1}
Wavelength splitting	$\delta\lambda$	10.0 cm^{-1}	No change
Spontaneous emission coupling factor	β	5×10^{-5}	No change

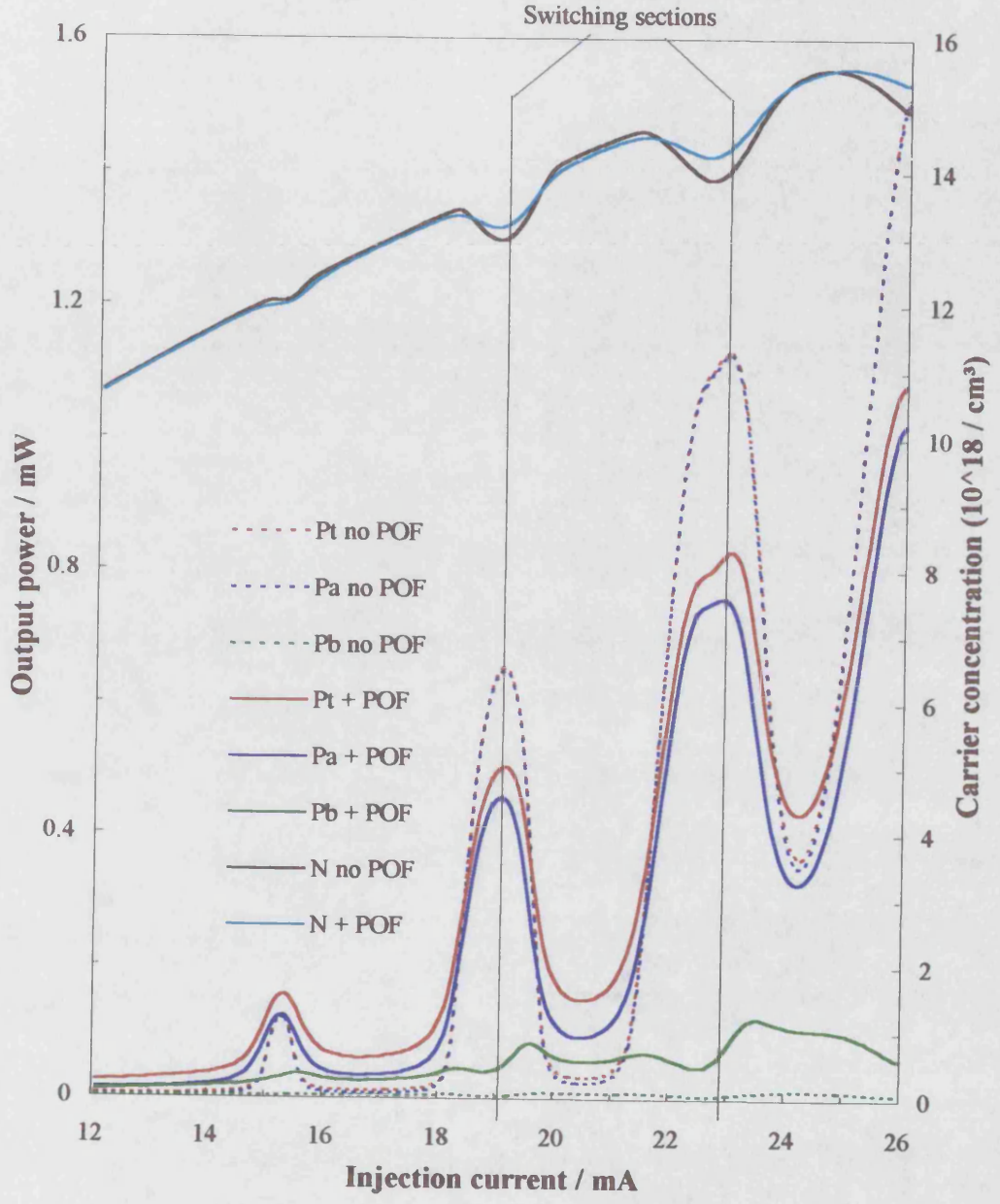

Figure 4.9: Theoretical cw L-I with and without POF illustrating cw polarisation switching

4.3 Dynamic polarisation switching

We have established that the influence of an external cavity on the cw polarisation state of the laser is enhanced at the L-I kinks. It is likely that dynamic polarisation switching is also enhanced under the same conditions. The dynamic process is activated by including a polarisation inverter in the external cavity to investigate this prospect.

4.3.1 Experimental arrangement

A quarter-wave retardation plate is used to convert the laser output from linear to circular polarisation, as illustrated in figure 4.10. Reflection by the mirror then inverts the sense of circular polarisation. The return pass through the quarter-wave plate converts the circular polarisation to linear polarisation orthogonal to that of the original laser output. Thus the combination of quarter-wave plate and mirror acts as a polarisation invertor. Switching is expected at twice the external cavity round-trip time, i.e. half the cavity frequency.

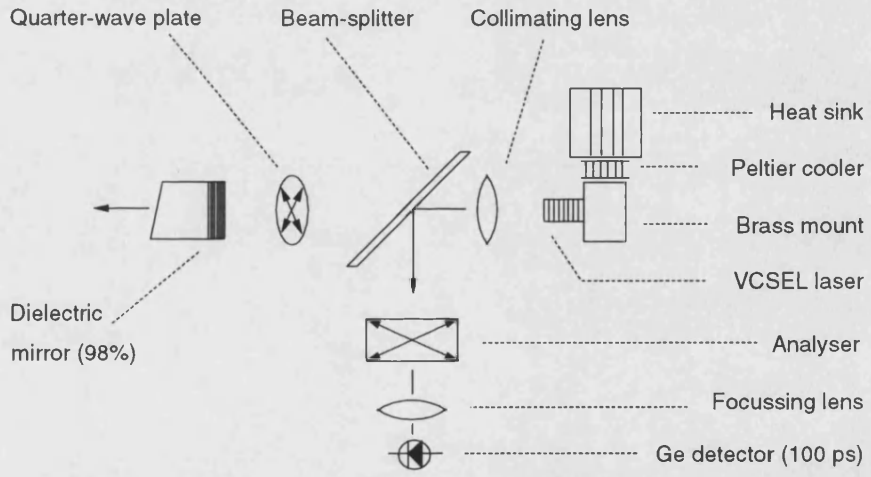

Figure 4.10: External cavity configuration for dynamic polarisation switching

The laser is driven with a constant injection current (dc bias) and therefore there is no requirement for a matching resistor. The output of a 100ps risetime germanium p-i-n diode detector is amplified by a 10 - 4200MHz minicircuit amplifier providing a gain of 28dB. The signal, however, is overwhelmed by low frequency noise of a larger amplitude preventing it from serving as a trigger signal and making an oscilloscope

unsuitable for displaying the signal. It is therefore observed in the frequency domain using an HP-8593A radio frequency (rf) spectrum analyser and phase information is lost.

4.3.2 High frequency switching

In the first instance low frequency (kHz) random pulses are observed on an oscilloscope trace as shown in figure 4.11. This represents chaotic switching [15] of the optical power caused by feedback instabilities and thus occurs mainly at the laser threshold current. Such phenomena are common in optical feedback systems and have been observed in polarisation switching experiments [16].

As expected from the observed effect of polarised external cavity feedback, dynamic polarisation switching takes place only at narrow current ranges ~ 1mA wide at 18mA and 23mA. Figure 4.12 illustrates the dynamic polarisation switching [40] rf spectrum of the laser output as monitored via the beamsplitter. The cavity length was initially set to 32.5cm yielding peaks at a frequency of 230 MHz and its odd harmonics. The two traces correspond to P_a and P_b as selected by the analyser and the difference in rf optical powers arises from the preferential reflectivity of the polarising beamsplitter R_{BS}. The presence of the odd harmonic frequencies is characteristic of square temporal pulses as expected from polarisation switching. Since bandwidth is sacrificed for the higher sensitivity this detector provides over faster photodetectors, the high frequency components are limited by the 100ps risetime of the detector.

Figure 4.13 shows the variation of the fundamental frequency electrical amplitude with analyser angle. The maxima at the extremes are the P_a and P_b pulses. They differ in amplitude as a result of the beamsplitter reflectivity polarisation sensitivity. This is proved later when observations are made through the mirror and both polarisations oscillate at equal amplitudes. Therefore, when R_{BS} is accounted for, the maxima become equal as necessarily expected from high frequency polarisation switching. The minimum near 60° is also a unique feature of this process and is the consequence of the antiphase relationship between pulses generated in P_a and P_b. When observed through a polariser set at an angle intermediate to the principal polarisation axes of the output, a negative interference of both sets of pulses is observed yielding a smaller pulse amplitude.

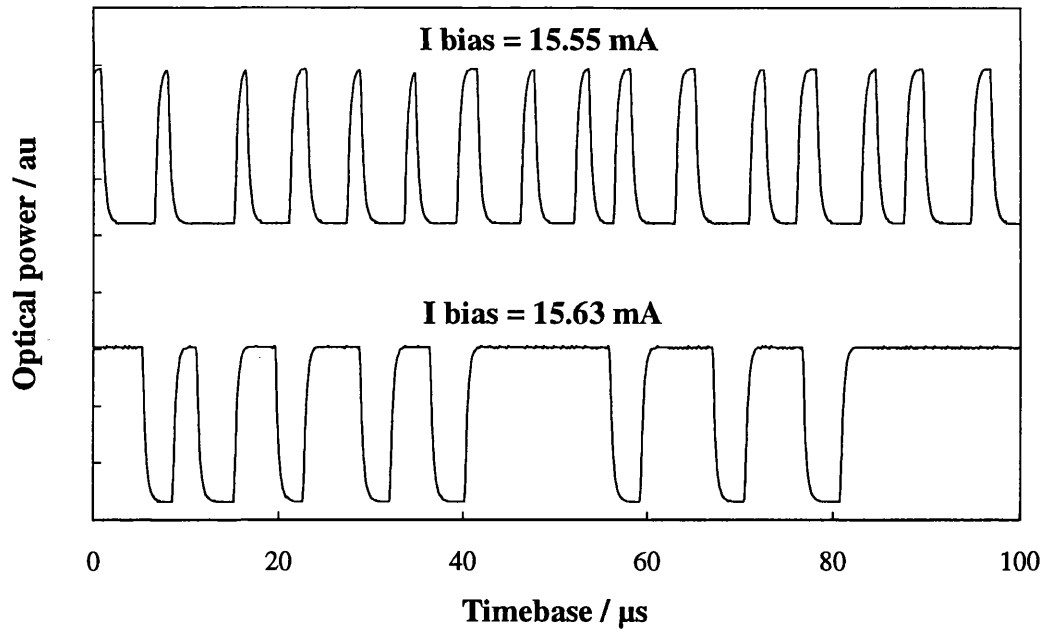

Figure 4.11: Chaotic switching of VCSEL near threshold under CW operation and external optical trigger

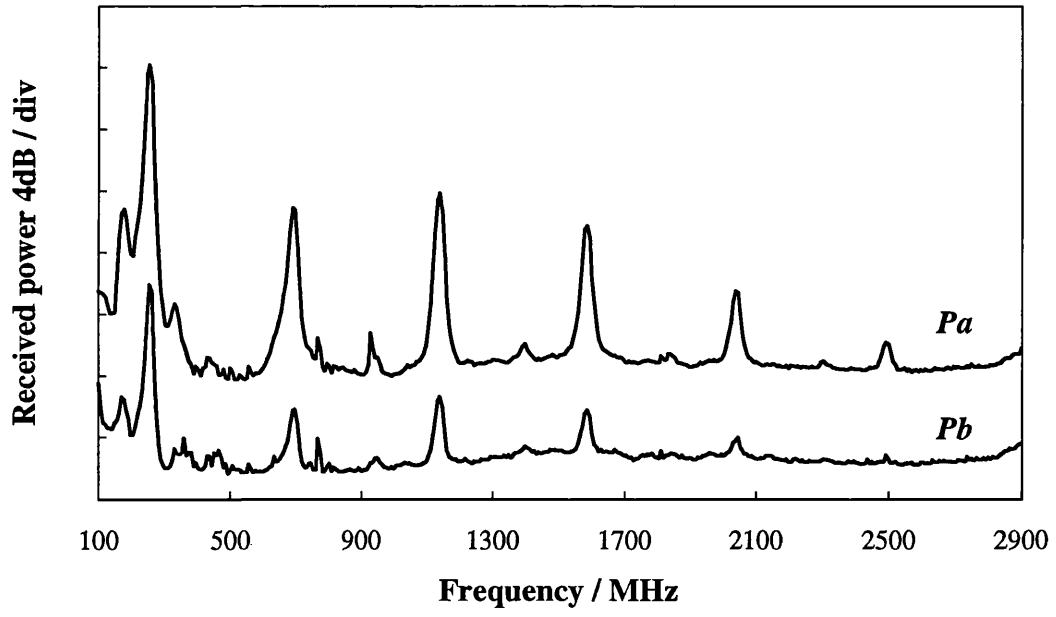

Figure 4.12: Output spectra of VCSEL in Pa and Pb demonstrating polarisation switching under external optical trigger at a fundamental frequency of 230MHz. The presence of odd harmonics indicates sqaure optical pulses

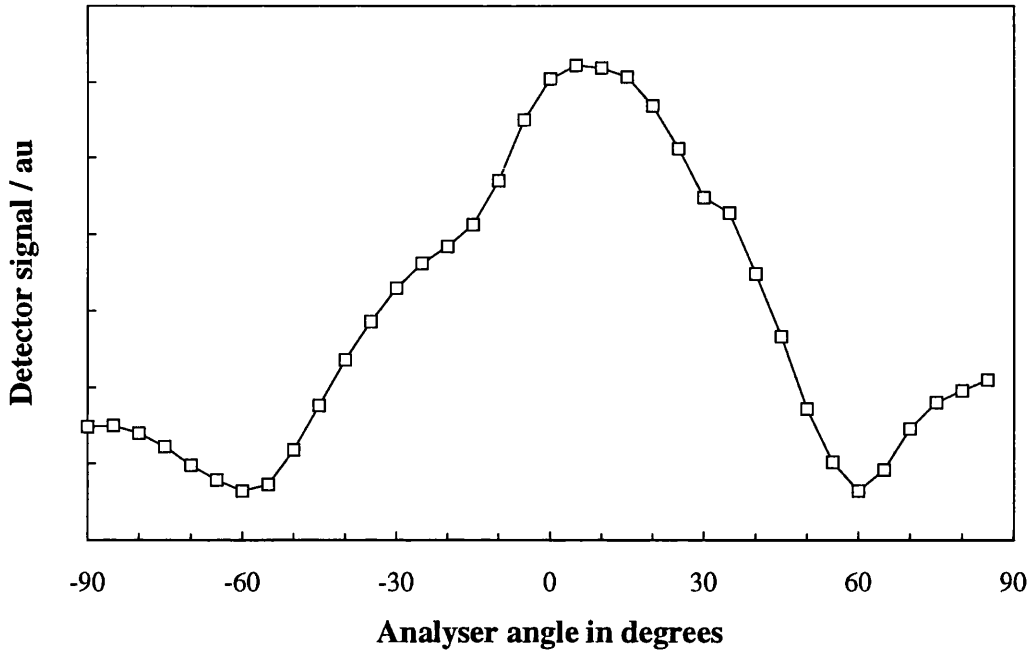

Figure 4.13: Polarisation switching signal amplitude vs. analyser angle

When the beamsplitter reflectivity, the amplifier gain and the detector sensitivity are accounted for, the observed electrical signal corresponds to an optical pulse oscillation intensity of 50 nW. This amplitude is much lower than the cw polarisation switching measurable in hundreds of microwatts. The rf switching process obviously involves only a tiny proportion of the available switching range. This is not surprising, considering that the modulation of P_b (δP_b) is caused by the modulation of feedback from P_a (δP_a) which itself is caused by δP_b. Furthermore and as the simulation predicts, the cw switching effect of the feedback is of the order of microwatts and the major change involves carrier concentration and thermal variations. RF trigger frequencies, however, do not allow the time for such changes and limit switching only to the optical profile redistribution, thus resulting in the small amplitude.

It is noticed that the rf spectrum around the fundamental frequency consists of multiple peaks. These peaks are a consistent feature of these traces and could not be eliminated by re-alignment of the external cavity or tuning of the injection current. These multiple

frequencies are multi-pass resonances of the external cavity. They have been observed in external cavity edge-emitting lasers and studied using a travelling wave model [41]. This phenomenon stems from resonant noise enhancement of the multi-pass signal. In the long term it may be eliminated by shortening the compound cavity to coupled cavity dimensions while simultaneously generating faster switching.

Higher frequency switching is subsequently generated by contracting the external cavity. This requires removing the beamsplitter and observing the output of the partial mirror through a second quarter-wave plate as illustrated in figure 4.14. Figure 4.15 illustrates the fundamental harmonics of the rf spectra of polarisation switching at 880 MHz, 912 MHz, 1 GHz and 1.1 GHz. The spectra are of the P_a outputs which are identical to their P_b counterparts. In this experimental configuration, setting the analyser at an angle mid-way between the polarisation orientations, i.e. at 45°, yields no signal. This proves that at high frequencies polarisation switching involves little switching in the total optical power because of the little variation in carrier density. Still faster switching at 1.5 GHz has been achieved but the fundamental peak became broad and low in power while higher harmonics were buried in noise as the detector bandwidth limit was reached. The frequency of switching in this experiment is therefore limited by the speed of the detector and is also close to the limit imposed by the physical sizes of the discrete optical components in the external cavity.

It is curious that the rf spectra obtained at other injection current ranges include all the frequency harmonics, odd and even, indicating mode-locking operation [42], chaotic behaviour [43] or self-pulsations [22], each feasibly induced by feedback. Such output is also obtained at appropriate drive currents when the quarter-wave plate is incorrectly oriented. It is worth pointing out that difficulties are encountered when attempting polarisation switching at frequencies between 400MHz and 600MHz. The rf spectrum shows multiple broad peaks at low power which may be associated with the transformation of the external cavity from a compound cavity to a coupled cavity. This frequency range corresponds to a cavity length of around 15 cm and may be further evidence of coherence collapse occurring in the laser.

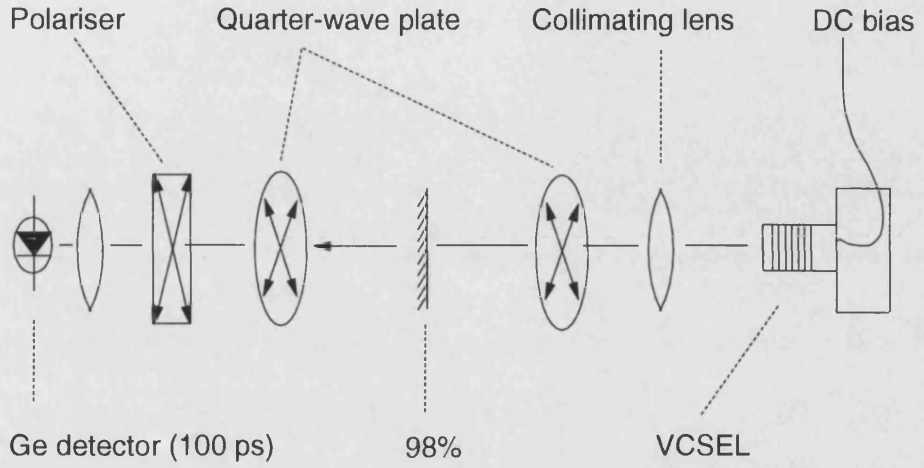

Figure 4.14: External cavity configuration for high frequency (gigahertz) polarisation switching

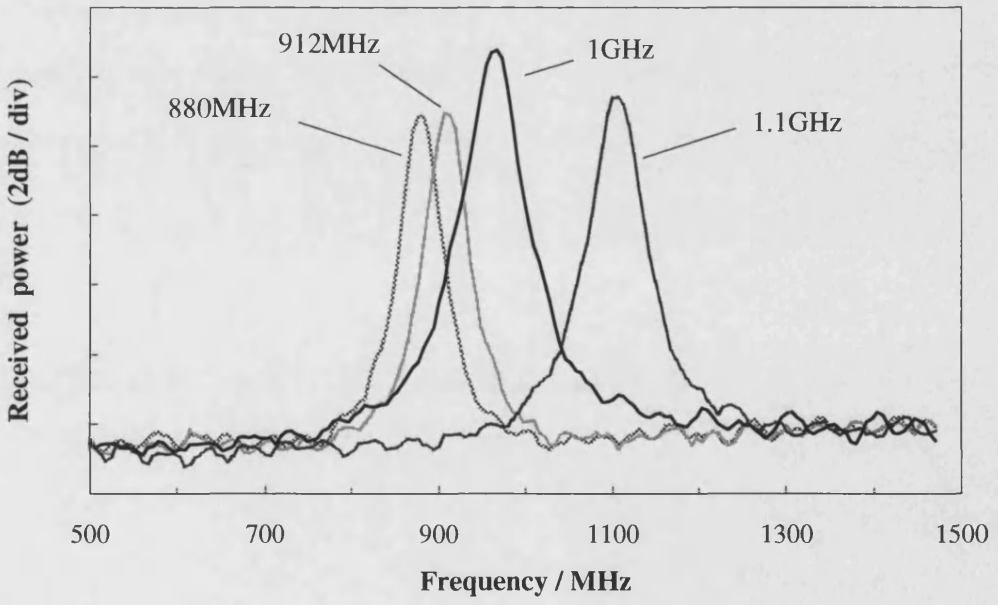

Figure 4.15: Fundamental harmonic frequencies of polarisation switching for short cavity lengths

Therefore, cw and rf polarisation switching is obtained only at the L-I kinks and is enhanced [40] by the coupled cavity effect and the compound cavity feedback together. To our knowledge, such a novel feedback system has not been applied to VCSEL devices. Regarding its applicability, this switching behaviour is on par with other feedback phenomena like feedback induced bistability.

Finally, it is interesting to note that, in our experiments, when other larger diameter VCSELs are triggered to perform similar polarisation switching, the effect is only that of chaotic self-pulsation. None of these lasers exhibited strong kinks as caused by a coupled cavity. Polarisation switching may therefore be enhanced further by proper design of a VCSEL to undergo deeper L-I kinks.

4.4 Conclusion

It has been shown that VCSELs are sensitive to polarised optical feedback, despite their high facet reflectivities, and are therefore suitable for dynamic polarisation switching. The switching amplitude has been enhanced by cross-saturation between polarised transverse modes. Dynamic all-optical polarisation switching is demonstrated at various frequencies reaching 1.5GHz and limited only by the bandwidth of a sensitive detector. The cavity length is also close to the limit imposed by the physical sizes of optical components in the external cavity.

The VCSEL's high sensitivity to polarised optical feedback in the cw state is accompanied by a sharp change in the total output power and in the carrier concentration. This opens opportunities for many applications that require highly sensitive lasers; one such application is investigated in chapter five.

4.5 References

[1] J.C.Cotteverte, G.Ropars, A.Le Floch, F.Bretenaker: *Polarization dragging in injected lasers* J. Quant. Elect. **30** (11) 1994

[2] T.Fujita, A.Schremer, C.L.Tang: *Polarization bistability in external cavity semiconductor lasers* Appl. Phys. Lett **51** (6) 1987

[3] H.Tanaka, J.Shimada, Y.Suzuki: *Highly efficient TE/TM mode switching of GaAsP/AlGaAs strained quantum well laser diodes* Appl. Phys. Lett. **64** (2) 1994

[4] H.Kawaguchi: *Absorptive and dispersive bistability in semiconductor injection lasers* Opt. and Quant. Elect. **19**, Special issue on bistability in semiconductor lasers 1987

[5] K.D.Choquette, R.E.Leibenguth: *Control of vertical-cavity laser polarization with anisotropic transverse cavity geometries* Phot. Tech. Lett. **6** (1) 1994

[6] T.Mukaihara, F.Koyama, K.Iga: *Engineered polarization control of GaAs/AlGaAs surface-emitting lasers by anisotropic stress from elliptical etched substrate hole* IEEE Phot. Tech. Lett. **5** (2) 1993

[7] K.D.Choquette, K.L.Lear, R.E.Leibenguth, M.T.Asom: *Polarization modulation of cruciform vertical-cavity laser diodes* Appl. Phys. Lett. **64** (21) 1994

[8] M.Shimizu, F.Koyama, K.Iga: *Polarization characteristics of MOCVD grown GaAs/GaAlAs CBH surface emitting lasers* Jap. J. of Appl. Phys. **27** (9) 1988

[9] K.D.Choquette, D.A.Richie, R.E.Leibenguth: *Temperature dependence of gain-guided vertical-cavity surface emitting laser polarization* Appl. Phys. Lett. **64** (16) 1994

[10] A.Chavez-Pirson, H.Ando, H.Saito, H.Kanbe: *Polarization properties of vertical-cavity surface-emitting lasers using a fractional layer superlattice gain medium* Appl. Phys. Lett. **62** (24) 1993

[11] A.Sapia, P.Spano, B.Daino: *Polarization switching in semiconductor lasers driven via injection from an external radiation* Appl. Phys. Lett. **50** (2) 1987

[12] P.Besnard, X.Jia, R.Dalgliesh, AD.May, G.Stephan: *Polarization switching in a microchip Nd:YAG laser using polarized feedback* J. Opt. Soc. Am. B **10** (9), 1993

[13] F.Robert, P.Besnard, M.Stephan, P.Paddon, A.D.May, D.Vakshoori: *Control of the polarisation state of a vertical cavity using polarised feedback* **CThI82** CLEO/Europe'94 proc. Amsterdam, The Netherlands 1994

[14] D.A.O.Davies, I.H.White, J.E.Carroll: *Applications of Polarisation switching in twin stripe semiconductor lasers* Jappanese J. Appl. Phys. **28** (3) 1989

[15] W.H.Loh, Y.Ozeki, C>L>Tang: *High-frequency polarization self-modulation and chaotic phenomena in external cavity semiconductor lasers* Appl. Phys. Lett. **56** (26) 1990

[16] W.H.Loh, A.T.Schremer, C.L.Tang: *Polarization self-modulation at multigigahertz frequencies in an external cavity semiconductor lasers* Phot. Tech. Lett. **2** (7) 1990

[17] S.Jiang, Z.Pan, M.Dagenais, R.A.Morgan, K.Kojima: *High-frequency polarization self-modulation in vertical-cavity surface-emitting lasers* Appl. Phys. Lett. **63** (26) 1993

[18] G.Z.Pan, S.Jiang, M.Dagenais, R.A.Morgan, K.Kojima, M.T.Asom, R.E.Leibenguth, G.D.Guth, M.W.Focht: *Fast polarization switching in a vertical cavity surface-emitting laser under optical injection* **SCL3.5** proc. LEOS'93 California, USA 1993

[19] W.H.Loh, C.L.Tang: *Numerical investigation of ultrahigh frequency polarization self-modulation in semiconductor lasers* J. Quant. Elect. **27** (3) 1991

[20] N.Badr and I.H.White, M.R.T.Tan, Y.M.Houng, S.Y.Wang: *Polarisation self-switching enhancement in a vertical-cavity surface-emitting laser by transverse modes saturation* **CWD6** proc. CLEO/Europe'94 Amsterdam, The Netherlands 1994

[21] Y.C.Chung, Y.H.Lee: *Spectral characteristics of vertical-cavity surface-emitting lasers with external optical feedback* Phot. Tech. Lett. **3** (7) 1991

[22] R.O.Miles, A.Dandridge, A.B.Tveten, H.F.Taylor, T.G.Giallorenzi: *Feedback-induced line broadening in cw channel-substrate planar laser diodes* Appl. Phys. Lett. **37** (11) 1980

[23] D.Lenstra, B.H.Verbeek, A.J.Den Boef: *Coherence collapse in single-mode semiconductor lasers due to optical feedback* J. Quant. Elect. **21** (6) 1985

[24] S.Jiang, Z.Pan, M.Dagenais, A.Morgan, K.Kojima: *Influence of external optical feedback on threshold and spectral charachteristics of vertical-cavity surface-emitting lasers* Phot. Tech. Lett. **6** (1) 1994

[25] J.L.A.Chilla, B.Benware, M.E.Watson, P.Stanko, J.J.Rocca, C.Wilmsen, S.Feld, R.Leibenguth: *Coherence of VCSEL's for holographic interconnects* Phot. Tech. Lett. **7** (5) 1995

[26] Y.Mori, J.Shibata, T.Kajiwara: *Optical polarization bistability in TM wave injected semiconductor lasers* J. Quant. Elect. **25** (3) 1989

[27] C.L.Tang, A.Schremer, T.Fujita: *Bistability in two-mode semiconductor lasers via gain saturation* Appl. Phys. Lett. **51** 1987

[28] H.Kawaguchi, I.H.White, M.J.Offside, J.E.Carroll: *Ultrafast switching in polarization-bistable laser diodes* Opt. lett. **17** (2) 1992

[29] H.Kawaguchi, T.Irie, M.Murakama: *Pitchfork bifurcation polarization bistability in laser diodes with external cavities* J. Quant. Elect. **31** (3) 1995

[30] H.Kawaguchi, I.S.Hidayat, Y.Takahashi, Y.Yamayoshi: *Pitchfork bifurcation polarisation bistability in vertical-cavity surface-emitting lasers* Elect. Lett. **31** (2) 1995

[31] G.Roupars, A.Le Floch, G.Jezequel, R.Le Naour, Y.C.Chen: *The inhibition mechanism in Polarisation bistable semiconductor lasers* J. Quant. Elect. **23** (6) 1987

[32] R.W.Tkack, A.R.Chraplyvy: *Regimes of feedback effects in 1.5μm distributed feedback lasers* J. Light. Tech. **4** (11) 1986

[33] H.Temkin, N.A.Olsson, J.H.Abeles, M.B.Panish: *Reflection noise in index guided InGaAsP lasers* J. Quant. Elect. **22** 1986

[34] R.W.Tkach, A.R.Chraplyvy: *Regimes of feedback effects in 1.5μm distributed feedback lasers* J. Light. Tech. **4** (11) 1986

[35] P.Spano, S.Piazzolla, M.Tamborrini: *Theory of noise in semiconductor lasers in the presence of optical feedback* J. Quant. Elect. **20** (April) 1984

[36] G.P.Agrawal: *Line narrowing in single-mode injection laser due to external optical feedback* J. Quant. Elect. **20** (May) 1984

[37] F.Prati, M.Travagnin, L.A.Lugiato: *Switching of transverse modes in vertical cavity surface emitting lasers* QMB5, EQEC'94 Amsterdam, The Netherlands

[38] J.Buus: *Unstable waveguiding in VCSELs* Phot. Tech. Lett. **6** (10) 1994

[39] P.McIlroy: *Calculation of the mode suppression ratio in Fabry-Perot, DBR and external cavity lasers* J. Quant. Elect. **26** (6) 1990

[40] N.Badr and I.H.White, M.R.T.Tan, Y.M.Houng, S.Y.Wang: *Enhanced polarisation self-switching in a vertical-cavity surface-emitting laser by gain saturation of transverse modes* Elect. Lett. **15** (30) 1994

[41] P.Besnard, B.Meziane, K.Ait-Ameur, G.Stephan: *Microwave spectra in external-cavity semiconductor lasers: Theoretical modelling of multipass resonances* J. Quant. Elect. **30** (8) 1994

[42] N.Onodera, Z.Ahmed, R.S.Tucker, A.J.Lowery: *Stability of harmonically driven mode-locked semiconductor lasers* Appl. Phys. Lett. **59** (27) 1991

[43] Y.Cho, M.Umeda: *Chaos in laser oscillation with delayed feedback; numerical analysis and observation using semiconductor laser* J. Opt. Soc. Amer. B **1** (June) 1984

CHAPTER

5

Bias Voltage of VCSEL Under Optical Feedback

This chapter details experimental work and a theoretical study investigating the effect of polarised optical feedback on the bias voltage across a VCSEL device. Its dependence on the injection current and the feedback polarisation is studied leading to novel results. These effects are modelled above and below threshold where they are also observed and correlated with the laser characteristics. This discovered phenomenon is used in an application-oriented experiment involving magneto-optic pattern detection where the signal is detected and enhanced by the VCSEL (patent application filed).

During the operation of a laser there is an equilibrium carrier concentration within the active region. This equilibrium exists between the carrier injection and the carrier depletion due to spontaneous, stimulated and non-radiative recombinations. If the depletion rate is altered by optical injection or feedback, the equilibrium will settle on a different carrier concentration within the active region. The laser junction voltage, however, being dependent on the carrier concentration, will follow its trend.

This reaction is inherent to the p-n junction and provides a mechanism for measuring the intensity of optical feedback or external optical injection into the laser that contributes to the recombination rate. VCSEL voltage dependence on the external optical injection wavelength has been investigated by others [1]. In this chapter the dependence on polarisation and intensity of feedback is examined experimentally and modelled theoretically.

An experiment is carried out using the effects discovered to detect the magnetic pattern encoded on a magneto-optical medium. Thus a laser may serve as a sensor as well as a source of optical power, reducing the component count and promoting the system performance in such an application.

5.1 Bias voltage measurement

The main objective of this section is to assess the effect of attenuating and rotating the polarisation of optical feedback on the bias voltage of the laser. The voltage response is also studied over a range of drive currents and the results are represented graphically in 3-D form for ease of visualisation. This response is also considered theoretically to determine its origin.

5.1.1 Experimental set-up

The experiments described in this section are carried out using VCSEL #1 which has been studied in chapters three and four. The relevant V-I and L-I curves are represented in figures 5.1 and 5.2 respectively and the latter demonstrates a laser threshold current of 15.7mA. The VCSEL is aligned in an external cavity with a laser diode lens for good optical coupling and a planar multilayer dielectric mirror for feedback. Figure 5.3

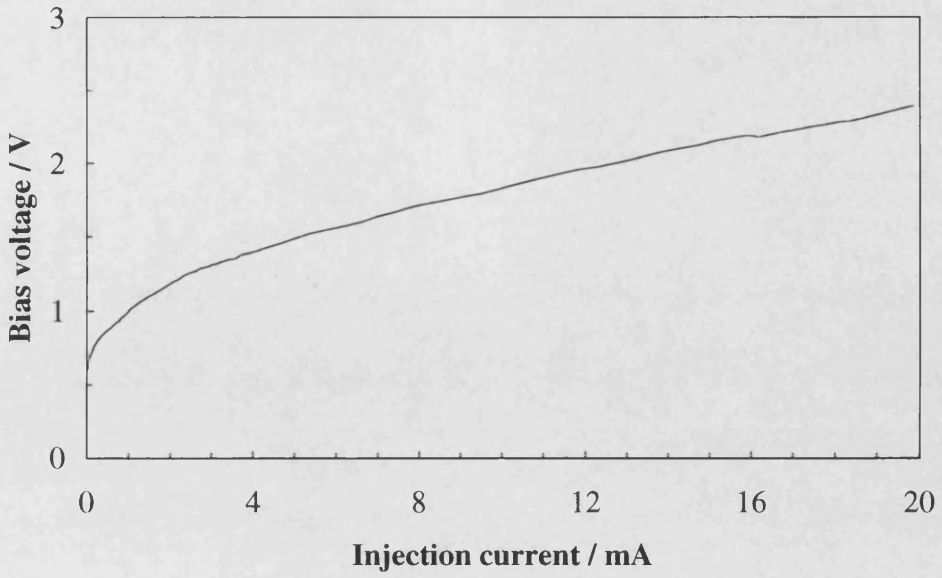

Figure 5.1: The voltage-current (V-I) characteristics of VCSEL #1

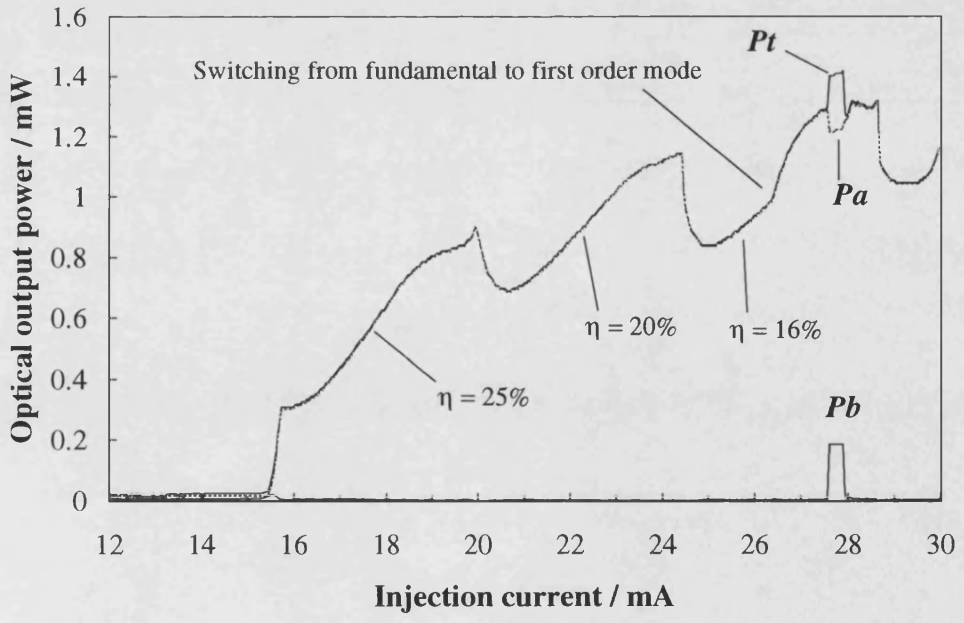

Figure 5.2: The light-current (L-I) characteristics of VCSEL #1

illustrates the feedback arrangement which reduces the laser threshold to 14.8mA. The polarisation of optical feedback is set by an intra-cavity polariser attached to a motorised rotating mount.

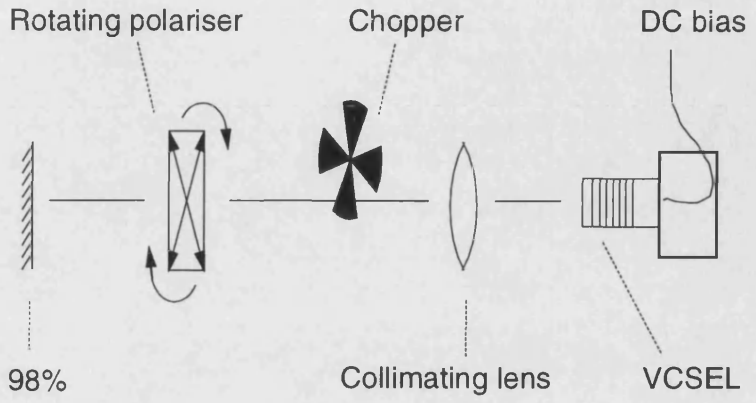

Figure 5.3: Experimental arrangement to measure the effect of polarised optical feedback on the laser bias voltage

The external cavity is chopped in an approximate square-wave pattern at some 400Hz causing a variation of the laser state of operation at the same frequency. This induces a small variation in the bias voltage which is amplified by the lock-in amplifier which uses the chopper signal for reference, see figure 5.4. This method of measurement yields higher sensitivity to variations in the signal compared to direct voltage measurements. Despite the chopper regularly interrupting the cavity, the low frequency of this occurrence qualifies the laser operation as alternate cw states.

The laser is driven from a voltage source through a fixed resistor (200 Ω) to limit the maximum current and a multi-turn variable resistor (2 kΩ) for fine control of the current (± 0.01mA). In order to avoid the problem of voltage fluctuation from mains driven sources, a 9 Volt battery is used.

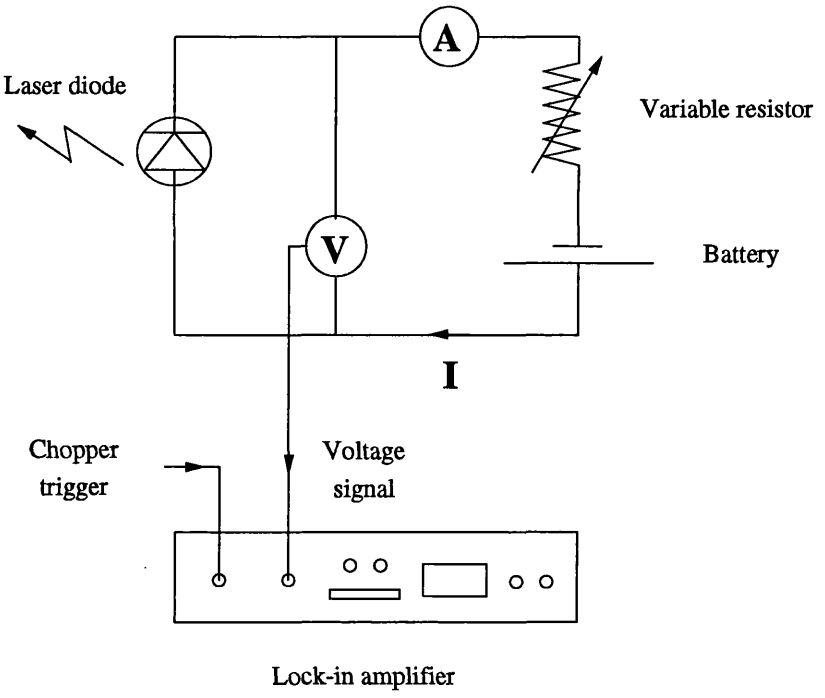

Figure 5.4: Electrical arrangement to detect small voltage changes across the VCSEL

5.1.2 Polarised optical feedback

The laser is driven dc while the polariser is rotated continuously through 90°. The amplifier output is recorded and the measurement is repeated at injection current increments of 0.5mA. Figure 5.5 is a 3-D stripe representation of the drop in bias voltage across the VCSEL caused by the presence of feedback over a range of drive currents from 10.5mA to 15mA. At 0° the polariser is parallel to the dominant laser polarisation P_a and conversely at 90° it parallels the suppressed optical polarisation P_b.

The effect of feedback on reducing the laser bias voltage appears at 11mA growing gradually with current. At 14.5mA it reaches a maximum amplitude of 10mV for feedback supporting P_a and 8mV for feedback supporting P_b. At a polariser angle range surrounding 45°, the drop in bias voltage is much smaller at a maximum of 3mV and appears at 13mA. Just above threshold, at 15mA, the effect is not only small but also opposite in polarity, i.e. the bias voltage increases when feedback is applied. This will be considered theoretically in section 5.2.2 below.

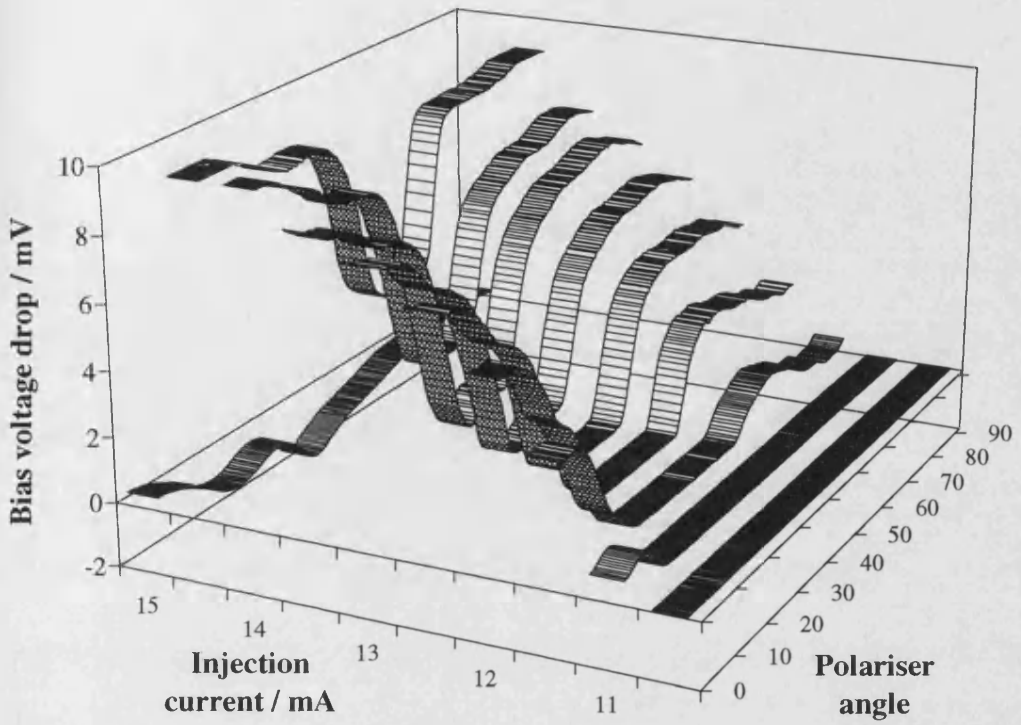

Figure 5.5: Variation of bias voltage with injection current and feedback polariser angle

5.1.3 Attenuated feedback

A second polariser (referred to as *the polariser*) is introduced into the external cavity between the first polariser (the attenuator) and the laser, as illustrated in figure 5.6. The attenuator then serves to attenuate the feedback while the polariser determines the feedback polarisation angle. The attenuator is continuously rotated from 0° to 90° for a series of polariser angles covering the same range at 10° increment steps. Figures 5.7 and 5.8 represent the drop in bias voltage at laser drive currents of 14.0mA (below threshold) and 14.8mA (just above threshold) respectively. Below threshold (figure 5.7) the drop in voltage has a maximum of 8mV and displays two peaks, one at (0°,0°) and another smaller one at (90°,90°). Above threshold (figure 5.8) the voltage rise is 2mV at the extreme and exhibits one peak at (0°,0°).

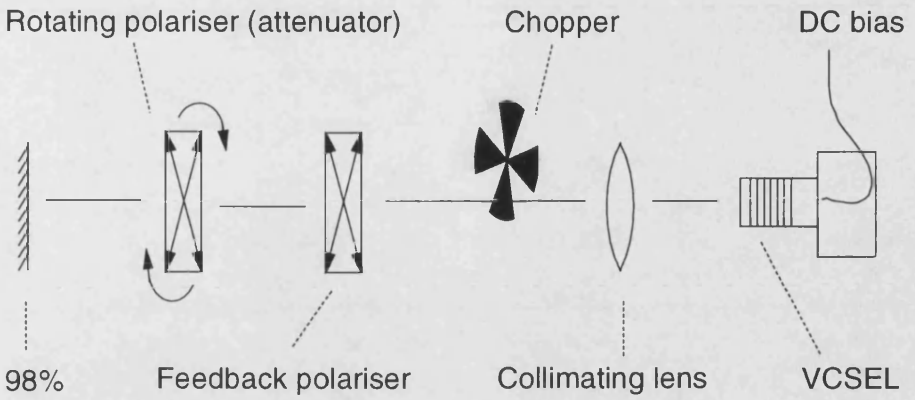

Figure 5.6: Experimental arrangement measuring the effect of attenuated polarised optical feedback on the laser bias voltage

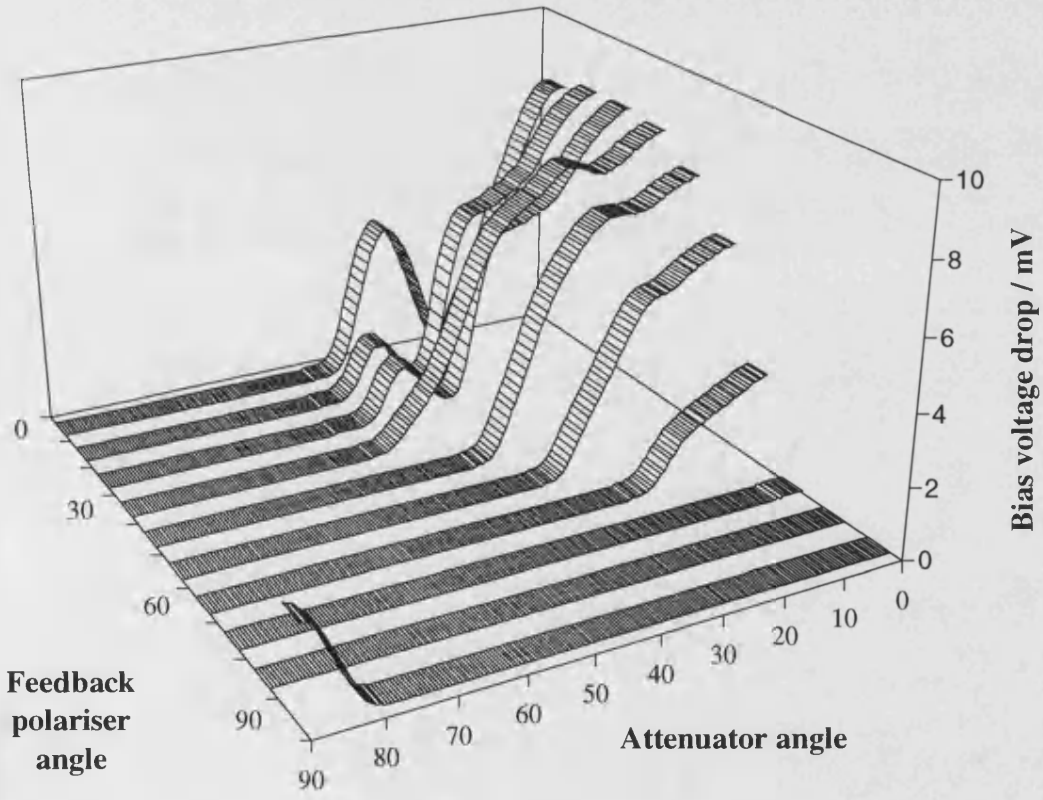

Figure 5.7: Drop in bias voltage under polarised and attenuated optical feedback at an injection current of 14.0mA (just below threshold)

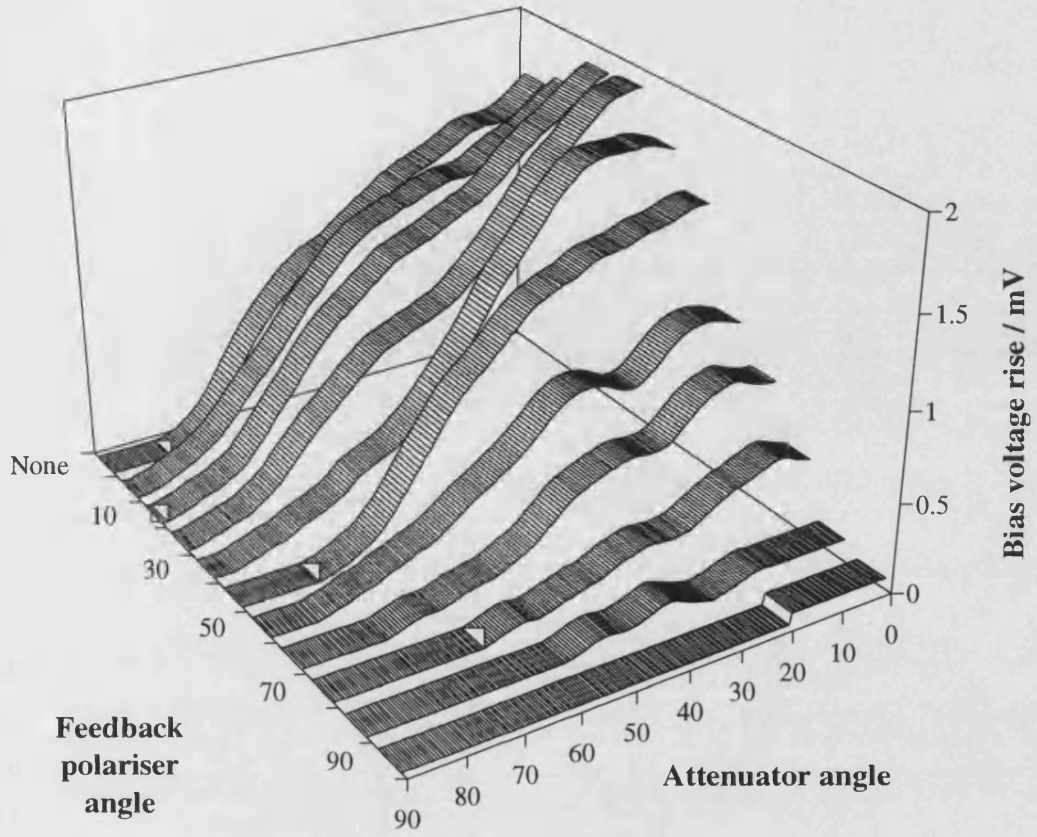

Figure 5.8: Rise in bias voltage under polarised and attenuated optical feedback at an injection current of 14.8mA (just above threshold)

5.1.4 Rotated polarised optical feedback

This section describes measurements similar to those carried out above in section 5.1.2 and illustrated in figure 5.3 but the polariser is replaced with a quarter-wave plate (QWP) to rotate the feedback polarisation. The combination of quarter-wave plate and mirror rotates plane-polarised light by twice the angle between the original polarisation and the principal axis of the quarter-wave plate. Multiple external cavity reflections add a further rotation per round trip. Therefore an offset angle of 45° rotates P_a to P_b and vice versa such that half of each output couples into the other.

The quarter-wave plate is rotated continuously from 0° to 90° for a series of laser injection currents at 0.5mA increment steps. Figure 5.9 illustrates the resulting laser bias voltage drop at drive currents from 9.5mA to 15mA. This graph is symmetric about the 45° line as expected from the action of a quarter-wave plate. It is also more logarithmic in shape than the corresponding measurement with the polariser in figure 5.5. Note the dip at 45° which evolves rapidly with current into a peak and later fades into the plateau. This indicates an initially weak optical coupling between P_a and P_b that rapidly improves preferentially even to self-coupling and remains level at higher currents below threshold.

Figure 5.10 is a representation of similar measurements above threshold where conversely the voltage rises and appears to be little influenced by rotating the quarter-wave plate. It may be noted, however, that the voltage rise in relation to the drive current resembles the L-I curve or perhaps the slope of the L-I curve. These matters are the subject of a theoretical discussion to follow in the next section. Note, however, the consistent dip in coupling between P_a and P_b at 45°.

5.2 Theoretical analysis

To the best of our knowledge the results described above are novel and particularly so for VCSELs. Before exploring intricate theoretical ideas concerning these results, however, it is prudent first to examine the electrical circuit used in the experiments and the possible sources of the voltage change. Consider the equivalent circuit in figure 5.11, where V_o is the battery voltage and V_b is the bias voltage measured across the VCSEL which is distinct from V_{pn}, the p-n junction voltage of the VCSEL. Each DBR mirror stack imposes an electrical resistance to the current injected into the laser. The total

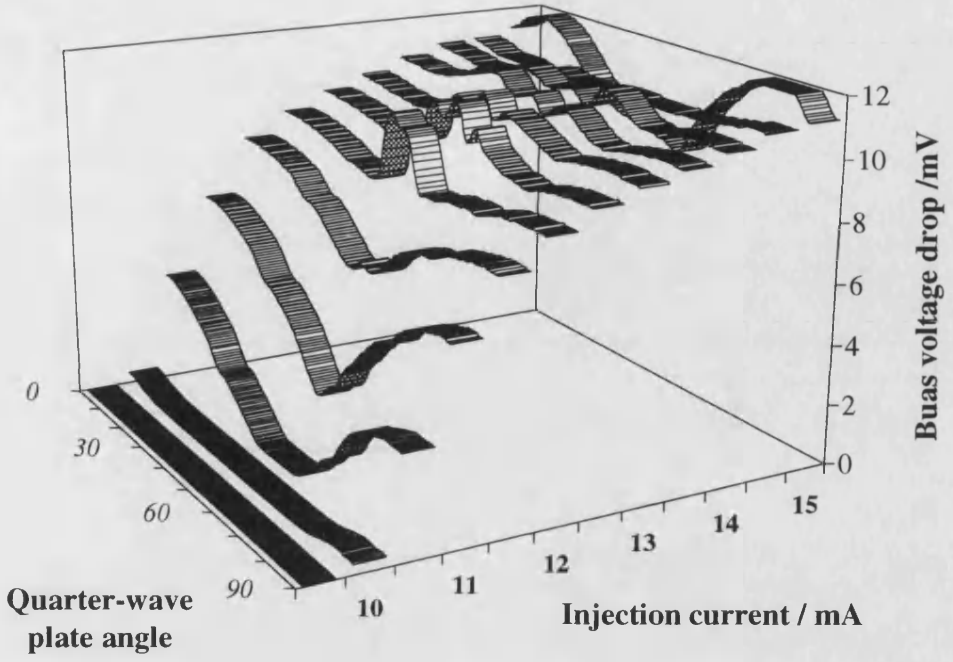

Figure 5.9: Drop in bias voltage under varied quarter-wave plate angle at a series of injection currents mainly below threshold

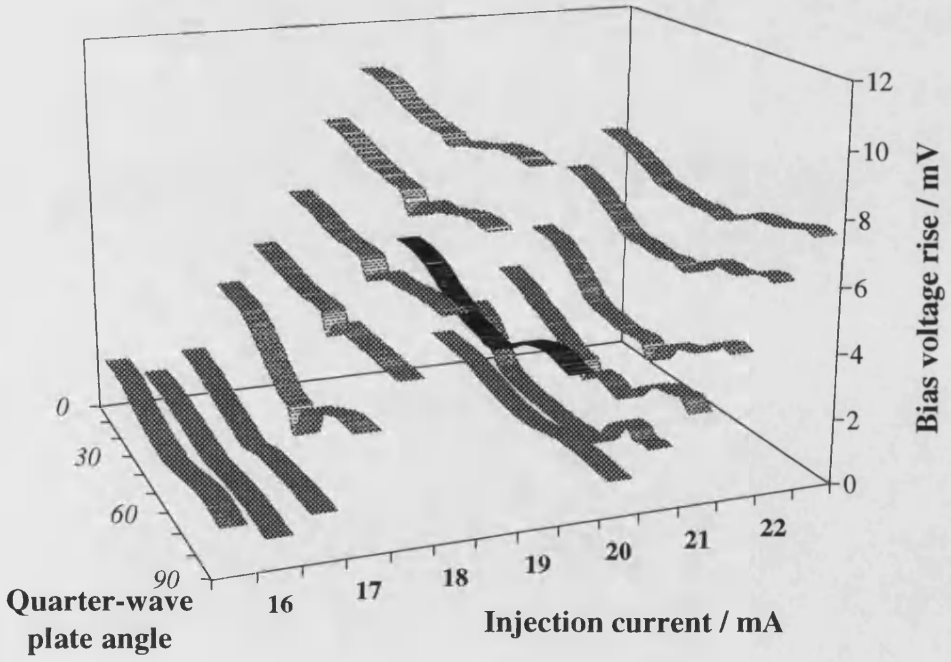

Figure 5.10: Bias voltage rise under varied quarter-wave plate angle at a series of injection currents above threshold

differential resistance R_M of the laser is represented by the slope of the laser's V-I curve of figure 5.1 assuming a constant junction voltage and is determined to be ~ 65 Ω. The injection resistance is expressed by R_D and is varied from 2.2 kΩ down to 200 Ω.

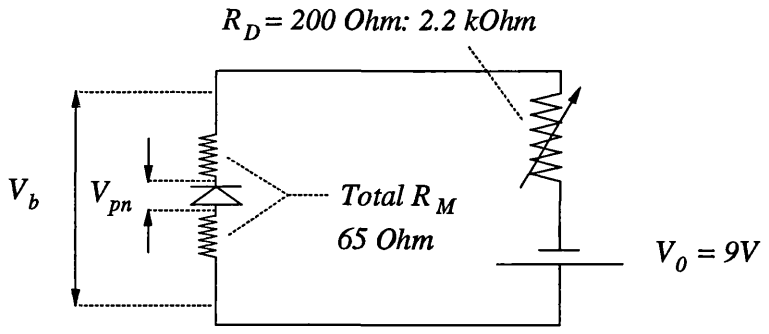

Figure 5.11: The electrical circuit representing the voltage source, drive resistance, DBR mirror resistance, laser bias voltage and p-n junction voltage

The bias voltage is the sum of the junction voltage and the potential drop across R_M:

$$V_b = V_{pn} + I R_M \quad \ldots\ldots \quad (5.1)$$

From an electrical perspective there are two mechanisms for the change in bias voltage: the junction voltage V_{pn} and the combined mirror resistance R_M. Assuming the latter is altered slightly and ignoring the second order effect of the change in drive current, the change of voltage is $\delta V_b = I\,\delta R_M$. Hence a drop in voltage of 10mV at a drive current of 14mA may be caused by a drop in R_M smaller than 1Ω. The assumption is that optical feedback causes more optical power to be released by the laser reducing its temperature and R_M.

In the absence of further information on the thermal dependence of the DBR mirror resistance, it is estimated that a temperature change of the order of a few degrees is necessary for the required change R_M. Let us re-use the temperature equation of (3.14):

$$\Delta T = Z_s (VI - P_{out})\, e^{\frac{-\Delta T}{250°C}} \quad \ldots\ldots \quad (3.14)$$

where the thermal impedance Z_s of VCSEL #1 is estimated at 1.0°C/mW. A simple calculation reveals that emitting 10μW more of optical power cools down the laser device by 0.01°C, quite unlikely to reduce R_M by 1Ω. Even including the fall in electrical power

dissipated in the device cannot account for cooling of the device of the order of 1°C.

The change in bias voltage must therefore originate from the junction voltage V_{pn}. It is expected that an increase in the optical power output may reduce the carrier concentration sufficiently to reduce the junction voltage and the bias voltage by 10mV. One study [1] of the bias voltage of an edge-emitting laser under injection locking demonstrates a voltage change smaller than ± 20μV. This is obtained under an optical power injection coupling of ~ 30nW which corresponds to ~ 1×10^{-5} of the injected laser output power. The polarity of the voltage change depends on the injected wavelength detuning relative to the lasing wavelength as reproduced in figure 5.12. When the injection wavelength equals the injected laser wavelength, the laser suffers a voltage drop of ~5μV.

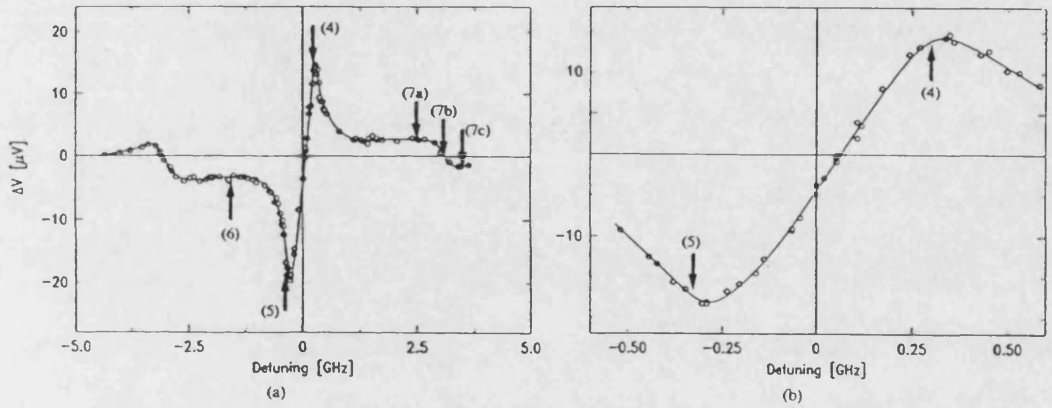

Figure 5.12: Measured change in the bias voltage of an AlGaAs edge-emitting laser (830nm) under optical injection vs. frequency detuning between injection and injected laser. Figure (a) is an overview while (b) expands the central part. The laser is driven at 65mA ($1.2 \times I_{th}$) emitting 3mW of optical power. The optical injection power is estimated at 30nW (after [1])

In comparison and considering its high output mirror reflectivity, the VCSEL displays a voltage drop far exceeding that expected under feedback (self-injection). What is even more surprising is the large bias voltage variation below laser threshold where the L-I of figure 5.2 shows negligible output power.

It may be then that only VCSELs display voltage changes in the millivolt range under optical feedback. This may arise from the characteristics of VCSELs that distinguish them from edge-emitting lasers. An obvious dissimilarity is the architecture of VCSELs resulting in their large transverse cross-sections supporting orthogonal polarisations and narrow output beams. A less obvious difference between VCSELs and their edge-emitting relatives is the high operational carrier concentration. This may yield a larger dependence of voltage on variations in the carrier concentrations. These matters are considered below in a series of calculations.

5.2.1 The junction voltage and the V-I curve

To understand changes in the V-I curve, it is necessary to formulate the relationship between the p-n junction carrier concentration and the voltage across it. The expertise of a colleague, Huw Summers, is applied at this point of investigation. His work over several years has generated a general procedure to make a wide range of quantum well calculations. One procedure is encoded in Quick Basic and when entered the quantum well thickness and material composition, it calculates the electron and hole energy levels, their masses and the energy bandgap. When entered into another C module, these parameters are used to calculate the density of states and the junction voltage at any carrier concentration. The details of these procedures are set out in the Appendix.

The C module is modified to calculate a curve of voltage against carrier concentration in the quantum well and the slope of that curve, the differential voltage; both are illustrated in figure 5.13. The latter represents the sensitivity of the voltage to small changes in the carrier concentration, which is deemed useful in this investigation. The module includes a junction temperature parameter which is varied between 300K and 360K. It is found to make only a small difference to the voltage and the differential voltage at low carrier concentrations. Figure 5.13 is obtained at the average temperature setting of 330K and is therefore assumed adequate for our purposes.

It ought to be pointed out that these procedures are designed for edge-emitting lasers, not VCSELs. This makes little difference, except where high carrier concentrations are reached in a VCSEL. The leakage of carriers into the barriers is not accounted for and

should lead to a reduction in their concentration in the quantum wells. This introduces an error smaller that 10% in the voltage and hence a similar error in the differential voltage.

Next, the C module is readapted and included in the VCSEL simulation project allowing the model to calculate the voltage against laser injection current. Again assuming a constant temperature of 330K, a theoretical junction V-I curve is produced and presented in figure 5.14 alongside the experimental device V-I curve. Comparing the two curves, the effect of the DBR mirror combined resistance on raising the device voltage becomes obvious. What is not obvious is the cause of the low experimental voltage at small currents.

This discrepancy may be understood by considering the lateral current spreading in a VCSEL which is determined by the depth of the proton implant. It has been shown [2] that a shallow implant allows more current spreading across the active region effecting a wider and more dispersed junction voltage profile. The average voltage over the electrical diameter then is lower than that over the optical diameter where the laser operates and the carrier concentration is averaged theoretically. This explains how the junction seems to conduct a current before it has reached the bandgap voltage and justifies the high theoretical current leakage of 40%.

Figure 5.14 also demonstrates a theoretical device voltage as calculated from equation (5.1). This curve is made parallel to the experimental curve by adjusting the total DBR mirror resistance and settling on $R_M = 50\ \Omega$. It is deduced that the current spreading dilutes the voltage generally by ~ .3V and slightly more at low currents. Incidentally, it has also been shown that VCSELs with shallow proton implants exhibit higher laser threshold currents, which is consistent with our measurements of VCSEL #1.

Reconsidering figure 5.13, it is interesting to note that the differential voltage is virtually constant above a carrier concentration of $5 \times 10^{18}\text{cm}^{-3}$. Hence a drop in the carrier concentration of $1 \times 10^{15}\text{cm}^{-3}$ reduces the p-n voltage V_{pn}, and the laser bias voltage V_b, by some 30μV. A voltage drop of 10mV corresponds to a carrier concentration fall of $3 \times 10^{17}\text{cm}^{-3}$ which constitutes a few percent of the average carrier concentration in the laser.

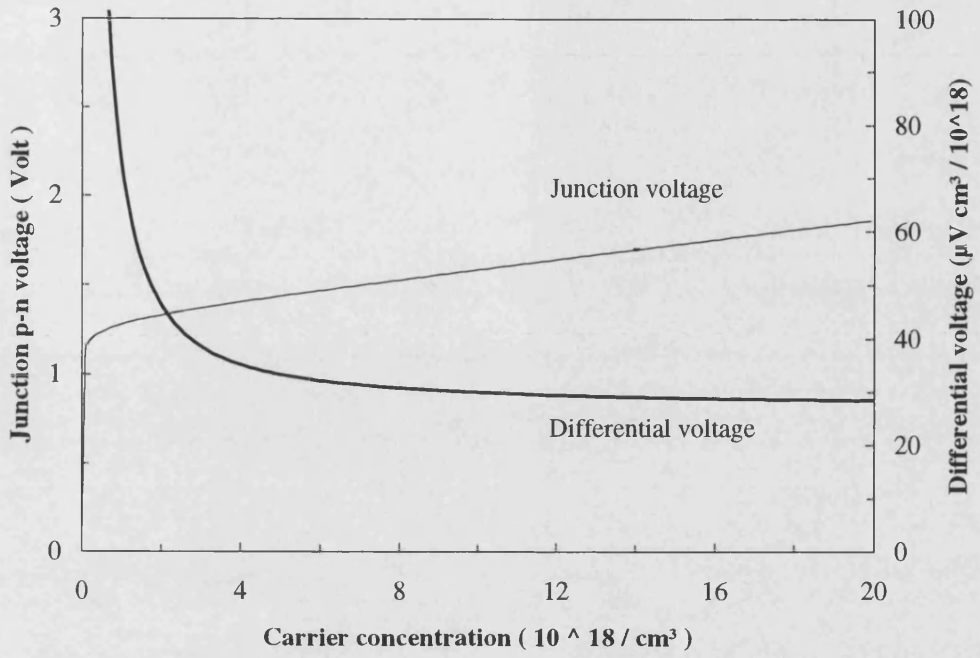

Figure 5.13: Calculated p-n juction voltage and differential voltage plotted against the carrier concentration

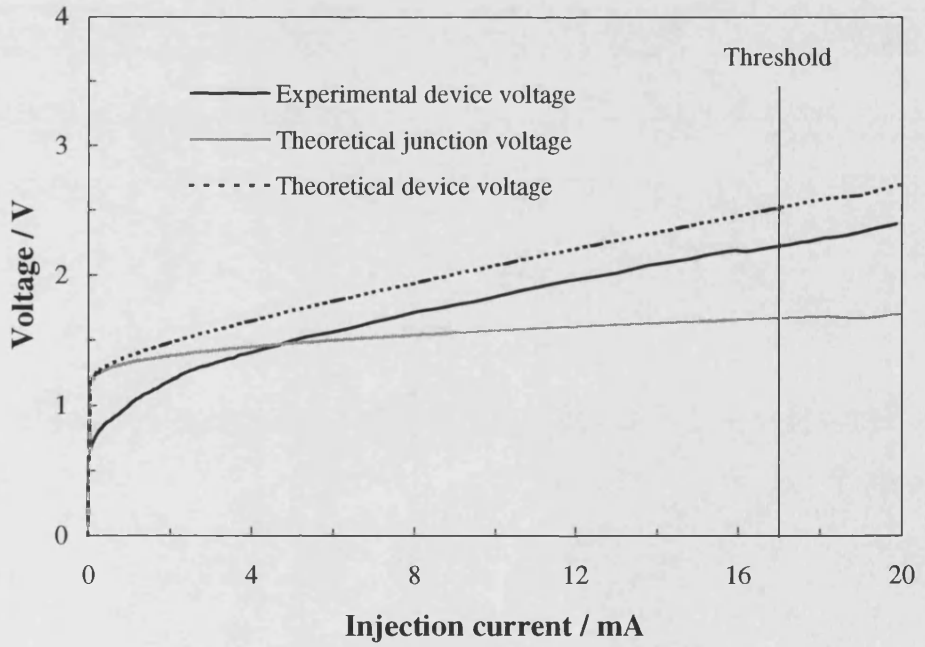

Figure 5.14: The experimental voltage-current (V-I) curve of VCSEL #1 compared with the theoretical junction voltage and hence device voltage

5.2.2 Optical feedback and the bias voltage

As was the case when investigating polarisation switching in chapter four, introducing the effect of an external mirror to the laser model makes little difference to the rate equations and their solutions. It was found in section 4.2.1 (chapter four) that cw polarisation switching may be modelled by reducing the optical loss for the suppressed mode and altering the gain saturation factors in its favour. This is justified by the lack of transverse optical guiding mechanism in the laser structure and the expected nonlinear local effect of gain saturation from focussed feedback light. In fact it is noted in figure 4.9 that the optical output power is reduced and the carrier concentration increased by POF that promotes the suppressed mode. It can also be seen that the effect is small at the foot of each L-I peak and grows to a maximum near the peak. Furthermore, the rise in carrier concentration is a good fraction of the total value as required by the calculation performed above. This suggests that a similar technique seems promising for modelling the observed behaviour described above.

Consideration has to be given also to the effective reflectivity of the coupled cavity constituting the laser output mirror. The coupled cavity is based on the assumption that the output light coherence is sufficiently long so as to experience coupled cavity effects. This does not apply to the highly incoherent spontaneous emission below the laser threshold, which explains the absence of voltage modulation with current from below threshold measurements in figures 5.5 and 5.9. Hence the reflectivity formula is altered to that of a coupled cavity above threshold and to a composite cavity below threshold.

In the endeavour to simulate the effect of quarter-wave plate feedback, the model sequence is modified as described below. Firstly, it solves the rate equations as per normal and calls the C module to calculate the junction voltage. Then it adds the external reflector, reduces the optical losses of P_b and alters the gain saturation factors, as set out in table 5.1. The rate equations are now solved again and the new carrier concentration is used to find the new voltage. The difference in voltage, the output powers, the carrier concentrations and the mirror reflectivity of the dominant mode are plotted against current in figure 5.15. This manner of solution presumes that the chopper frequency (~ 400Hz) is low enough to allow each state of operation to settle into cw action.

Table 5.1: Feedback parameters

Parameter description	Symbol	Value without feedback	Value with feedback
Modal loss difference	$\delta\alpha$	10.0 cm^{-1}	4.0 cm^{-1}
Gain self-saturation of P_a	ε_{aa}	30 x 10^{-17} cm^3	70 x 10^{-17} cm^3
Gain self-saturation of P_b	ε_{bb}	30 x 10^{-17} cm^3	70 x 10^{-17} cm^3
Gain suppression of P_a by P_b	ε_{ab}	30 x 10^{-17} cm^3	70 x 10^{-17} cm^3
Gain suppression of P_b by P_a	ε_{ba}	30 x 10^{-17} cm^3	70 x 10^{-17} cm^3
Spontaneous emission coupling factor	β	1 x 10^{-5}	No change
Reflectivity of external mirror	R_X	0%	98%
Quarter-wave plate transmissivity	T	0%	95%
Coupling factor between lens and laser	f	0%	95%

The changes in parameters set out above simulate POF promoting both polarised laser modes. The voltage difference in figure 5.15 shows a resemblance to the equivalent experimental results in figure 5.10. Naturally, the voltage rise maxima depend largely on the variation of the parameters in table 5.1. The details of the process are likely to have dynamic dependencies which require more specialised and interactive modelling. However, the model demonstrates that at a kink in the L-I curve, the bias voltage of a laser is highly sensitive to optical feedback. This essential fact is the basis of a dedicated experiment that will be described in the following sections.

The model also successfully simulates the sharp drop and polarity reversal of the measured δV_b (figure 5.5) at the correspondingly sharp laser turn-on. What it fails to simulate, though, is the depth of the voltage drop below threshold. This has perhaps more to do with the design of the rate equations than with the substance of the model. The photon density solutions of the rate equations account for the optical power contained in the specified optical laser modes. This in fact constitutes most of the optical power in a laser operating above its threshold. Below threshold, however, the small optical power in the cavity is distributed over the spontaneous emission spectral range. The inaccuracy introduced is usually minor except in the current range just below threshold. There the optical gain does not quite match up to the optical loss but spontaneous emission

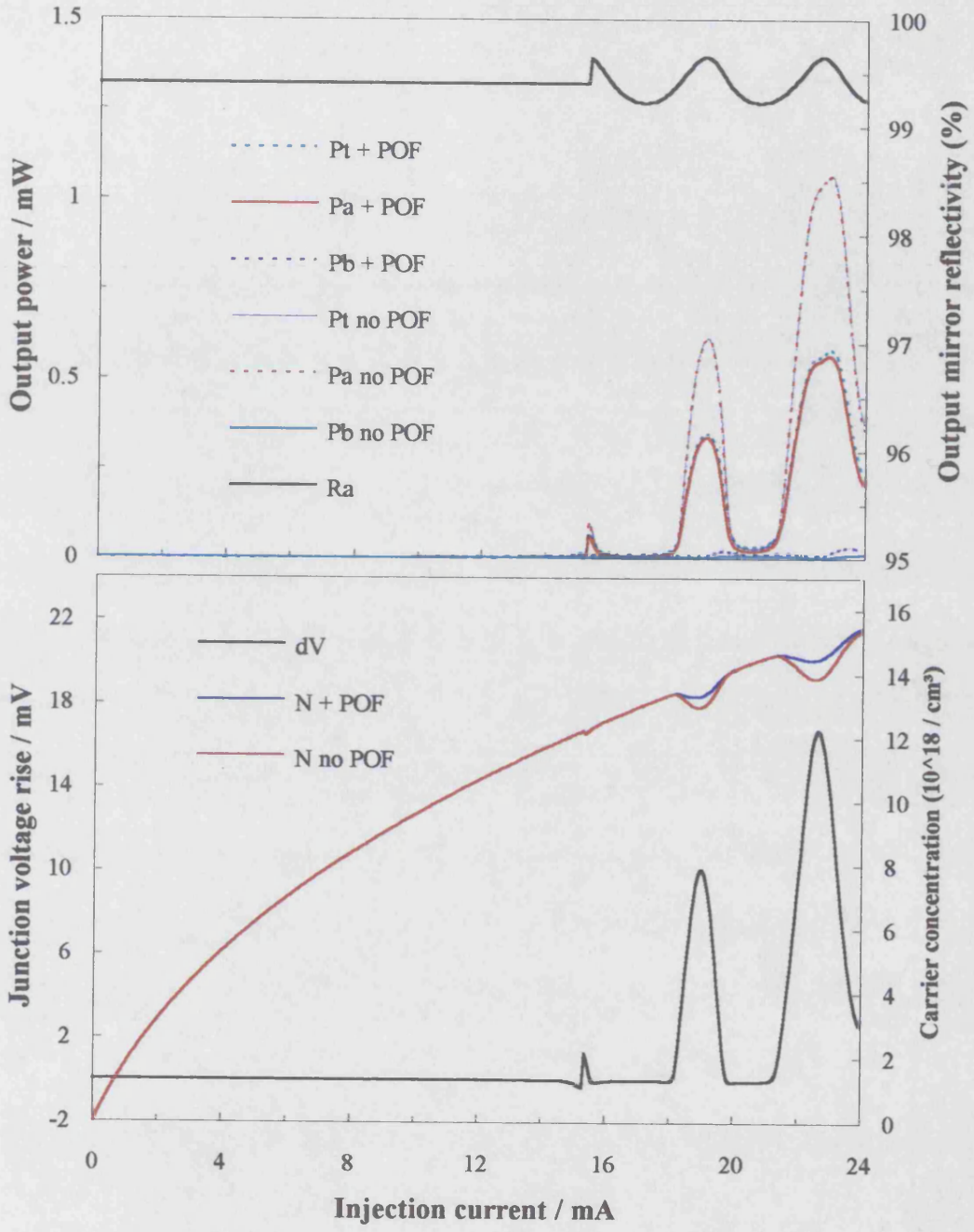

Figure 5.15: Theoretical cw L-I with and without optical feedback (above) illustrating changes in the carrier concentration (N) and device voltage (dV) (below). P_t is the total output power

is amplified enough to deplete some carriers. The amplified spontaneous regime is beyond the range of the standard rate equations and is better explored using modified amplifier equations.

Another aspect of the bias voltage change is its dependence on the feedback ratio. To simplify the matter, this is investigated at a constant current. The model is modified again to solve the rate equations with no optical feedback up to the first L-I peak which also results in the first peak in the voltage change. While maintaining a constant injection current, the external cavity effective reflectivity (including all optical losses) is scanned from nil to unity. Figure 5.16 displays the evolution of the bias voltage rise with the effective reflectivity and the gradual fall in total optical power. This voltage curve is approximately linear over small reflectivity changes, although the slope drops dramatically above 85%. This may be useful in determining the effects of small reflectivity changes on the bias voltage.

It is relevant to point out that the changes in voltage discussed above are accompanied by a change in the injection current. As expected, a δV_b of +10mV induces a δI of approximately -15μA through a drive resistance R_D of ~ 600 Ω. This naturally causes a small but opposite change in the device voltage (δV_b ~ -1mV) but is considered a negligible second order effect.

Measurements of changes in device voltage under variable optical feedback are motivated by the possible use of a VCSEL as a detector. Consider operating VCSEL #1 at a point where the bias voltage sensitivity to feedback intensity is greatly enhanced, such as the peak of one L-I kink. This can then provide a method of detecting very small feedback changes via the laser bias voltage. This may be of great significance in applications where one device can play both roles of transmitter and detector. One such application involving the magneto-optical Kerr effect is considered in the next section.

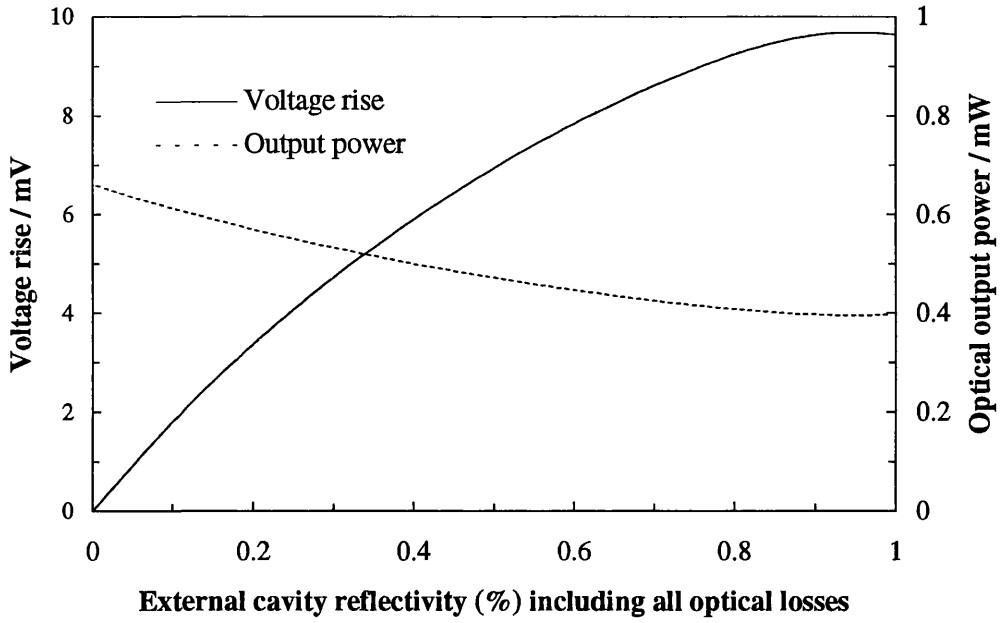

Figure 5.16: Variation of peak voltage rise with the external reflectivity at a constant injection current of ~19mA (L-I peak)

However, despite all the precautions taken to prolong the life of VCSEL #1, at this point of experimentation it ceased to operate. This is perhaps not surprising considering that most experiments performed so far were carried out under cw laser operation. Although VCSEL #1 has served for longer than expected, its failure is quite a set-back because it is a unique and irreplaceable device. Nonetheless, the original plan is pursued as documented below.

5.3 Detection of the magneto-optic (MO) Kerr effect

When plane-polarised laser light is reflected from a magneto-optically active material, it will become elliptically polarised with its major axis rotated with respect to the original direction by a small angle (θ_k) due to the polar Kerr effect. The sense of rotation depends on the polarity of the magnetic field in the material.

This effect can be used to modulate the intensity of optical feedback to the laser diode and hence its bias voltage. Although the voltage modulation is expectedly small, it may be enhanced greatly, as discovered above, by operating the laser at a kink in the L-I curve. This may prove to be an alternative method of magneto-optic data retrieval that is less cumbersome and faster than standard detector systems. As discussed in the introductory chapter, the bulk of the optical head and hence the long access time in magneto-optic read/write disk systems is one of the limiting factors for their usage and market penetration at present. Therefore the feasibility of data detection is explored experimentally in the remainder of this chapter.

5.3.1 Device characterisation

As demanded by the catastrophic termination of VCSEL #1 and after experimenting with several other laser devices, none of which were smaller than 24μm in diameter, one laser was found that demonstrated the best experimental result. VCSEL #2 is a 34μm diameter laser operating at 980nm with a threshold just above 10mA. Its V-I and polarisation resolved L-I curves are presented in figures 5.17 and 5.18 respectively. The V-I curve reveals a changing differential forward bias resistance that averages at ~ 84 Ω between 0mA and 40mA. It may also be noted that unlike VCSEL #1 the voltage bias at small currents tends to ~ 1.1V for this device, close to the theoretically expected 1.2V. This indicates low current spreading because of a deeper proton implant which, in comparison, also results in a higher junction resistance and a higher bias voltage curve.

It can be seen from the L-I curve that the laser operates in two orthogonal polarisations (P_a at 15° and P_b at 105°) as observed through a Glan-Thompson polariser. Figure 5.19 illustrates several near field images of the laser output captured with a CCD camera by two colleagues, Philip Dowd and Lutz Raddatz. Figures 5.19a to 5.19e follow the evolution of the P_a output from the fundamental mode at 11.5mA to first order at 13.5mA

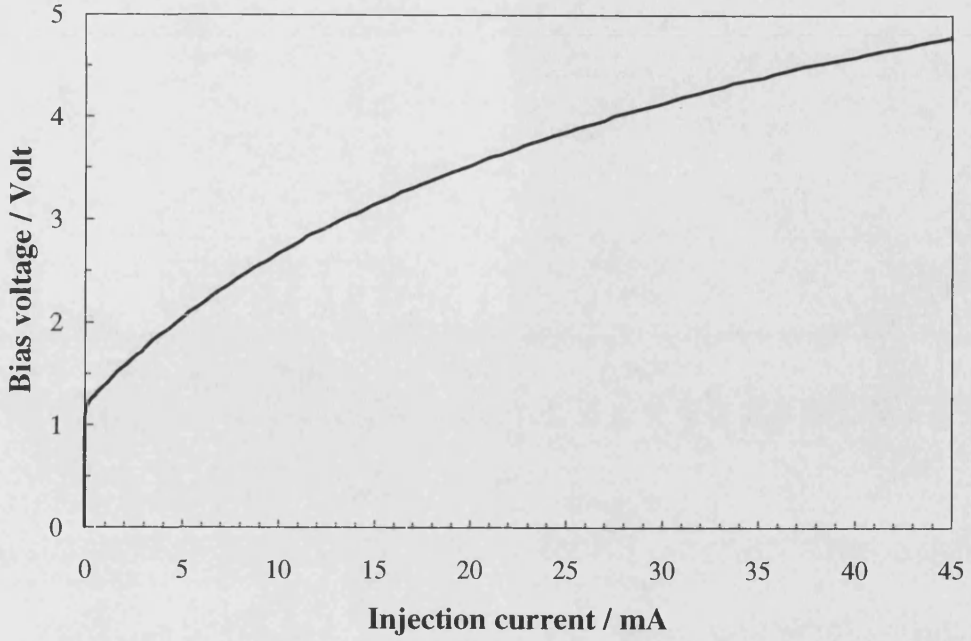

Figure 5.18: Voltage-current curve of VCSEL #2 demonstrating little current spreading and a high differential resistence

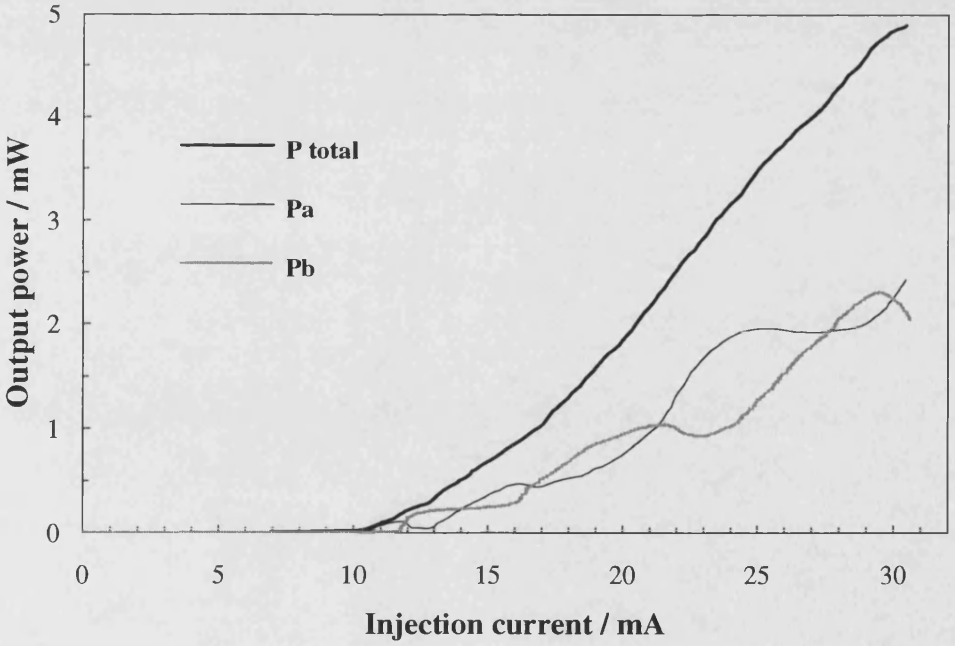

Figure 5.19: Polarisation resolved L-I characteristics of VCSEL #2 demonstrating alternate transverse mode switching

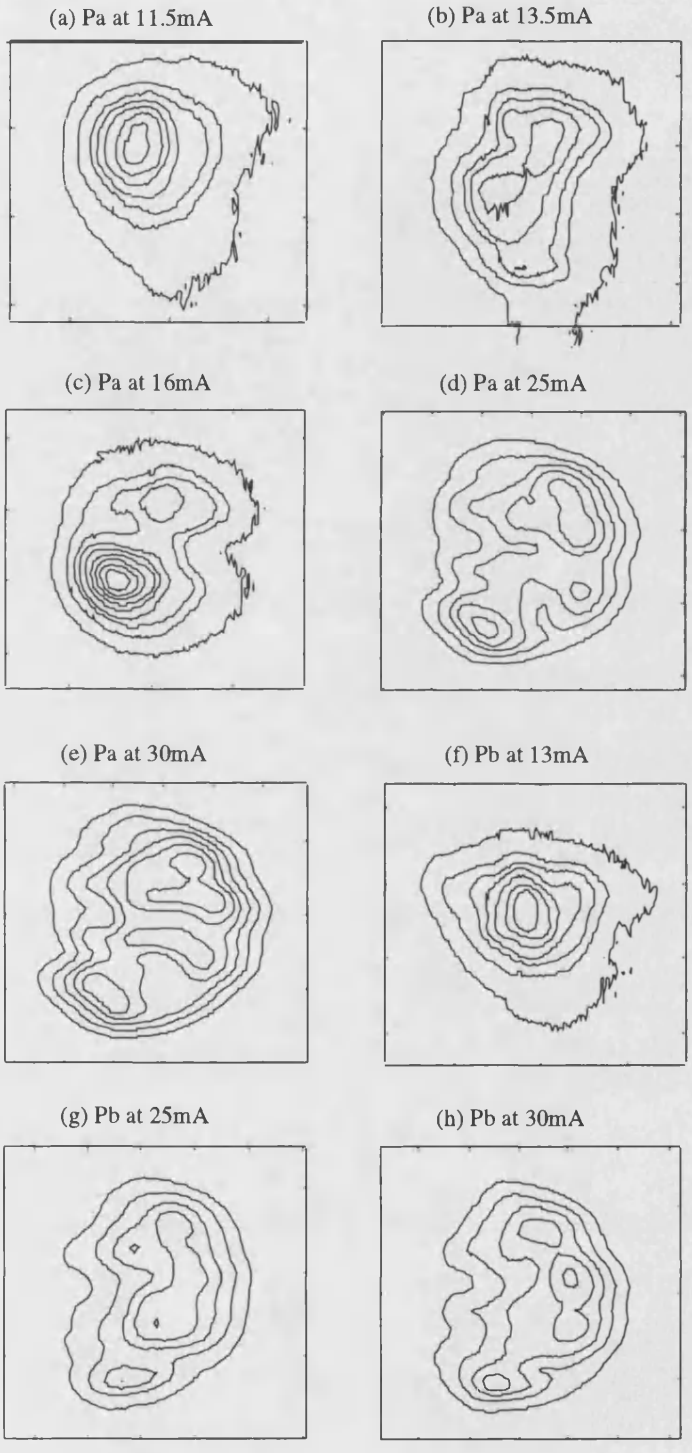

Figure 5.19: Near field images of VCSEL #30 for P_a and P_b demonstrating the evolution of the transverse mode structure over a current range correlating with the kinks in the L-I curve

and 16mA and to what appears to be the second order mode at 25mA and third order mode at 30mA. The near fields indicate that the oscillation in the L-I curve of P_a is a product of the transverse mode switching. Figures 5.19f to 5.19h similarly show the single transverse P_b mode at 13mA and what seem to be the first order mode at 25mA and the second order mode at 30mA. Obviously then the laser regularly introduces higher order transverse optical modes with increasing current injection.

It may be noted that the differential internal efficiency of the laser increases for these higher order modes, hence the gradually increasing slope of the total output power. Of most interest for our purposes, however, are the kinks in the P_a and P_b curves where negative slopes are observed. At these points of operation the laser bias voltage may prove highly sensitive to optical feedback.

5.3.2 Magneto-optic sample characteristics

The MO sample used in the following experiments is a Cobalt/Platinum (Co/Pt) multilayered structure material of 10 alternating layer pairs with no protection overcoat. This sample has been courteously provided by Dr C.D.Wright of the Information Storage Research Group at the Department of Electrical Engineering at the University of Manchester. The sample is approximately 3mm x 3mm in dimensions and is magnetised in one longitudinal direction except for a series of linear domains 2mm long of opposite magnetisation, as schematically presented in figure 5.20a. Such a magnetic pattern appears as intensity contrast in a polar Kerr micrograph, reproduced in figure 5.20b.

The image is expanded non-isotropically, i.e. the dimension perpendicular to the pattern is grossly expanded relative to the parallel dimension. It is obtained by scanning a small region of the sample using a laser microscope system. The black irregular marks in the images are surface defects which may have existed in the sample before processing or may have been caused by the patterning process itself. The magnetic pattern which has been defined by a laser beam consists of lines (marks) and intermediate spaces of background magnetisation. Their widths are unequal and vary between 10μm and 54μm as listed in sequence in figure 5.20.2. This sample is designed for optimum performance

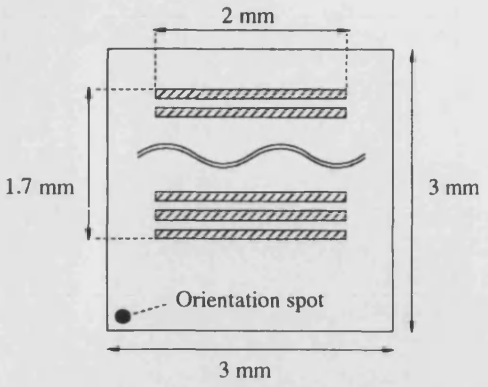

Figure 5.20a: Schematic diagram illustrating the dimensions of the MO sample and the pattern

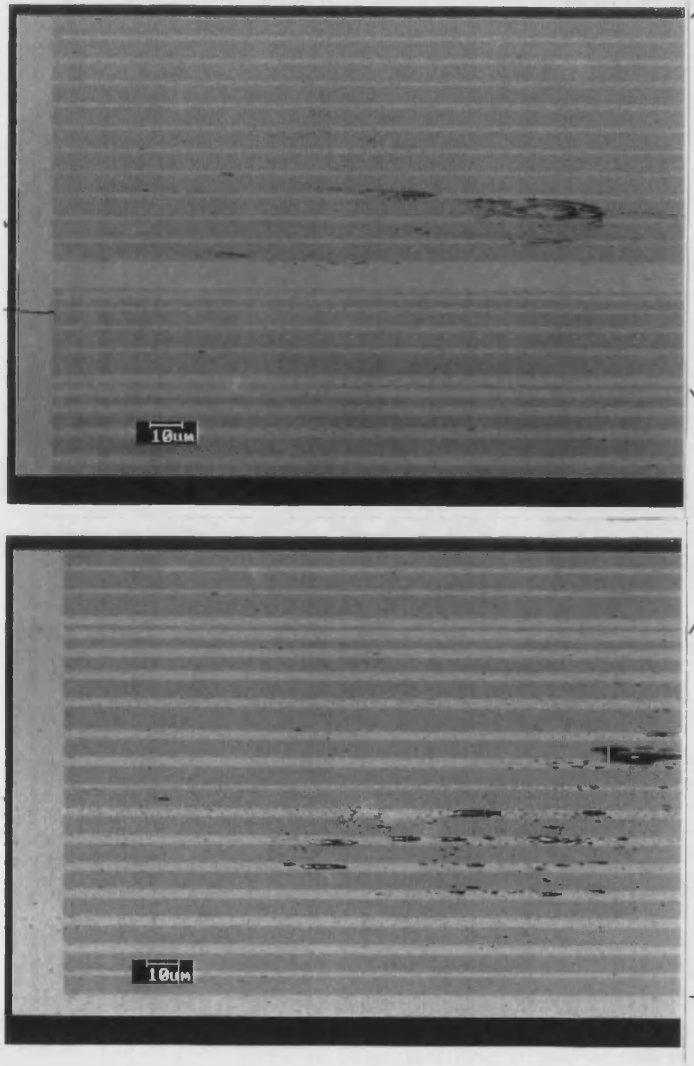

Figure 5.21b: Polar Kerr micrographs of the sample illustrating the magnetised pattern

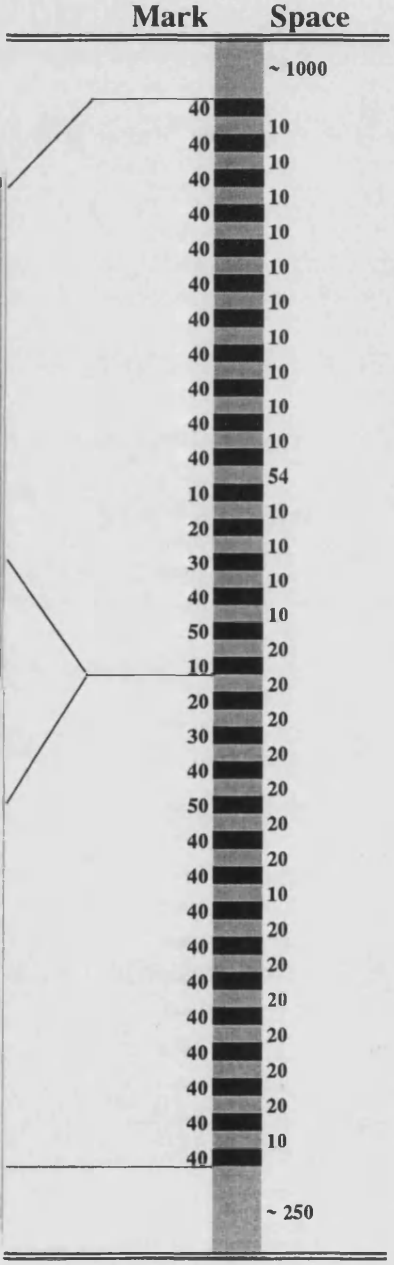

Figure 5.21c: Table of MO pattern line width and spacing in microns

at a wavelength of ~ 800nm where both reflectivity and Kerr angle are at a maximum. At the operating wavelength of the laser, however, its measured reflectivity is a substantial 60% and θ_k is estimated at 0.2°.

5.3.3 Experimental arrangement

The aim of this experiment is to detect the magnetic pattern on the MO sample using the enhanced sensitivity of the laser bias voltage to optical feedback. Hence VCSEL #2 is aligned in an external cavity formed with the MO sample as illustrated in figure 5.21. The sample is mounted on a Micro Control mirror mount for good angular control of the sample surface and a Photon Control micropositioner for accurate positioning. One lens collimates the laser output beam and another focuses the beam onto the sample. For this purpose, two 8.0mm Melles Griot laser diode lenses are used with a quoted numerical aperture of 0.50 and a spot size of 1.02μm at a wavelength of 830nm. An intra-cavity plane glass beamsplitter redirects part of the reflected beam to a Ge p-i-n detector via a polariser and a lens. An intra-cavity Glan-Thompson polariser is inserted between the laser and the beamsplitter to linearly polarise the probe laser beam.

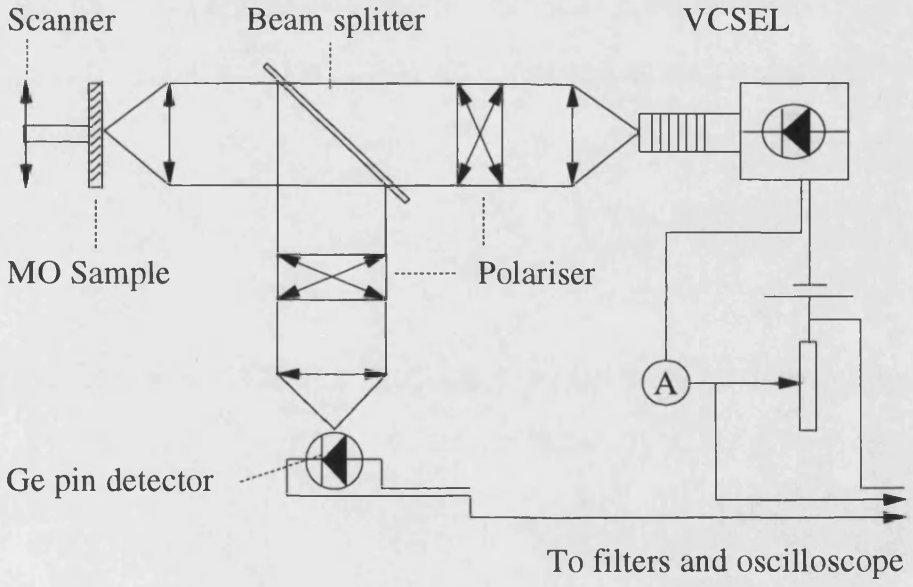

Figure 5.21: Experimental arrangement for detecting the magnetic pattern stored on an MO sample using a detector and independently the bias voltage sensitivity of VCSEL #2

With its magnetised lines aligned vertically, the MO sample is mounted on a scanner that sweeps it horizontally with a sinusoidal motion set to a period of 80ms. The detector signal and the laser bias voltage are observed simultaneously on a Tektronix scope via an amplifying plug-in head with a frequency band filter. Also attached to the sample mount is a Linear Variable Differential Transformer (LVDT) gauge for direct measurement of the sample position. The laser is operated on a cooled mount at a roughly constant temperature around 17°C. Overall temperature variations are therefore unlikely to play a significant part in the experiment.

5.3.4 Pattern detection

The plane-polarised light spot scans the pattern lines at a linear speed approximately 18mm/s and is reflected with a small ellipticity in polarisation. This is analysed by each polariser and the polarising beamsplitter, reducing the intensity of both beams. Scanning the sample then causes an intensity modulation of both the detector beam and the laser feedback beam in response to the magnetised lines. The MO pattern may subsequently be observed through the detector and also in the laser bias voltage level.

Observing the beam via the polariser and detector reveals the pattern of magnetisation which is illustrated in figure 5.22 representing the maximum signal amplitude of ~ 400μV. The pattern is clearly distinguished from the rest of the sample surface starting at ~ 1 mm and ending at ~ 1.7 mm. Rotating the detector polariser varies the depth of the voltage modulation. At particular angles the pattern fluctuations disappear and within some angle ranges the signal is inverted as in figure 5.23. This represents the highest detection sensitivity of 16% (and a signal amplitude of ~ 170μV) for the polarisation rotation involved.

When the laser bias voltage is searched for the pattern a small signal between 50μV and 100μV is found that is obscured by noise, especially that caused by surface irregularities and defects. Under particular conditions, however, the voltage signal is enhanced by the laser. At a drive current of 25.5mA ± 0.1mA and a polariser angle of 3° ± 5°, the bias voltage pattern signal is rapidly enhanced to a best amplitude of 550μV. Noise may be reduced by setting the low frequency and high frequency filters available on the scope.

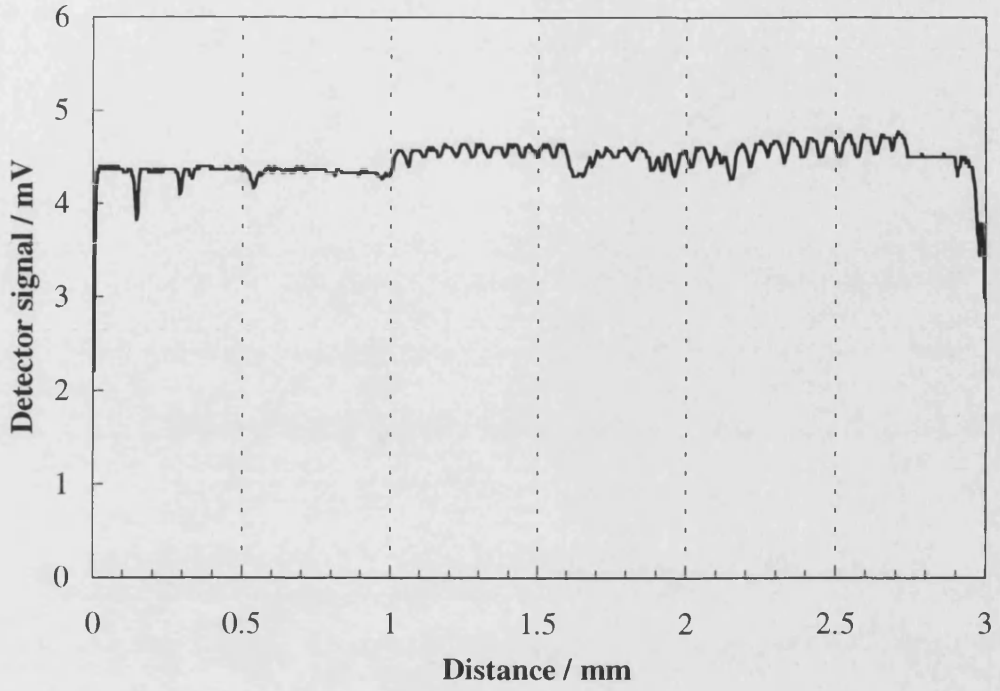

Figure 5.22: Detector voltage signal of the MO sample illustrating a maximum positive sensitivity of 400μV (+9%) to the magnetic pattern encoded

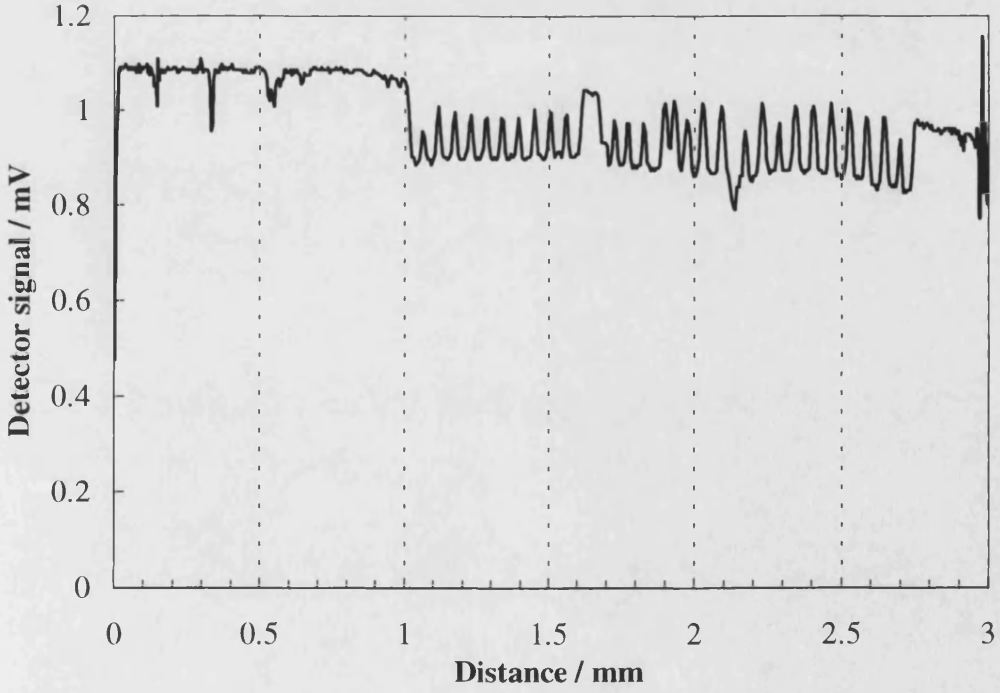

Figure 5.23: Detector voltage signal of the MO sample illustrating a maximum negative sensitivity of 170μV (-16%) to the magnetic pattern encoded

The observed signal is illustrated in figure 5.24 along with the simultaneous unoptimised detector signal. The voltage detected pattern is distinct between 1.3mm and 1.5mm on the sample and corresponds to a few lines 40μm wide each spaced by 10μm.

The pattern does not appear complete in one scan because our method of scanning the sample inevitably incorporates a longitudinal component of motion. This moves the sample in and out of the lens focus, dilating the incident spot size, smearing the Kerr effect and diluting the voltage signal. This obstacle is overcome in a real dedicated system where the focus is maintained interactively and the signal is optimised. Nonetheless, the whole pattern may be observed a few lines at a time in the above arrangement by simply retuning the focus appropriately. This enhancement may be correlated to the kink in the L-I of P_a around 25mA which exhibits a negative slope. A similar result is observed at a drive current of 23.1mA ± 0.1mA and a polariser angle of 0° ± 5° where the signal is enhanced to 300μV. This may also be correlated to the L-I kink of P_b at 22mA where a negative slope is displayed.

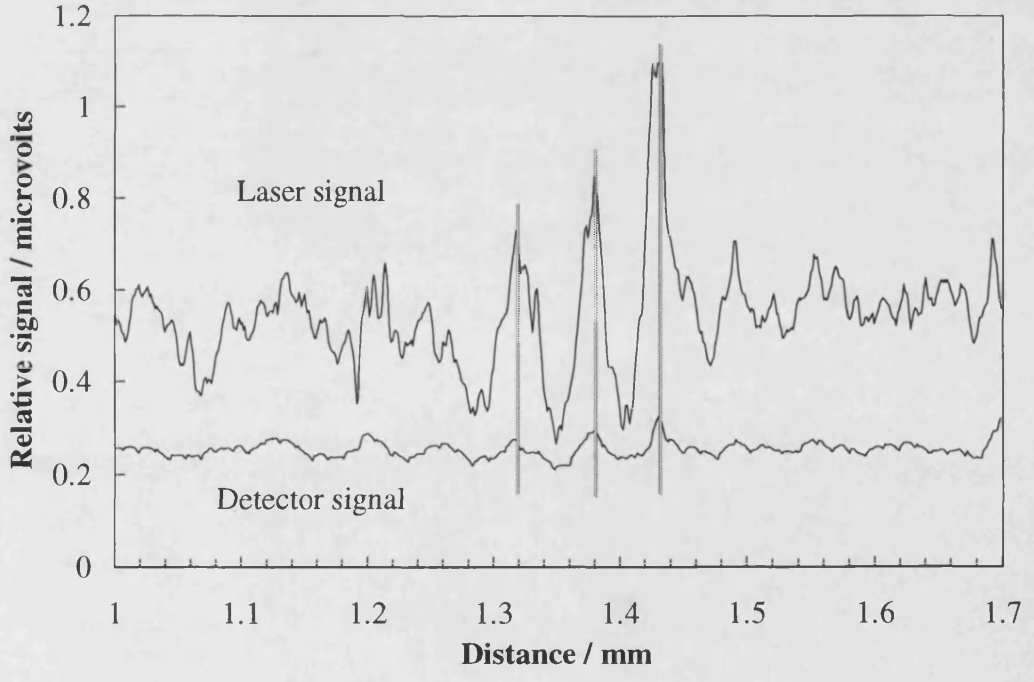

Figure 5.24: Laser bias voltage correlates with the detector voltage illustrating magneto-optic pattern detection

The experiment is also carried out using other optical components such as a quarter-wave plate and a half-wave plate; both produced no significant results. When detecting the voltage signal, precautions were taken not to allow the detector signal to couple to the voltage signal within the oscilloscope. This was tested for by disconnecting the detector signal cable altogether while still observing the unaffected bias voltage signal. A greater enhancement may be achieved by optimising the laser design so as to display deeper kinks.

This experiment is a proof of principle of magneto-optic pattern detection using the VCSEL. Although in a commercial system the magnetic data bit is submicron in size and the data transfer rate is ~ 6MHz, such a system also provides interactive focussing and tracking and optimised optics. A commercial disk medium is also protected from oxidation and disconfiguration by the substrate and overcoat. Hence, further and more dedicated investigation is warranted to make this system a reality. Meanwhile, a patent application based on this experiment and the results illustrated above has been filed by Hewlett-Packard Corporation.

5.4 Conclusion

This chapter documents the first observations of bias voltage modulation of a semiconductor laser by optical feedback with a dependence on the feedback polarisation. It is discovered that kinks in the L-I curve of a VCSEL enhance the voltage modulation to ~ 10mV; such modulation also takes place below laser threshold. A theoretical study is carried out culminating in a simulation of this novel effect and a fundamental understanding of its origin. It can result, it is shown, from large gain compression and suppression factors induced by the feedback.

An innovative experiment is designed to utilise this effect in detecting a pattern magnetised on a magneto-optic material. This pattern causes the rotation of plane-polarised light by the polar Kerr effect and modulates the feedback to the laser. The voltage signal is amplified tenfold at the L-I kink allowing enhanced detection of the pattern (patent application filed).

Our results demonstrate the possibility of eliminating several optical components from the optical head of a magneto-optic data retrieval disk system, reducing the track to track access time. This could potentially provide the key to MO computer hard drives of revolutionary capacity combined with competitive random access times.

5.5 References

[1] M.P.van Exter, C.Biever, J.P.Woerdman: *Effect of optical injection on bias voltage and spectrum of semiconductor laser* J. Quant. Elect. **29** (11) 1993

[2] C.J.Change-Hasnain, J.P.Harbison, G.Hasnain, A.C.Von Lehmen, L.T.Florez, N.G.Stoffel: *Dynamic, polarization, and transverse mode characteristics of vertical cavity surface emitting lasers* J. Quant. Elect. **27** (6) 1991

Conclusion

This conclusion expresses the ideas introduced in the first two chapters and summarises the experimental work and theoretical analysis carried out in remaining chapters. Proposals for future work are also offered in the light of current technology status and requirements.

This thesis is been devoted to investigating the optical polarisation behaviour of vertical-cavity surface-emitting lasers (VCSELs) particularly under optical feedback. VCSELs have had a remarkable impact on semiconductor laser technology and have enjoyed rapid progress. It is expected that they will replace edge-emitting lasers in some applications and that they will perform new functions in addition.

The introductory chapter gives a general view of semiconductor lasers in terms of architecture. A comparison between edge-emitting lasers and VCSELs illustrates the various advantages of the latter class. The features of VCSELs that will simplify their implementation include convenience in wafer-level testing, inherently better quality surface-emitted output beams, achievable microamp threshold currents, and the viability of tunable individually addressable 2-D arrays. VCSELs have also opened new opportunities for this technology in multichip communications, 2-D optical displays and 3-D optical integration where all-optical operation is approaching optical processing. In particular the optical polarisation diversity of VCSELs is a significant feature that affords them great potential and therefore, polarisation switching applications are considered.

Additionally, the application of semiconductor lasers in optical data storage has lead to their proliferation in the personal and domestic environment. VCSELs are in a position to enter this technology bringing new solutions that enhance performance. A review of data storage techniques covers magnetic media, particularly hard disks, and the available optical media: CD-ROM, WORM, re-writable and magneto-optical disks. It is concluded that the optical head mass and sophistication limits access time to data, a problem possibly alleviated by VCSEL.

In the second chapter, the physical principles of semiconductor laser operation are established and followed by a general review of VCSEL technology with particular attention to their optical polarisation. The mirror and cavity designs, transverse confinement and the semiconductor materials used are briefly presented and the operational characteristics of VCSELs described. Interest in VCSELs is demonstrated by the rapid pace of the development of 2-D arrays, microcavity devices and 3-D integrated components, specifically refractive and defractive lenses for optical fibre and free-space interconnections.

Chapter three examines the unique light-current output characteristics of a VCSEL device exhibiting deep continuous-wave (cw) modulation. This is attributed to residual gain anisotropy, cavity birefringence, a coupled cavity formed with the substrate, and the inevitable wavelength drift due to device heating. The coupled cavity is an example of a simple but effective 3-D integrated optical device. The physical processes involved are rationalised and formalised into a mathematical rate equation model which is solved numerically. Besides extracting several internal laser parameters, the model is used for predicting the effects of varying them. In particular polarisation switching is anticipated to occur under further external cavity feedback and to be enhanced by the coupled cavity.

The sensitivity of this VCSEL to polarised optical feedback by undergoing cw polarisation switching is demonstrated experimentally in the fourth chapter. Using the theoretical model, the cross-saturation between the orthogonally polarised transverse optical modes is found to cause this switching. Dynamic all-optical polarisation switching is achieved at frequencies up to 1.5GHz and limited by the detector bandwidth. The model also predicts that cw polarisation switching is accompanied by a considerable change in the carrier concentration within the laser and in the bias voltage across it.

Chapter five documents the first observations of bias voltage modulation by polarised optical feedback angle variation. The voltage is modulated on the order of 10mV with feedback polarisation angle, expectedly above threshold and surprisingly below it. The model is expanded to account for this novel effect which is attributed to gain compression and suppression factors.

Exploiting this behaviour, the laser is used as a source under feedback and simultaneously as a detector of the polarisation rotation induced by the polar Kerr effect. As predicted in chapter three, the laser response is enhanced at the kinks in the L-I curve. This experiment demonstrates the feasibility of using a VCSEL for magneto-optical (MO) pattern detection for MO storage applications (patent application filed).

Future work

The work presented in this thesis has generated many ideas for future work. With regards to the polarisation switching, the ultimate aim is to achieve ultra-high switching frequencies with sufficient modulation power for detection and optical processing. Obtaining switching at 5GHz requires an external cavity length of 15mm which is possible using a spherical (ball) lens. Achieving 50GHz, however, requires a cavity length of 1.5mm which is comparable to the optical thickness of the substrate. Therefore, it seems necessary to form an external cavity with a quarter-wave plate (QWP ~ 1mm thick) affixed to the laser and mirrored on the far side with a multilayer dielectric coating, thereby dispensing of the lens altogether. Achieving higher frequencies still necessitates thinning the substrate down or even using a top-emitting VCSEL. In fact, it would be interesting to investigate the consequence of including the QWP in the laser cavity by eliminating the top mirror.

The problem of small modulation power may be solved by inducing bistability in the laser. Mathematically this requires a set of gain saturation terms that promotes gain cross-saturation highly. In physical terms this may be induced by introducing impurities into the laser cavity at the fabrication stage. Bistability, however, involves the redistribution of the carrier profile across the laser which limits the frequency response to ~ 10GHz at best. Another option is to reduce the output mirror reflectivity, down to

~ 97% perhaps, improving the effect of the external cavity. Minimising the birefringence would also bring the two polarised modes into closer competition which probably makes them more sensitive to feedback.

Alternatively, one may utilise the coupled cavity formed with the mirrored QWP described above, whose constructive interference depends on the mode wavelength. Magnifying the cavity birefringence by defining a more elliptical lateral cavity for instance, would therefore increase the wavelength splitting between the polarised modes. As predicted in section 3.3 by using the model, this allows the suppressed polarised mode an advantage over the dominant mode at the appropriate temperatures and injection currents. In other words, polarisation switching may be enhanced further by the coupled cavity with additional spectral splitting.

If a dynamic polarisation switching device is to be utilised as a clock in an all-optical system, then some system-oriented measurements need to be obtained, such as the timing jitter of the pulse train. One also needs to demonstrate signal recovery from another clock at a similar wavelength range (960-990nm). For this purpose and others like pulse reshaping and retiming, it is desirable to demonstrate wavelength conversion, in particular from 790nm, 870nm, 1.3μm and 1.5μm wavelength lasers used for optical fibre systems.

CW polarisation switching has been useful in determining some of the laser parameters, e.g. gain anisotropy, wavelength splitting (cavity birefringence), thermal impedance, wavelength drift rate with temperature and the substrate facet reflectivity. Similarly and utilising the model developed, it is possible to characterise one device from each batch or wafer, for quality control for example.

CW polarisation switching may be used as an all-optical polarisation logic gate for all-optical processing applications. In such a configuration, and with its bias voltage dependent on the optical injection polarisation, the device may serve as an unobtrusive electrical sensor of the optical state of the laser, imbedded in the optical system.

Having demonstrated the validity of MO pattern detection via the device bias voltage, the next step is to enhance the voltage signal and to apply this behaviour to a real MO storage system environment. It is predicted that the deeper the L-I modulation by the

coupled cavity, the more the kinks enhance the voltage signal. Therefore, improving the cavity by polishing the substrate and perhaps even applying a high reflectivity (HR) coating, while reducing the laser output mirror reflectivity, may enhance the voltage signal to a few millivolts.

Emphasis thereafter should be shifted to detecting a signal from real size data bits (~ .7μm in diameter). Using shorter wavelength VCSELs for this purpose may be advantageous because of the smaller spot sizes obtainable. It would also be appropriate to demonstrate a data flow rate of ~ 20MHz as expected from an operational system. The effect of surface defects from the protective substrate of an actual MO disk may be diffused by focussing the laser beam through the transparent substrate onto the MO material.

Finally, in the light of the discoveries made, the results achieved, the ideas acquired and the insight gained, it is believed that VCSELs will have a bright future indeed.

Appendix

The Quick Basic module calculates the energy band levels of the quantum well materials by non-linear mole fraction interpolation from experimental data for similar material compositions. The effective electron, light-hole and heavy-hole masses are similarly interpolated from appropriate experimental data. The resultant energies lead to the depths of the conduction and valence energy wells, as illustrated in figure A.1. Knowing the particle effective masses and the quantum well width (layer thickness), Schrödinger's equation is solved for the finite quantum well in the vertical direction (axial). This module is used once to calculate the confined state energies (E_1, E_2, E_3 ... etc) for all three particles.

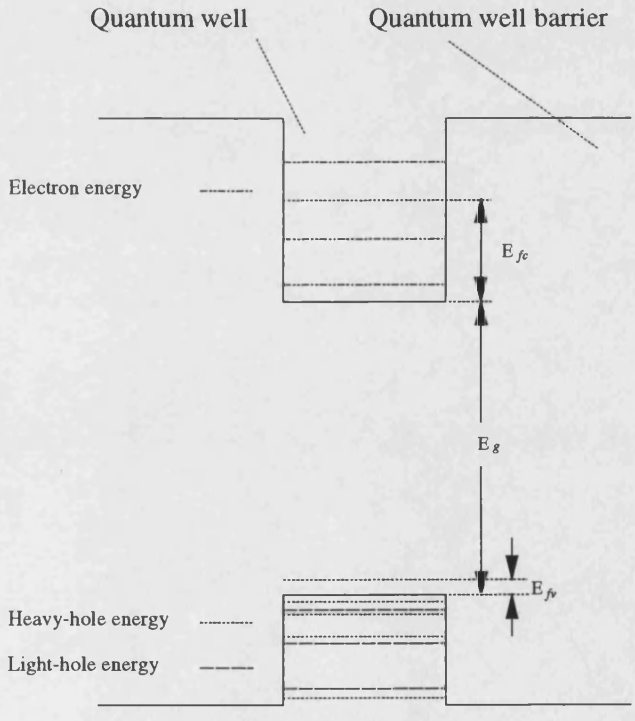

Figure A.1: The finite quantum well and the confined state energies of conduction electrons and valence holes (light and heavy)

The C module is designed to compute the bias voltage for a given carrier concentration value, using the products of the first module. Initially, the Fermi level positions of the cladding layers and the quantum well layers are calculated. The electron filling of the quantised subbands is estimated as a function of energy $f_c(E_c)$, and the total electron concentration in the conduction band is calculated by:

$$N = \int_{subbands} \rho_c(E) f_c(E) dE$$

where the function $\rho_c(E)$ is the density of states with respect to energy, and the integral is over all energies and all subbands. The program engages into iterations until the resultant carrier concentration matches the given value. Then the process is repeated for the valence band taking into account the light-holes and heavy-holes. Finally, the Fermi-level energies in both bands are added to the band gap culminating in the electron-voltage across the device from which the bias voltage is extracted.

$$V_{bias} = (E_{fc} + E_{fv} + E_g) / e$$

where e is the electron charge.